Summer 2014

FLEXIBLE TETHERS IN MULTI-CHROMOPHORIC SYSTEMS: LINKING PHOTOPHYSICS WITH ASSEMBLY

Jeffrey M. Lucas

University of Massachusetts - Amherst, jmluc0@chem.umass.edu

FLEXIBLE TETHERS IN MULTI-CHROMOPHORIC SYSTEMS:
LINKING PHOTOPHYSICS WITH ASSEMBLY

A Dissertation Presented

by

JEFFREY MORGAN LUCAS

Submitted to the Graduate School of the
University of Massachusetts Amherst in partial fulfilment
of the requirements for the degree of

DOCTOR OF PHILOSOPHY

September 2014

Department of Chemistry

FLEXIBLE TETHERS IN MULTI-CHROMOPHORIC SYSTEMS:
LINKING PHOTOPHYSICS WITH ASSEMBLY

A Dissertation presented

by

JEFFREY MORGAN LUCAS

Approved as to style and content by:

_____
Paul M. Lahti, Chair

_____
Michael D. Barnes, Member

_____
S. Thayumanavan, Member

_____
Ryan C. Hayward, Member

                                    _____
                                      Craig T. Martin, Department Head
                                      Department of Chemistry

DEDICATION

To my wife Jing, and to my parents, family, colleagues, friends and mentors. All of you

have added such quality to my life; I am truly blessed.

ACKNOWLEDGEMENTS

To my family and friends, and to my grandparents, Alfred and Viola Marzullo and Harold and Margaret Lucas, who began their lives in the United States with next to nothing, who strove to succeed when opportunities were limited, who worked themselves to the bone so that I could have the life that I have today, I say thank you for your patience, love, support and inspiration. I hope that I have made all of you proud. I share my success with you today, for this thesis is not only mine, but yours as well.

Finally, to my wife Jing, my beacon of light on the stormy sea of life, I say thank you most of all. Without you, I would be a pale shadow of the man I am today. Cheers to our success, in anything and everything; building our lives together has been, and continues to be, my greatest joy. J&J, forever.

ABSTRACT

FLEXIBLE TETHERS IN MULTI-CHROMOPHORIC SYSTEMS:
LINKING PHOTOPHYSICS WITH ASSEMBLY

SEPTEMBER 2014

JEFFREY MORGAN LUCAS, A.S., SCHENECTADY COUNTY COMMUNITY
COLLEGE

B.S., SIENA COLLEGE

PH.D., UNIVERSITY OF MASSACHUSETTS AMHERST

Directed by: Paul M. Lahti

Aggregation and folding events in conjugated polymers have a dramatic effect on the photophysics, and in turn, the efficiency of said species in organic electronic devices. The factors that lead to twisting, bending and folding in conjugated polymers have been studied in numerous polymeric materials, but due to the variability of these events, they remain poorly understood.

To probe the spectroscopic signatures of folding and to link them with conformational and morphological features formed by these species in the solid state, a series of alternating co-polymers were then synthesized, incorporating the 2- and 4-carbon tethers with oligo-phenylenevinylene derivatives. Static absorption, photoluminescence and TEM images of drop-cast films indicate that the length of the linker has a dramatic effect on the fluorescence and morphological behavior of segmented alternating copolymers. Given that the linker length also shows variations in resistance to thermal reorganization, incorporating flexible linkers into polymeric systems provides a method of tuning morphological features within polymeric thin films by changing the length of the flexible tether.

In a study to further test the folding capacity of aliphatic linkers, dyads of trimethoxystyrene-functionalized fluorenone linked by 2-, 4-, and 8-carbon flexible tethers were studied by static absorption spectroscopy and both static and time-resolved photoluminescence (TRPL) spectroscopy. The unique behavior of the 2-carbon tethered system is attributed to an ability to fold into a geometry that favors intramolecular excimer emission, while the other linkers possess too large a number of conformational degrees of freedom to favor folding events.

TABLE OF CONTENTS

LIST OF TABLES

LIST OF FIGURES

LIST OF SCHEMES

CHAPTER 1

GENERAL BACKGROUND AND GOALS OF RESEARCH

1.1 Overview

During the past century, folding and aggregation of molecules, polymers and oligomers has become an intense field of study due to their prospective use in numerous chemical and biological applications[1-4]. The photochemistry of aggregates of conjugated organic molecules and polymers has been of particular interest due to novel and promising test applications as biological sensors[5], fluorescent materials[6], photoresists[7], and organic electronics[8-11], all of which are emerging as robust fields for practical use.

A single conjugated chromophore or polymer chain has a set of reasonably well-defined photophysical characteristics and expected processes that it may undergo during photo-excitation and relaxation[12,13]. However, in solid-state applications such as organic electronic devices, individual molecules are in close contact or even surrounded by other molecules of the same species, as well as by other molecular or polymeric species that make up the other device components. This "close contact" chemical environmental can have a significant effect on the photophysical processes exhibited by photoactive species[14,15].

In a general case that is very important to this dissertation, two chromophores may interact after one is photo-excited to cause energy transfer to the unexcited chromophore, whether they are separate molecular systems, or chromophores within the same molecular or polymer chain. For example, Förster resonance energy transfer (FRET) comes from dipole-dipole coupling interactions between a singlet excited state chromophore and a singlet ground state chromophore, resulting in the relaxation of the

1

excited molecule, the donor (D), and the formation of an excited state in the other chromophore, the acceptor (A), without the exchange of a photon. This process can occur over extended distances (10-100 nm), without direct intermolecular contact between donor and acceptor. After FRET, the accepting species may fluoresce, or become a new donor in FRET[13,16].

One requirement for FRET to occur involves the overlap between the donor's emission spectrum and the acceptor's absorption spectrum. The emission and absorption spectra of a particular species represent the range of energy donation states (donor) and
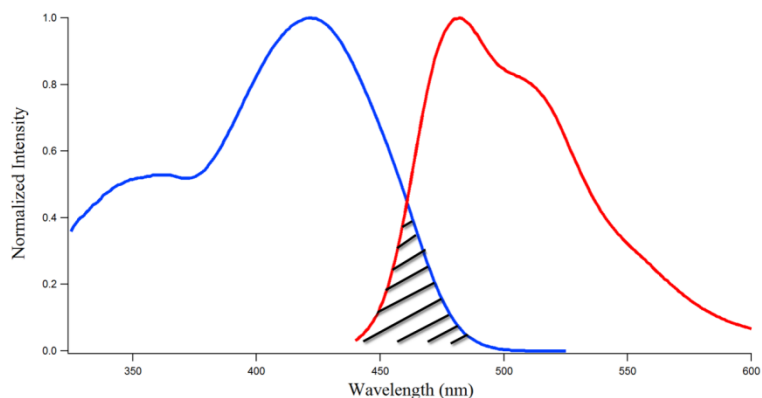
Figure 1.1: Figure depicting the spectral overlap (black shaded area) between a donor fluorescence spectrum (red) and an acceptor absorption spectrum (blue).

energy acceptance states (acceptor) for FRET. Overlap between the donor system emission spectrum and the acceptor absorption spectrum (Figure 1.1) can be considered analogous to string harmonics with two strings vibrating at constructive frequencies; if one musical note is an integer multiple of another, then the two tones will form a harmonic. The analogous dipolar overlap between donor and acceptor, which arises from spectral overlap, enables Förster energy transfer[16]. While the spectrum represents all molecular orientations in a sample, on an individual donor-acceptor pair basis the dipolar overlap depends strongly on relative orientation between the donor and acceptor

chromophores. This dissertation is, in part, concerned with limiting geometries and distances for interchromophore interactions.

Interchromophore interaction -- and, indeed, effective conjugation length of any individual chromophore -- is also influenced by structural and conformational defects in a nominally conjugated chain. The vast majority of conjugated polymers have conjugation defects that are intrinsic to the structural characteristics of the polymeric species (such as bond torsions and structural folding), as well as structural errors arising from limitations of the methods by which the polymers are synthesized[17-19]. Furthermore, some conjugation defects may arise from air oxidation if samples are exposed to oxygen during purification or thin film processing. This dissertation also probes effects of some specific structural and folding characteristics of members of fluorenone-containing conjugated chromophores, and of the poly(phenylenevinylene) family of chromophores.

The work in this dissertation was strongly impelled by work on one of the most-studied conjugated polymers, poly(p-phenylenevinylene) (PPV). PPV derivatives have been intensely studied, in part, due to their highly fluorescent behavior and efficacy in several different optoelectronic applications[20,21]. Most germane to this dissertation, although this class of conjugated polymer undergoes FRET in bulk solution and in the solid state[22], one of its most interesting behaviors is the ability of a single polymer chain to exhibit intrachain energy transfer in an environment where interchain communication does occur[23]. Considering that PPV derivatives have been reported to be sensitive to oxidative degradation[24], and have been shown to possess varying amounts of other conjugative defects that can arise from intrachain folding and aggregation, studies that

can identify any spectroscopic signatures of these situations can help identify previously reported variations in photophysical behavior exhibited by PPV derivatives.

This dissertation also addresses issues related to some specific structural and folding characteristics of members of fluorenone-containing conjugated chromophores, specifically, the propensity of fluorenone-based systems to form excimeric interactions, and how this tendency can be utilized as a molecular ruler to measure the through-space distance between conformationally accessible sites between in tethered, multi-chromophoric systems. Additionally, this work yielded implications that may serve to understand the expected emission profiles of asymmetrical excimer-forming chromophores.

1.2 General Goals of Research

As stated above, conjugation defects can greatly affect the photophysics and morphology of conjugated systems in ways both subtle and difficult to control. While a large amount of research has been aimed at fine-tuning the photophysics and morphology of conjugated systems through variations in *processing* conditions, my research utilized the installation of conjugation defects or variations in individual compounds in a controlled manner. Photophysical assays of the resulting compounds were used to find telltale spectroscopic signatures of folding and other chromophore assembly of conjugated chromophores. The resulting structure-property correlations offer guidelines to design materials with more stable and predictable optoelectronic properties and crystalline packing in conjugated polymers containing fluorenone and oligophenylenevinylene chromophores.

This dissertation work developed synthetic methods to installing controlled conjugation defects interruptions (as conjugation defects) in the form of aliphatic carbon

4

chains as part of segmented, alternating copolymers. Copolymer structural variation effects on photophysical behavior were characterized, and in some cases correlated with their morphological behavior. Chapter 2 outlines the synthesis and characterization of oligo(p-phenylenevinylene) (oPV) chromophores that were incorporated into segmented alternating copolymers with aliphatic carbon chains of different lengths to simulate defects in conjugation. These systems were photophysically characterized in solution and in thin films, and their transmission electron microscopy (TEM) provided some details their general morphology variations in films. In Chapter 3, the synthesis and characterization of a series of flexibly-linked fluorenone-based dyads is discussed, in which the length of the linking conjugation defect is varied from 2-8 carbons. This work showed how excimer formation between fluorenone pendants provides a probe for dyad folding of fluorenone-incorporating chains, and found the flexible chain length scale at which the folding of the installed defects is most prominent. Chapter 4 summarizes the synthesis of a new model septithiophene chromophore, results of investigating the chromophore's electronic spectral behavior, and gives recommendations for methods by which the septithiophene chromophore could be incorporated into segmented alternating polymers for tests of oligothiophene folding and self-assembly. Chapter 4 also describes the proposed synthesis and photophysical characterization of a series of fluorene-fluorenone dyads that have the potential to identify the origin of variations in fluorescence emission seen in partially oxidized samples of poly(fluorene). Finally, Chapter 5 describes in detail all experimental and synthetic methods that I applied or developed during completion of the above-mentioned projects.

1.3 References

(1)   Brunsveld, L.; Folmer, B. J. B.; Meijer, E. W.; Sijbesma, R. P. Supramolecular Polymers. *Chemical Reviews* **2001**, *101*, 4071-4098.

(2)   Huser, T.; Yan, M.; Rotherberg, L. J. Single chain spectroscopy of conformational dependence of conjugated polymer photophysics. *Proceedings of the National Academy of Sciences* **2000**, *97*, 11187-11191.

(3)   Tretiak, S.; Mukamel, S. Density Matrix Analysis and Simulation of Electronic Excitations in Conjugated and Aggregated Molecules. *Chemical Reviews* **2002**, *102*, 3171-3212.

(4)   Stefani, M. Protein misfolding and aggregation: new examples in medicine and biology of the dark side of the protein world. *Biochimica et Biophysica Acta (BBA) - Molecular Basis of Disease* **2004**, *1739*, 5-25.

(5)   Turner, A. P. F. Biosensors: Sense and sensibility. *Chemical Society Reviews* **2013**, *42*, 3175-3648.

(6)   Basabe-Desmonts, L.; Reinhoudt, D. N.; Crego-Calama, M. Design of fluorescent materials for chemical sensing. *Chemical Society Reviews* **2007**, *36*, 993-1017.

(7)   Ichimura, K. Preparation of water-soluble photoresist derived from poly(vinyl alcohol). *Journal of Polymer Science: Polymer Chemistry Edition* **1982**, *20*, 1411-1417.

(8)   Höfle, S.; Pfaff, M.; Do, H.; Bernhard, C.; Gerthsen, D.; Lemmer, U.; Colsmann, A. Suppressing molecular aggregation in solution processed small molecule organic light emitting diodes. *Organic Electronics* **2014**, *15*, 337-341.

(9)   Chen, Z.; Cai, P.; Chen, J.; Liu, X.; Zhang, L.; Lan, L.; Peng, J.; Ma, Y.; Cao, Y. Low Band-Gap Conjugated Polymers with Strong Interchain Aggregation and Very High Hole Mobility Towards Highly Efficient Thick-Film Polymer Solar Cells. *Advanced Materials* **2014**, *26*, 2586-2591.

(10)   Hadjichristidis, N.; Hirao, A.; Tezuka, Y.; Du Prez, F.: *Complex Macromolecular Architectures: Synthesis, Characterization, and Self-Assembly*; Wiley, 2011.

(11)   Spencer, S. D.; Bougher, C.; Heaphy, P. J.; Murcia, V. M.; Gallivan, C. P.; Monfette, A.; Andersen, J. D.; Cody, J. A.; Conrad, B. R.; Collison, C. J. The effect of controllable thin film crystal growth on the aggregation of a novel high panchromaticity squaraine viable for organic solar cells. *Solar Energy Materials and Solar Cells* **2013**, *112*, 202-208.

(12)   Anslyn, E. V.; Dougherty, D. A.: *Modern Physical Organic Chemistry*; University Science Books: Sausalito, California, 2006.

(13)   Lowry, T. H.; Richardson, K. S.: *Mechanism and Theory in Organic Chemistry*; Harper and Row Publishers: New York, 1987.

(14)   Brunetti, F. G.; Kumar, R.; Wudl, F. Organic electronics from perylene to organic photovoltaics: painting a brief history with a broad brush. *Journal of Materials Chemistry* **2010**, *20*, 2934-2948.

(15)   Günes, S.; Neugebauer, H.; Sariciftci, N. S. Conjugated Polymer-Based Organic Solar Cells. *Chemical Reviews* **2007**, *107*, 1324-1338.

(16)   Lakowicz, J. R.: *Principles of Fluorescence Spectroscopy*; Springer, 2007.

(17)   Clafton, S. N.; Beattie, D. A.; Mierczynska-Vasilev, A.; Acres, R. G.; Morgan, A. C.; Kee, T. W. Chemical Defects in the Highly Fluorescent Conjugated Polymer Dots. *Langmuir* **2010**, *26*, 17785-17789.

(18)   Strobl, G. R.: *The Physics of Polymers: Concepts for Understanding Their Structures and Behavior*; Springer, 2007.

(19)   Baughman, R. H.; Chance, R. R. Point defects in fully conjugated polymers. *Journal of Applied Physics* **1976**, *47*, 4295-4300.

(20)   Heun, S.; Mahrt, R. F.; Greiner, A.; Lemmer, U.; Bassler, H.; Halliday, D. A.; Bradley, D. D. C.; Burn, P. L.; Holmes, A. B. Conformational effects in poly(p-phenylene vinylene)s revealed by low-temperature site-selective fluorescence. *Journal of Physics: Condensed Matter* **1993**, *5*, 247-260.

(21)   Junkers, T.; Vandenbergh, J.; Adriaensens, P.; Lutsen, L.; Vanderzande, D. Synthesis of poly(p-phenylene vinylene) materials via the precursor routes. *Polymer Chemistry* **2012**, *3*, 275-285.

(22)   Saini, S.; Bagchi, B. Photophysics of conjugated polymers: interplay between Förster energy migration and defect concentration in shaping a photochemical funnel in PPV. *Physical Chemistry Chemical Physics* **2010**, *12*, 7427-7433.

(23)   Yu, Z.; Barbara, P. F. Low-Temperature Single-Molecule Spectroscopy of MEH-PPV Conjugated Polymer Molecules. *The Journal of Physical Chemistry B* **2004**, *108*, 11321-11326.

(24)   Bianchi, R. F.; Balogh, D. T.; Gonçalves, D.; Faria, R. M.; Irene, E. A. Photo-oxidation Phenomenon of MH-PPV Films Studied by Ellipsometry and Infrared Spectroscopy. *Molecular Crystals and Liquid Crystals* **2002**, *374*, 457-462.

CHAPTER 2

MORPHOLOGICAL AND PHOTOPHYSICAL EFFECTS OF CONJUGATION-INTERRUPTING TETHERS IN OLIGO(P-PHENYLENEVINYLENE) COPOLYMERS

2.1 Overview

2.1.1 Introduction

This chapter describes the synthesis, solution-based optoelectronic properties, as well as thin-film steady-state and time-resolved photoluminescence, transmission electron microscopy and DFT geometry optimization computations of a series of oligo-p-phenylenevinylene copolymers and the corresponding monomeric chromophore. Probing and controlling the morphological characteristics of organic molecular and polymeric materials is critical for their use in electronic devices[1-7]. For example, contemporary organic photovoltaic active layer film morphologies are tuned at meso- and nano-scales by solution processing and thermal annealing of active layer constituents, where the morphology of the active layer is often determined by the kinetics of phase separation and domain crystallization[8,9]. The resultant morphology is often at least partly disordered, containing crystalline domains separated by amorphous regions, the size-scales of which often require carefully controlled conditions to reproduce[10,11].

Organic conjugated polymers are typically very rigid, but these rigid-rod chromophores can bend at structural defects[12,13], as stated in Chapter 1. This can hinder crystallization in some cases, but bending and folding can lead to intrachain pi-stacks in other cases. Such defects can also lead to a range of effective conjugation lengths in long chromophores that nominally are pure with just one structure. This in turn affects absorption and luminescence behavior, often giving a broadened range of behavior. One strategy to retain chromophoric purity, enhance processibility, and avoid changes in

luminescence behavior by encouraging *amorphous* solid state film formation -- without

π-chain stacking and its attendant photophysical effects -- is to employ segmented

alternating block copolymers in place of homo-polymeric species[14-18].
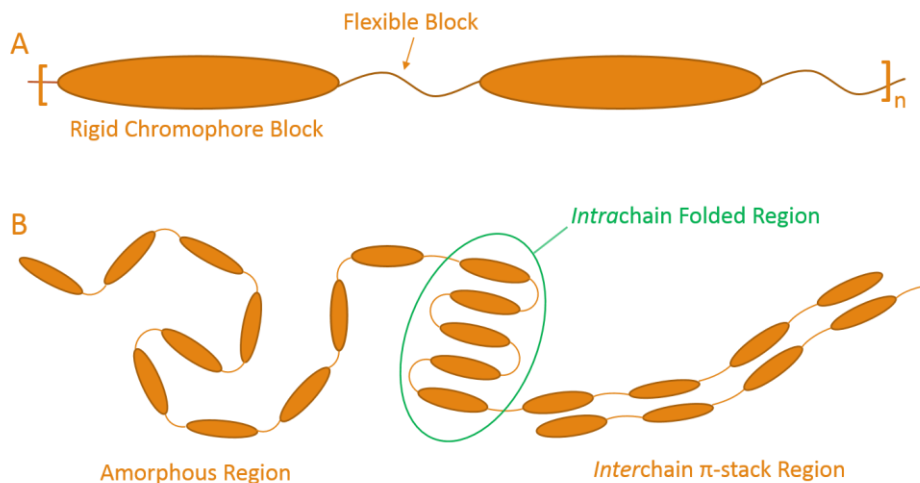
Figure 2.1: Schematic of (A) a segmented alternating copolymer, and (B) generalized examples of segmented chromophore environments in the solid state.
The non-conjugated flexible linkers that connect the chromophoric units are meant to

provide enough flexibility to allow easy processing during film casting. However, there

remains the possibility that rigid chromophore segments of the copolymer may fold to

give intrachain chromophore-stacked regions like a carpenter's rule (Figure 2.1).

2.1.2 Exemplifying the Effects of Folding and Aggregation in Conjugated Systems: Poly(p-phenylenevinylene)

The work in this dissertation was strongly impelled by work on one of the most-

studied conjugated polymers, poly(p-phenylenevinylene) (PPV). PPV derivatives have

been intensely studied, in part, due to their highly fluorescent behavior and efficacy in

several different optoelectronic applications[19,20]. Most germane to the present work,

although this class of conjugated polymer undergoes FRET in bulk solution and in the

solid state[21], one of its most interesting phenomena is the ability of a single polymer

chain to exhibit intrachain energy transfer in an environment where inter-chain communication does occur[22]. In a 2004 study by Yu and coworkers[22] and a subsequent study by Barbara and coworkers in 2006[23], the normally broad emission spectrum obtained from bulk solution and solid state samples of MEH-PPV was probed by single-molecule spectroscopy (SMS) conducted over 20-300 K. These studies found a bimodal distribution of both blue-fluorescent and red-shifted emitting sites in poly[2-methoxy-5-(2-ethylhexyloxy)-1,4-phenylenevinylene] (MEH-PPV). At low temperatures (~20 K), the blue-emitting chromophores that emit with high intensity at room temperature are fewer in number, and are superseded by the red-shifted (~20 nm) fluorescent process. This effect was attributed to an increase in chromophore-chromophore FRET, and it was hypothesized that the conformational structure of the polymer chain played a role in the emission wavelength at individual sites[22].

The morphological hypothesis put forth by the Barbara group proposed that although PPV is a rigid-rod chomophore, it has the ability to deviate from a rigid conformation in the solid state by forming twists and folds in the polymeric backbone, which gives rise to the above-mentioned variations in photophysics. This is consistent with observations published a separate study by Summers and Buratto[24], in which PPV was shown to form thin films that contain a variety of nanostructures, including "sheet-like" regions and "ribbon-like" regions. These regions were also reported to differ in their fluorescence spectra, with different morphological features giving variations in spectral curvature, and with the sheet-like regions giving emission that is significantly blue-shifted in comparison to the ribbon-like features[24].

With the precise origin of the variations in MEH-PPV solid state emission spectra still unclear, Barbara's morphological the hypothesis was further examined by Barbara and coworkers[25], who published a study examining changes in the emission spectrum of MEH-PPV as a function of thin-film processing conditions. Slight variations in emission wavelength akin to those seen in the temperature-dependent SMS studies were seen for MEH-PPV blended dilutely into poly(methyl-methacrylate) (PMMA) films. The spectral shape (emission energy distribution) was found to be dependent on the processing procedure used to fabricate the thin films. Films that were quickly covered by borosilicate glass cover slips after deposition of the PMMA solution favored red-shifted emission, while thin films that were left uncovered to dry more slowly favored blue emission. The authors presumed that the changes in morphology were correlated with different conformations, and that polymer chain conformation may influence the emission spectrum of MEH-PPV, since polymer chains in the samples left to dry slowly have the opportunity to organize while solidifying, while covering the film before drying might restrict reorganization to produce a kinetically-trapped morphology[25]. In the same study by Barbara's group[25], samples that were allowed to dry under a nitrogen atmosphere were shown to produce more stable emission intensity as a function of sample standing time, in comparison to samples that were allowed to air dry, which produced unstable emission that tended to "blink" and "flicker"[25]. It was proposed that during the air drying process, MEH-PPV was reacting with oxygen to produce small amounts of photoluminescent impurities that gave rise to the blue spectral emission. In a separate study from Bazan and Buratto's groups[26], various amounts of fluorescent site blinking was observed in SMS of oligo(p-pheynylenevinylene) (oPV) isolated in three non-emitting polymer matrices of

11

varying dielectric and viscoelastic properties. Contrary to the proposals from the study by

Barbara[25], Buratto postulated that the variations in single molecule emission stability

arise from disparities in torsional strain on the polymeric backbone and differences in

freedom of movement imparted by the local matrix environment. However, although the

SMS experiments published by Buratto were conducted in a specially-designed chamber

filled with nitrogen gas to eliminate oxidation during data collection, the polymer

matrices were allowed to dry in the open air during thin film fabrication, and considering

the study done by Barbara's group, varying amounts of fluorescent impurities brought

about by photo-oxidation could have been produced during this time.

The above-mentioned studies by the Barbara and Burrato groups both noted that it

is possible for PPV derivatives to undergo varying amounts of twisting, folding and

aggregation, and although the two groups have debated the origins of these structural

variations, it is clear that such variations in polymer structure can have strong effects on

both emission stability and spectral curvature. However, considering that PPV derivatives

are quite sensitive to oxidative degradation[27], and have been shown to possess varying

amounts of other conjugative defects intrinsic to the polymeric structure, studies that can

identify spectroscopic signatures of folding or aggregation due to specific defects may

identify the source of the above-mentioned variations in photophysical behavior.

2.1.3 Concerning the Role of Different Types of Conjugation Defects in Affecting Photophysical Properties of Polymeric Systems

The vast majority of conjugated polymers have conjugation defects that are

intrinsic to individual polymeric species, and to the methods by which the polymers are

synthesized[28-30]. Furthermore, some conjugation defects may arise from degradative

processes, such as air oxidation if the samples are exposed to oxygen during purification or thin film processing[27].

Structural defects in individual polymer chains that arise from the mechanisms of specific polymer synthesis can also cause irregularities in *aggregate* structures. For instance, different methods of making PPV can produce different amounts of cis- and trans-double bond linkages (Figure 2.2) that influence the bulk polymer properties[31,32]. While all-trans PPV forms crystalline phases in thin films[33,34], the presence of cis-defects can cause unpredictable, amorphous irregularities in the crystalline morphology, which has been associated with localization of excitons within a single polymer chain[35-37]. Although methods have been devised to produce *nearly* all-trans PPV[38], full elimination of the remaining small amounts of synthetic cis-defects in these polymers remains a problem unsolved.

All Trans   Cis Defect
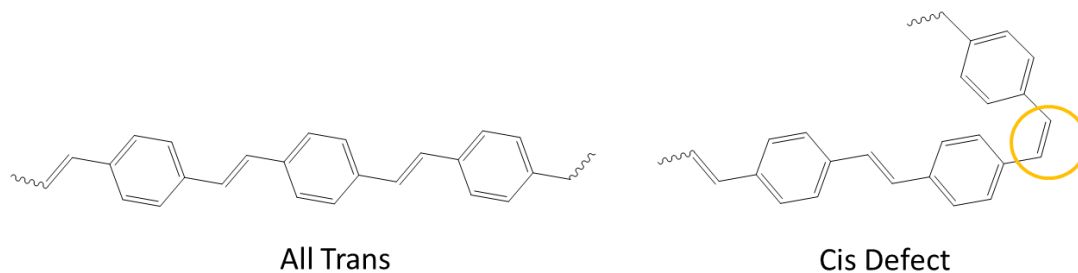
Figure 2.2: All-trans PPV and PPV with a cis-defect.

Despite efforts to reduce such structural defects, irregularities in polymer chain conformation are often simply intrinsic to polymeric structure, while others can arise during polymer purification and thin film processing. As shown in Figure 2.3, slight twists in a PPV polymer backbone stemming from steric effects between neighboring

aromatic rings can interrupt the continuity of the π-conjugated backbone in polymers[39,40].

**Twist in Polymeric
Structure**
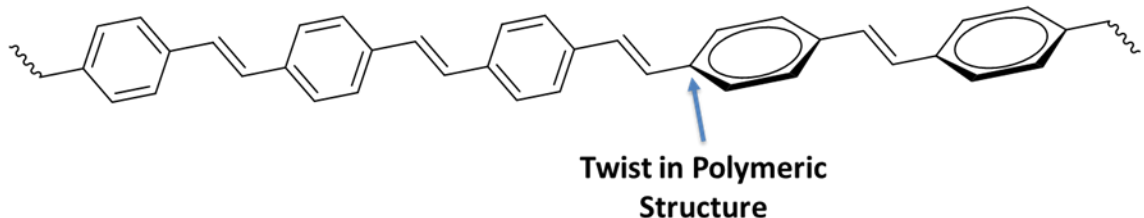
Figure 2.3: Schematic illustrating twisting of the polymeric backbone in poly(p-phenylenevinylene).

The average distance between such torsional defects influences a polymer chain's effective conjugation length, and will vary from polymer to polymer and even between individual chains of the same polymer. Indeed, conformational conjugation-interrupting defects can clearly occur even in polymers that are completely devoid of synthetic

Figure 2.4: Typical conformations of a 100-segment PPV homopolymer generated by Monte Carlo simulations. See Hu et al[41] (permission license number 3401051508068).

defects. Conjugation defects[41-43] through degradation were important in the aforementioned studies by the Barbara group[22,23,25]. While the actual chemical structures of these defects are not fully understood, studies have shown that MEH-PPV and other PPV derivatives can react with oxygen in solution, converting a small number of sp^2 vinylene carbons to sp^3 carbons through a radical mechanism initiated by ultraviolet light[41]. The presence of these defects allows the polymer chains to undergo a conformational conversion from a straight, rod-type polymer to a folded, coil-type polymer during thin film fabrication[42,43]. In a study by Hu and coworkers, the number of sp^3 carbons that interrupt the length of conjugation in a PPV chain was varied in Monte Carlo computational studies, and had a great effect on the computed structure[43]. For example, the equilibrium structure of the defect-free homopolymer of 100 repeat units was calculated to be highly extended, while inclusion of a 5% defect density produced a polymer in a somewhat extended "defect-coil" conformation, in which the polymer defects can be seen as "kinks" in the polymer chain (Figure 2.4, V). However, when intersegment interactions were added to the calculation, the "defect-coil" conformation easily collapsed into a folded "defect-cylinder" conformation with a low energy barrier to rearrangement[43].

The computational study by Hu and coworkers provides permissive evidence that defects within a polymer chain can cause folding events that allow through-space, intrachain chromophore interactions. This hypothesis may provide an explanation for photophysical variations seen in MEH-PPV, and experimental work that attempts to model such folding events and correlate them with photophysical processes may shed

light on the sometimes puzzling photophysical behavior seen in PPV derivatives and similar polymeric species.

2.1.4 Segmented Alternating Copolymers Composed of PPV chromophores and Aliphatic Tethers

A substantial body of research utilizes non-conjugated tethers that link oligo-phenylenevinylene chromophores together in segmented alternating copolymers. Although some of these studies were not conducted for the purpose of probing defect-induced polymeric folding, information that is relevant to my dissertation can still be extracted from the work. For example, Karasz and coworkers[44,45] studied 2.5- and 3.5-oligophenylenevinylene type segmented copolymers as blue and green OLED emitters (Figure 2.5A). They used systems with structure PV2.5Fn, where 2.5 is the degree of phenylenevinylene (PV) oligomerization, F stands for the flexible linker unit (termed "flexor" in some parts of this dissertation), and n is the number of atoms linking the PV units. Systems having n = 4, 6, 8, and 10 were studied, and some systems showed variability in their solid state emission spectral maxima over 565-580 nm, depending on OLED fabrication conditions. The Karasz group's work indicated these segmented copolymers to be amorphous in x-ray diffraction studies, despite the variable solid state spectral results with processing. In a more recent study, Plunkett and coworkers[46] compared the solution and solid film electronic spectral behaviors of oPV chromophores to those of corresponding segmented copolymers connected by flexible linkers as shown in structures PV2.5OE5, PV4.5OE5, PV5.5OE5, PV2.5OEO5, PV4.5OEO5, PV5.5OEO5 (OE for oligoethylene type linkage, OEO for oligoethyleneoxide type linkage). These copolymers (Figure 2.5B) have quite long chromophores up to a 5.5-degree of oligomerization, that might be inclined to π-stack, save for the stack-hindering, large,
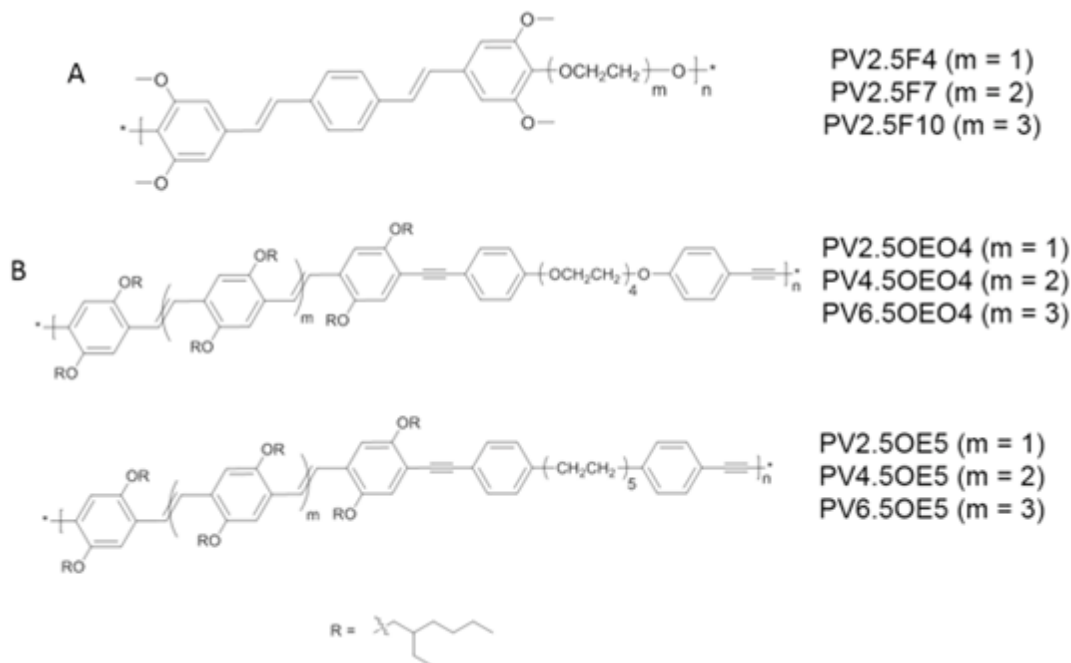
Figure 2.5: Chemical structures of oligophenylenevinylene segmented alternating copolymers studied by (A) Karasz et al[45], and (B) Plunkett et al.[46]

branched ethylhexyloxy pendant groups attacked to each phenylene group of the oligo-PV unit. The flexible linker units are likewise quite long at up to 15-atoms in length, allowing substantial freedom of motion by the chromophores in a single chain, at least in principle. The solution phase behaviors of the systems were very similar to one another, with both absorption and emission spectra for all of the polymers being very similar to those of the control oligo-PV monomers. But, in the solid film studies, they found evidence that the longer oligo-PV systems experienced some degree of electronic coupling between chromophores, which was evidenced by the low energy vibronic features seen in the thin film emission spectrum for PV5.5OEO4 (Figure 2.6). Since this feature seen in the PV5.5OEO4 thin film emission spectrum was absent in PV5.5OE5, Plunkett and coworkers concluded that the oligoethyleneoxide-linked systems had more folded regions with interactions between chromophores than did the oligoethylene-linked systems.
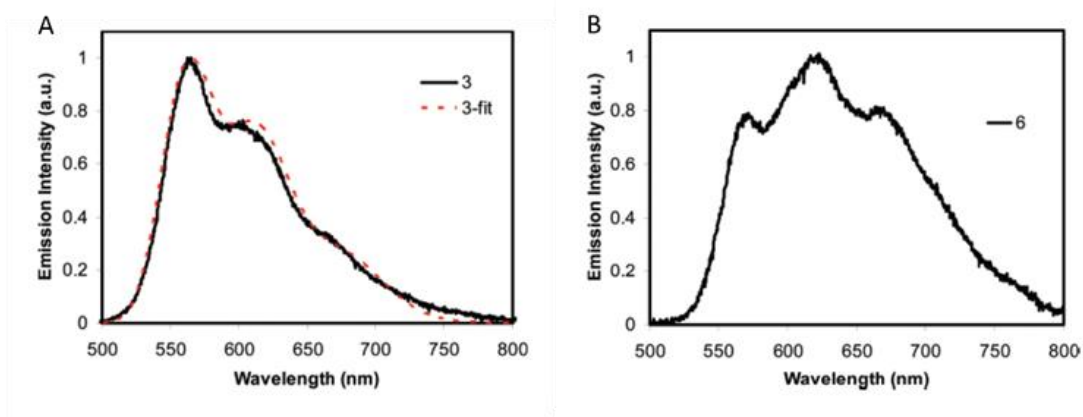
Figure 2.6: Thin film emission spectra of PV5.5OE5 (A) and PV5.5OEO4 (B). Adapted with permission from Plunkett et al[46], Macromolecules 2012, 45, 5051. Copyright 2012 American Chemical Society.

The long flexible linkers in Plunkett's studies allow for folding and (apparently some) assembly of elongated linear chromophores, but the hindering pendant side chain, branched substituents used in that work should disrupt chromophore stacking to a major extent, whether inter-chain or intra-chain (folding). In contrast, my work was intended to gauge the effects upon photophysical behavior and possible chromophore aggregation of using *shorter* flexible linkers that act more like a simple pivot -- or like a simple defect in a nominally fully conjugated linear polymer chain. These systems can be considered
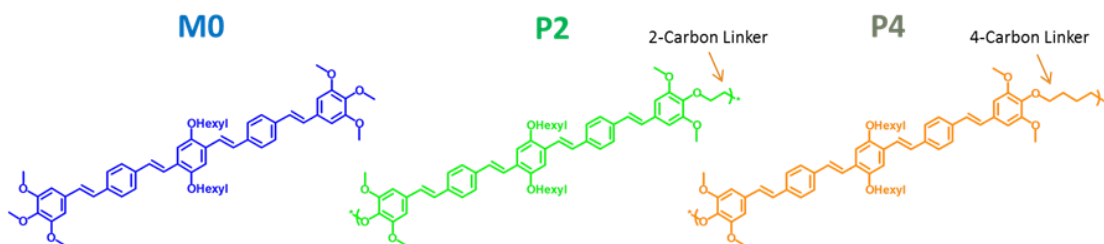
Figure 2.7: Chemical structures of M0, P2 and P4, indicating the variations in flexible tether length.

reasonable analogues of PPVs having conjugation-interrupting sp^3-defects, with varying but controlled flexibility of the defects. Shorter linkers with more limited degrees of conformational freedom should increase interchromophore contacts in the copolymer

18

solids, because a higher percentage of the possible conformer space should fold

chromophores into proximity in an intrachain fashion. This chapter describes the

synthesis, static and time-resolved photophysical characterization, and tunneling electron

microscopic (TEM) morphological study of copolymeric 4.5-oPV chromophores linked

by flexible 1,2-ethandiol and 1,2-butandiol units, shown in Figure 2.7 as P2 and P4,

respectively. The corresponding monomeric chromophore M0 was also synthesized for

comparison to the block copolymers. Joelle Labastide of the Barnes group carried out

time-resolved photophysical characterizations for this study, and Dr. Lang Wei of the

Lahti group carried out TEM and electron diffraction (ED) characterization.

2.2 Results and Discussion

2.2.1 Molecular Design
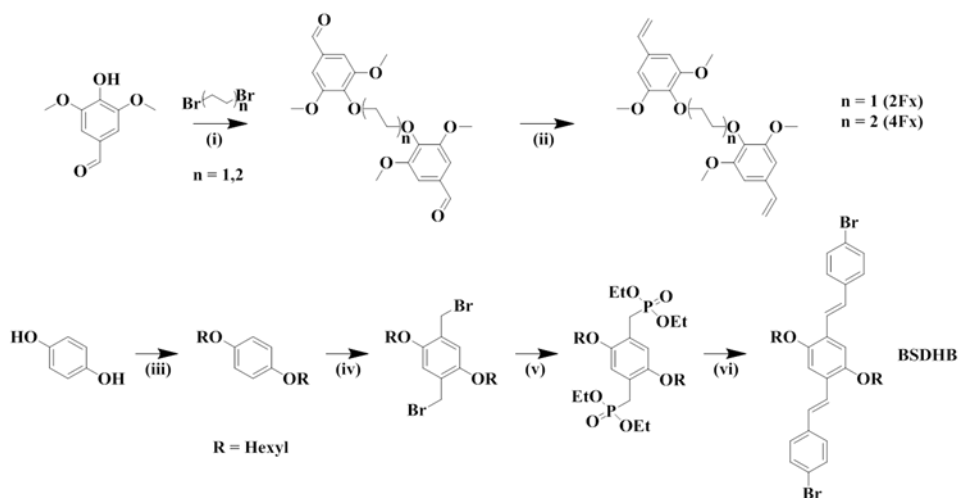
Scheme 2.1: Synthetic routes to monomers 2Fx, 4Fx and BSDHB.

Scheme 2.1 outlines the syntheses of the monomeric units used to make M0 and

the corresponding, conjugated-nonconjugated block copolymers P2 and P4. The flexible

linker units were synthesized by linking two syringaldehyde groups with the appropriate

1,n-dibromoalkane ($n = 2, 4$) by base-promoted Williamson etherification, followed by

Wittig vinylation of the terminal aldehyde groups to give 2Fx and 4Fx, respectively. A central oPV unit 1,4-bis(4-bromostyryl)-2,5-dihexyloxybenzene (BSDHB) was made with solubilizing pendant straight-chain hexyloxy side chains, starting by alkylating hydroquinone via a literature methodology[47] similar to that used in forming the flexible linked unit, but with an increased reaction time due to the reduced nucleophilicity of hydroquinone in comparison to syringaldehyde. The solubilizing pendant chains were used in this design, because initial work on a version of M0 without the side chains showed lower than desirable solubility in typical organic solvents to be used for solution photophysical tests and film formation. After 3 days of reaction time and recrystallization from ethanol, 1,4-dihexyloxybenzene was isolated as large, colorless platelets. After bromomethylating the alkylated species with paraformaldehyde and hydrobromic acid according to literature procedures[47], the bromomethyl groups were converted to phosphonate ester groups using microwave-assisted Arbuzov conditions with triethylphosphite. The microwave-assisted conditions simplified the synthesis by eliminating the need for a reaction solvent, and utilizing microwave irradiation in place of the typical thermal heating reduced reaction time to 20 min from a typical, conventional duration of 24 h. Removal of the excess triethyl via vacuum distillation yielded a colorless, highly viscous oil; several hours of applying vacuum to the oil gave 1,4-bis(diethylphosphonatomethyl)-2,5-dihexyloxybenzene as colorless, cubic crystals. This compound was then coupled with 4-bromobenzaldehyde by a microwave-assisted Horner-Wadsworth-Emmons (HWE) procedure using sodium hydride as the base to give 1,4-bis(4-bromostyryl)-2,5-dihexyloxybenzene. As with the Arbuzov reaction, utilizing microwave assisted conditions gave rapid product formation for the HWE reaction.

Coupling the use of a stronger base in comparison to the alkoxide reagents conventionally used for HWE olefination, and the ability to run the reaction at a temperature beyond the boiling point of the solvent in the pressurized microwave reaction vessel led to near-total conversion of the reactants into product after 5 min of reaction time, as opposed to the 24 h that I found to be needed using conventional, thermal heating reaction conditions. Additionally, no column chromatography was necessary for purification of 1,4-bis(4-bromostyryl)-2,5-dihexyloxybenzene; the resultant crude product required only an aqueous workup and recrystallization from ethanol to give material of high purity by ^{1}H NMR spectroscopy.
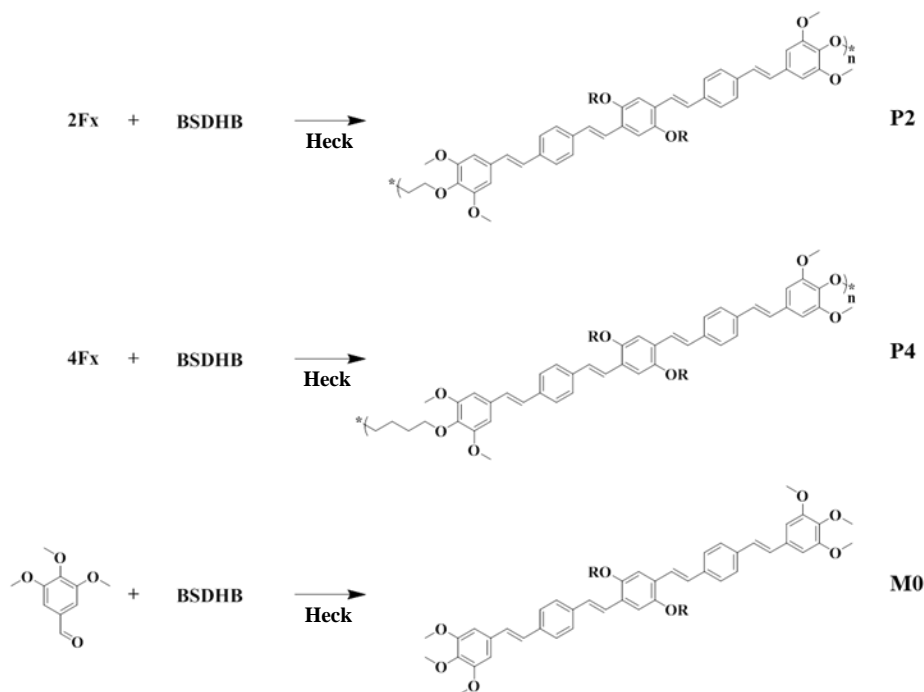
Scheme 2.1: Polymerizations and cross-coupling reaction to form P2, P4 and M0.

As shown in Scheme 2.2, 1,4-bis(4-bromostyryl)-2,5-dihexyloxybenzene was then coupled with 2FX and 4FX using a microwave-assisted, Heck-type polymerization to give polymers P2 and P4, respectively, having GPC molecular weights of $M_n = 3500$

21

(Đ = 2.65, degree of polymerization = 4-5) and $\bar{M}_n$ = 3000 (Đ = 1.33, degree of polymerization = 3-4), respectively. The Heck polymerizations for this synthetic route were adaptations of those developed in previously published literature, which reported couplings conducted using conventional heating techniques[48]. In my work, the reaction times were reduced from several days to two hours by using microwave irradiation. However, the reaction temperature was kept in a similar range as to that which was reported (~90 °C) to prevent the thermal decomposition of the solvent *N,N*-dimethylformamide. The polymers were purified by Soxhlet extraction with hexanes and then methanol, followed by dissolution of the remaining residue in chloroform and precipitation into cold methanol. Although these are not high polymers, they have the desired alternating block copolymeric structure needed to assess effects of controlled conjugation-interrupting flexible units. Their dispersity indices show the presence of longer chains in P2 and P4, with $\bar{M}_w$ corresponding to degrees of polymerization of 11-12 and 5-6, respectively.

For the final assembly of M0, a similar procedure was used as for the polymerizations[48], with a 2.2:1 ratio of trimethoxystyrene to 1,4-bis(4-bromostyryl)-2,5-dihexyloxybenzene to minimize mono-coupled product. To purify this reaction, column chromatography was necessary to separate the multiple components of the crude reaction mixture. Detailed synthetic procedures and characterization data for all intermediates can be found in Chapter 5.

2.2.2 Spectral Properties

Steady state solution phase UV-Vis absorption measurements for M0, P2, and P4 (Figure 2.8) all show strong, overlapping bands at about 350 and 418-425 nm with

lineshapes that are typical for oPVs. The similarity of the solution absorption and PL

spectra is consistent with expectation for $\pi \rightarrow \pi^*$ transitions in the same oPV

chromophore, with little or no perturbation from conformational twisting or from inter-

chromophore association.
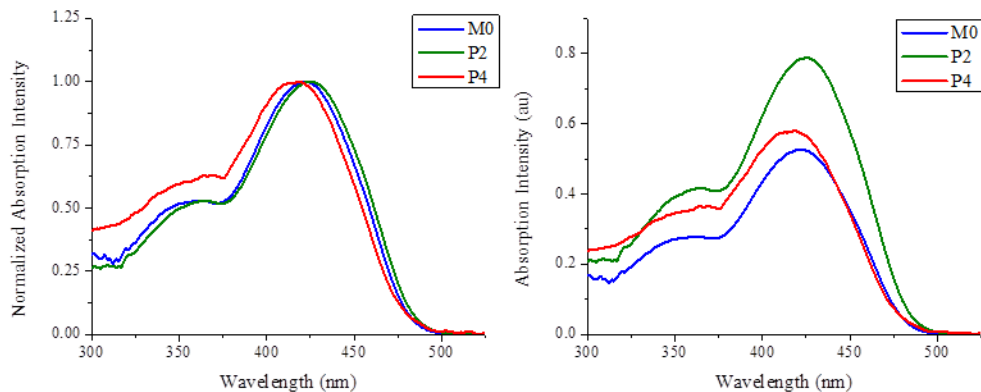
Figure 2.8: Steady state absorption of M0, P2 and P4 in chloroform (0.01 mM): (a) spectra normalized with respect to peak maxima, (b) spectra shown with absorptivity ordinate.

The alkoxy groups in all of the systems studied probably contribute to the small

UV-vis solvatochromic blue shifts (≤6 nm; see Table 2.1) seen when changing from

nonpolar toluene (PhMe) to polar acetonitrile (MeCN). Static photoluminescence (PL,

Table 2.1: Solution-phase absorption and photoluminescence maxima for M0, P2 and P4 in toluene (PhMe) chloroform (CHCl3) and acetonitrile (MeCN).

	ABS λ_{max}[nm] PhMe	ABS λ_{max}[nm] CHCl$_3$	ABS λ_{max}[nm] MeCN	PL λ_{max}[nm] PhMe	PL λ_{max}[nm] CHCl$_3$	PL λ_{max}[nm] MeCN
M0	424	422	418	485 (510)	482 (510)	484 (507)
P2	426	425	418	483 (514)	484 (514)	481 (510)
P4	418	415	414	480 (511)	482 (511)	480 (510)

Figure 2.9) spectra show the highest energy λ_{max} = 480-485 nm with minor variations in

the intensities of the next, lower energy vibronic transition at about 505 nm. The bands

are summarized in Table 2.1. The quantum yields for M0, P2, and P4 in chloroform
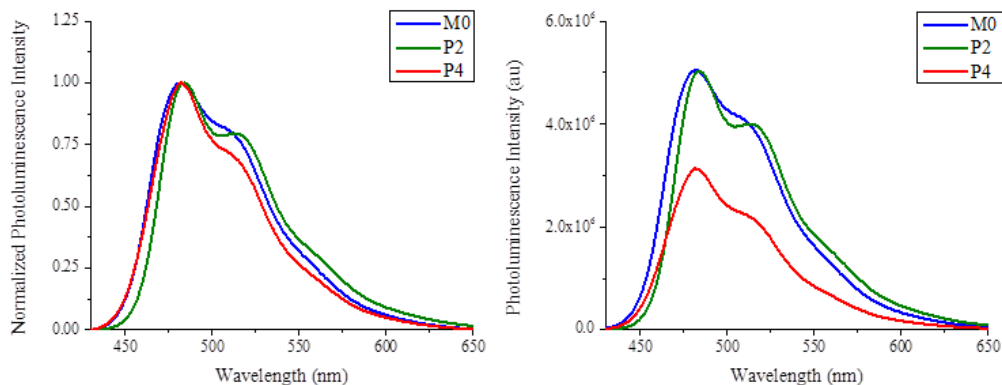
Figure 2.9: Solution-phase photoluminescence spectra of M0, P2 and P4 in chloroform (0.01 mM): (a) intensities normalized with respect to peak maxima, (b) absolute intensity spectra.

Uniquely in the cases that I studied, M0 in an acetonitrile solution analyzed

immediately after dissolution (without further treatment) shows its highest intensity at the

longer wavelength 505 nm band rather than the 480 nm band, but upon sonicating the

solution for several minutes, the typical spectra with maximum at 480 nm was obtained

(Figure 2.10).
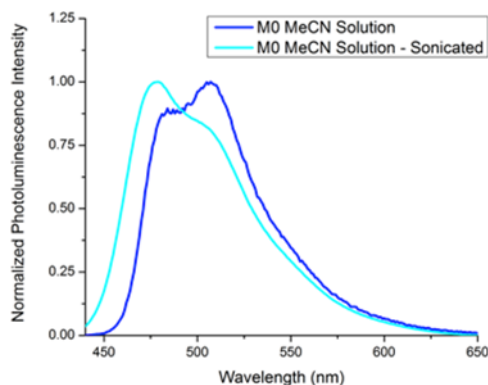
Figure 2.10: Normalized photoluminescence spectrum of 0.01 mM M0 in acetonitrile, both before (blue) and after (cyan) sonication.

Considering theoretical work done by the Spano research group[49,50] on aggregate emission in PPV derivatives, if oligophenylenevinylene chromophores form π-stacked aggregates (H-aggregates), the 0-0 fluorescent transition will be somewhat quenched, and the lower energy vibronic bands will increase in intensity. It is therefore possible that the high contribution of the 0-1 transition to the overall fluorescence profile seen in the acetonitrile solutions before sonication arises from emission from H-aggregates that either remained undissolved upon addition of the solvent, or were formed in solution. Furthermore, the change in spectral curvature post sonication was presumably due to a breaking up of aggregates during sonication.

Time-resolved photoluminescence lifetime studies in toluene (PhMe), chloroform (CHCl$_3$), and acetonitrile (MeCN) for 0.01 mM solutions of M0, P2, and P4 all show decay behavior fitting two major processes with $\tau_1 \approx 0.14$–0.55 ns and $\tau_2 \approx 1.1$–1.3 ns: even if a third decay function is included (Table 2.2), its contribution is negligible. The τ_2 process predominates under most conditions, and trends slightly slower and more predominant in more polar acetonitrile. In PhMe and CHCl$_3$, the fast τ_1 process contributes the most relatively to P2 PL decay (almost half), and the least to P4: in MeCN, all of the compounds have nearly the same decay lifetimes and relative contribution for both major processes. Taking into account that a multi-chromophoric relaxation process, possibly a cooperative aggregate relaxation, will have a faster decay constant than the decay constant for the relaxation of an isolated chromophore[51,52], τ_1 was assigned to the former type of process and τ_2 to the latter. Given the result for the non-sonicated MeCN sample of M0, the time-resolved results make it quite reasonable to postulate the presence of aggregates influencing photophysical behavior in other solvents.

Overall, the presence or absence of the nonconjugating linker to create a segmented

copolymer did not greatly vary the solution phase photophysical behaviors of the 4,5-

PPV chromophore in M0, P2, and P4 under the same conditions, except for the

significant decrease in steady state PL quantum yield in P4 relative to the others, from

over 50% to 44%.

Table 2.2. Solvent effects on solution TRPL decay time constants (τ) and
contribution to overall fluorescence decay curve (A) for M0, P2, and P4.

		τ_1 [ns] (A$_1$)	τ_2 [ns] / (A$_2$)	τ_3 [ns] / (A$_3$)
M0	PhMe	0.399 (0.327)	1.161 (0.671)	10.01 (0.002)
P2		0.641 (0.457)	1.279 (0.534)	8.432 (0.003)
P4		0.164 (0.150)	1.067 (0.838)	2.935 (0.012)
M0	CHCl$_3$	0.397 (0.195)	1.224 (0.798)	4.032 (0.006)
P2		0.200 (0.307)	1.332 (0.690)	8.375 (0.003)
P4		0.548 (0.159)	1.230 (0.816)	3.605 (0.025)
M0	MeCN	0.151 (0.140)	1.324 (0.859)	10.28 (0.010)
P2		0.141 (0.108)	1.298 (0.876)	4.204 (0.016)
P4		0.152 (0.110)	1.275 (0.877)	4.609 (0.013)

But, solid state behavior was much more influenced by nonconjugating linker

length. Steady state UV-vis spectra of thin films drop-cast from chloroform (Figure 2.11)

show absorption peaks at ~450 nm for all three systems.
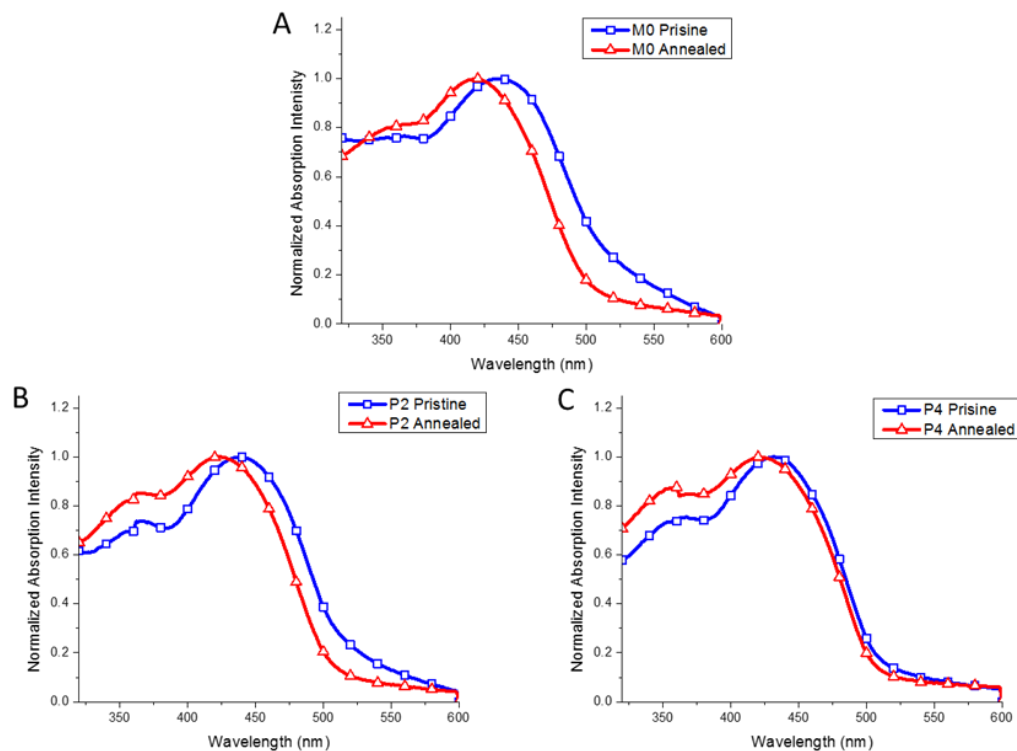
Figure 2.11: Normalized steady state absorption spectra of M0 (A), P2 (B) and P4 (C) pristine and annealed thin films dropcast from chloroform. Spectra were normalized with respect to peak maxima.

Similarly prepared samples exhibit featureless PL spectra with maxima at 550 nm and the same lineshapes for M0 and P2: however, PL is essentially *quenched* in pristine P4 films (Figure 2.12) under the same spectral acquisition conditions. Upon annealing at 120 °C for 5 min, the absorption maxima for *all* of the systems blue-shift, with the smallest effect for P4 (Figure 2.12). Under the same annealing conditions, the solid film PL intensity of P2 is reduced, but the PL intensity of M0 is virtually *quenched*. Film samples *and* bulk solid samples of P4 show very little PL before annealing, and none after. The low intensity of PL in films of P4, and strongly decreased PL intensity in annealed films of M0, is event evident to the naked eye, whereas P2 retains a visible blue-white luminescence post-annealing. ATR-IR spectroscopy shows no post-annealing formation of carbonyl bands to indicate oxidative cleavage of oPV units in any of M0,
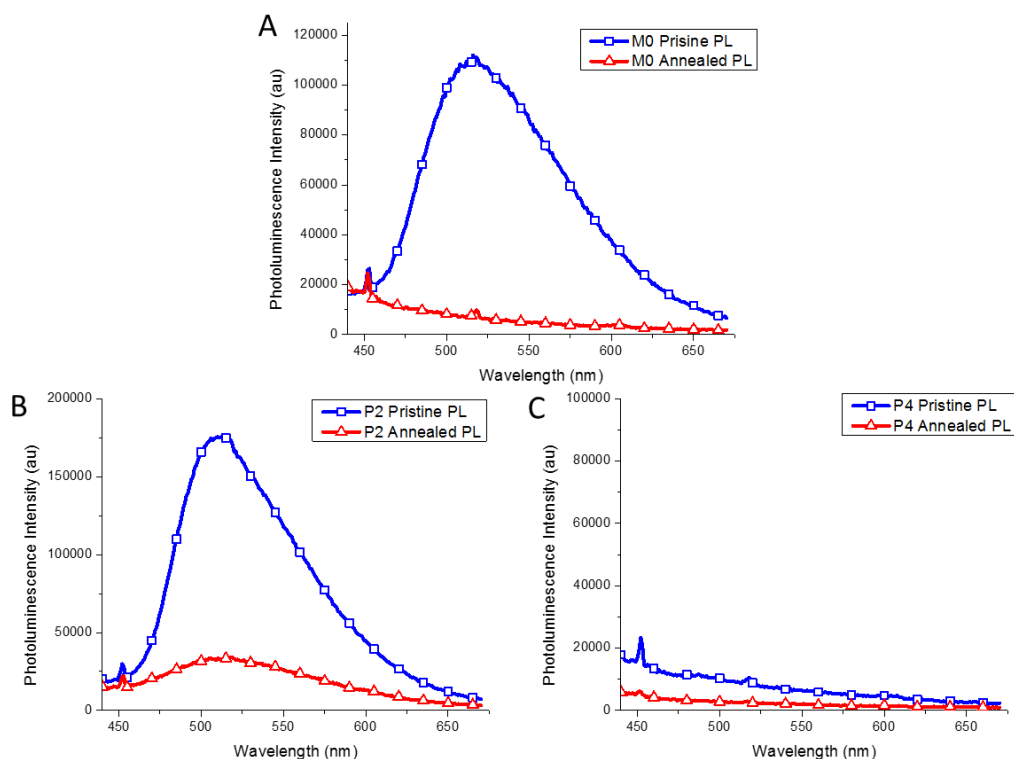
Figure 2.12: Steady state photoluminescence spectra of M0 (A), P2 (B) and P4 (C) pristine and annealed thin films dropcast from chloroform.

P2, and P4. The changes in absorption and (particularly) PL induced by annealing indicate chromophore movement from a kinetically trapped, pristine distribution of sites, to more thermodynamically favorable arrangements with different ensemble photophysical behavior.

TRPL lifetime decay measurements were conducted using the same drop-cast films used to obtain the static PL spectral measurements, both before and after thermal annealing. The same tri-exponential model used for the solution TRPL was used to analyze the film TRPL data. Again, the decay profiles are well-described by two decay components, with essentially negligible contribution from a third. As shown in Figure 2.13 and Table 2.3, M0 film PL decay is quite different from that in P2 and P4.

28
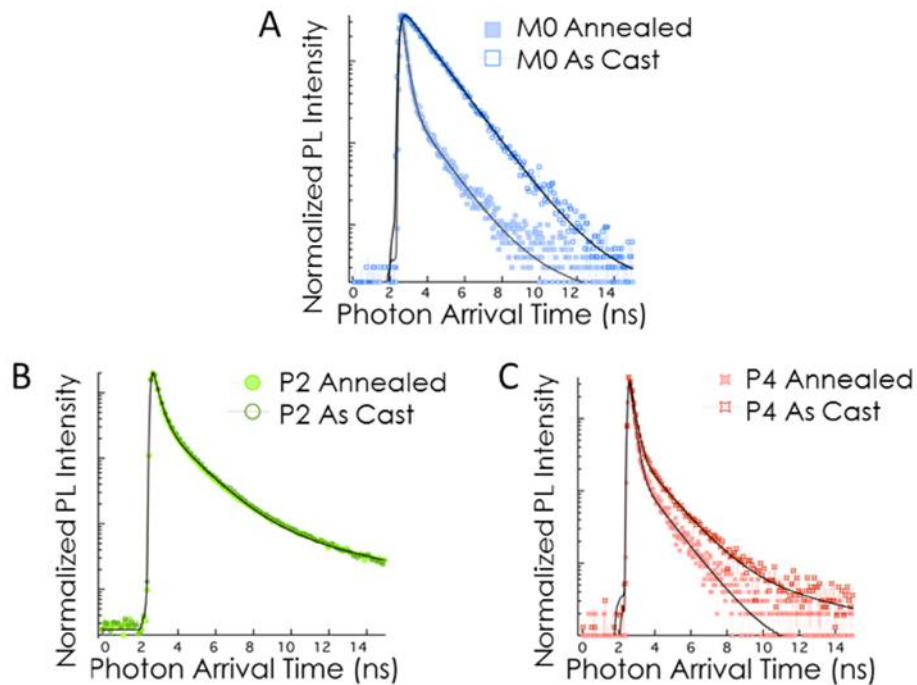
Figure 2.13: Normalized time-resolved photoluminescence spetra for M0 (A), P2 (B) and P4 (C), both before (dark colors) and after (light colors) annealing.

Table 2.3: TRPL decay constants (τ) and their relative contributions to the overall fluorescence decay (A) for dropcast films of M0, P2, and P4, pristine and annealed (120 °C for 5 min) drop-cast films.

		τ_1 [ns] / (A_1)	τ_2 [ns] / (A_2)	τ_3 [ns] / (A_3)
M0	pristine	nil	1.45 (0.999)	8.97 (0.001)
P2		0.31 (0.849)	1.50 (0.145)	7.09 (0.006)
P4		0.22 (0.935)	1.34 (0.064)	6.23 (0.001)
M0	annealed	0.22 (0.930)	1.33 (0.068)	6.51 (0.002)
P2		0.31 (0.848)	1.48 (0.146)	7.19 (0.006)
P4		0.21 (0.954)	1.35 (0.046)	nil

The pristine sample decay is essentially mono-exponential with $\tau_2 = 1.45$ ns, but post-annealing only 6.8% of this process remains; instead 93% of decay arises from a fast decay process with $\tau_1 = 0.22$ ns. The dramatic change indicates that the emitting chromophores undergo major changes in structure or (more likely) local environment. Since the slower of the two processes matches very closely with solution-phase oligophenylenevinylene chromophore lifetimes that have been previously reported[53-55], the 1.45 ns decay process was attributed to relaxation of excited state M0 chromophores in sites having little inter-chromophore interaction. The fast decay process was attributed to relaxation of π-stacked or otherwise closely-interacting chromophores. Here, as an exciton diffuses between interacting chromophores, each chromophore gives the opportunity for fluorescence relaxation, which in turn gives a higher overall probability of relaxation.

Pristine P2 exhibits essentially biexponential TRPL decay behavior, about 85% of which comes from fast decay with $\tau_1 = 0.31$ ns, with the rest coming from a $\tau_2 = 1.50$ ns process attributed to non-interacting chromophores by analogy to the M0 assignment. Interestingly, there is essentially *no change* in this decay behavior post-annealing. Whatever emitting sites are present in the quite weakly emitting, pristine P4 has similar qualitative behavior to P2, but more of the τ_1 fast decay process: annealing somewhat increases the τ_1 contribution.

As evidenced by the transition from τ_2 dominance to τ_1 dominance in M0 decay dynamics during thermal annealing, the emitting monomer sites must undergo drastic reorganization during annealing, while an analogous reorganization for the segmented alternating copolymers is much less evident. This evidence indicates that connecting

oligophenylenevinylene chromophores with aliphatic tethers disfavors chromophore reorganization, leading to more photophysically stable thin films in comparison to the monomeric species.

The assumption that τ_2 arises from isolated chromophore relaxation while τ_1 comes from a multi-chromophore relaxation process is reasonable, considering the conformational freedom of M0, P2 and P4. M0 has a substantial ability to reorganize in comparison to the segmented copolymers due to the absence motion-restricted connecting cross-chromophore tethers. Also, as argued by Barbara and coworkers[13], interchromophore attractions draw chromophores together to impart an overall stability to the system. So, it is not unreasonable to assume that M0 chromophores migrate during thermal annealing to form interchromophore interactions, thus giving rise to a dramatic increase in τ_1 after annealing. Later discussion, below, will show that the pendant side-chain substituents in M0 probably even favor cofacial chromophore organization. However, the chromophores in P2 and P4 are motion-restricted, and -- as evidenced by the large contribution of τ_1 seen in both samples before annealing -- the two systems form interchromophore interactions during *initial* film casting. This effect is more prominent for P4, given the higher contribution of the pre-annealing τ_1 process in comparison to P2. While it is evident that the tethers in P2 and P4 *do* restrict chromophore migration in comparison to the monomer, the finding that the $\tau 1$ contribution for P4 is increased while P2 decay dynamics remain constant shows that some chromophore reorganization can occur in P4, but little or none in P2. At least one contributor to this behavior will be given at the end of the chapter, by computations showing that intrachain folding in P2 seems disfavored, while P4 folding to put chromophores in contact appears straightforward.

2.2.3 Transmission Electron Microscopy

The length of a linker -- or lack of one -- has a major effect on solid state

photophysics of the segmented copolymer chromophores used in this study, which

presumably arises (at least in part) from morphological differences among M0, P2, and

P4 in the solid phase. In an effort to probe these differences, the pre- and post-annealed

films were examined by TEM (Figure 2.14). Pristine M0 films show a number of striated

domain regions that electron diffraction (ED) rings indicate to be single crystalline or

nearly so, since they produce well-defined patterns of electron diffraction (ED) spots,

rather than the rings seen in thicker regions of the film (Figure 2.14). After annealing,
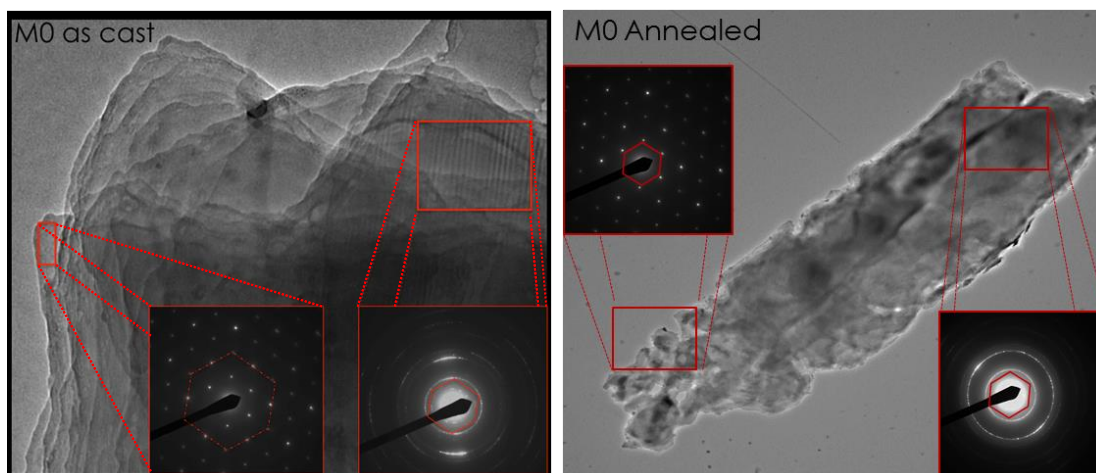
Figure 2.14: TEM micrographs of M0 prisine (left) and annealed (right) thin films. Areas outlined in red indicate the areas from where the corresponding electron diffractogram was measured.

M0 samples exhibit a decreased number of ED rings, and the ED patterns of the single-

crystalline regions are simplified, with fewer diffraction spots and a change from

irregular to isotropic spot shapes.

The TEM micrographs show that pristine P4 forms also forms sheet-like layers;

however, the micrographs do not show the well-defined grain boundaries and analogous

striated regions as seen in pristine M0. The samples show multiple ED rings, indicating significant crystallinity with some orientation. After annealing, the ED rings show a few individual ED spots indicating the presence of crystalline domains that can be seen in the micrographs as isolated, irregularly striated, pill-shaped crystallites.
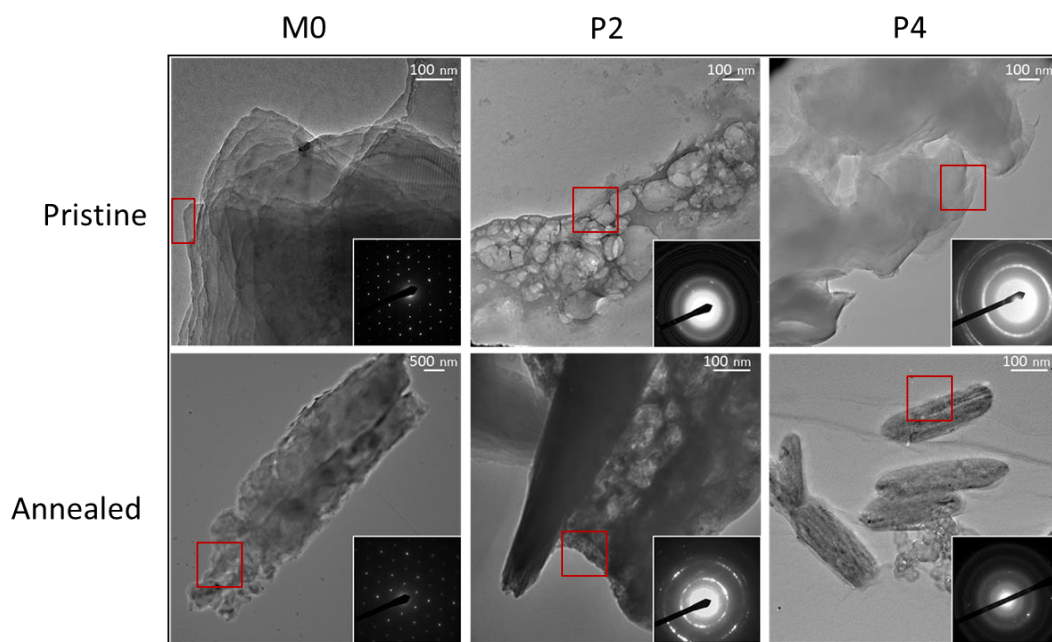
Figure 2.15: Transmission electron micrographs of M0, P2 and P4 drop-cast films. Areas outlined in red gave the electron diffractograms shown.

To correlate the solid film static and time-resolved PL results with the TEM results, it is important to remember that the PL results provide insight regarding only *emitting* sites in the solid films, while TEM shows overall, heterogeneous regions of film. M0 has many highly crystalline domains on a mesoscale before annealing, and also shows relatively good film PL when pristine. The simplification of the M0 ED pattern after annealing coupled with a near-complete quenching of the bulk PL and the increased participation of the fast decay process (τ_1) suggest that a repeat chromophore-chromophore spacing that results in stacking of the M0 π-systems became more common

in the M0 film post annealing. The striking similarities between the M0 and P4 micrographs and qualitative presence of crystallinity seen in their ED patterns suggests that the individual chromophores in P4 may be associating in a similar manner as M0 chromophores. The quenched PL of the M0 annealed film and of both P4 pristine and annealed films, coupled with the similarities in decay dynamics of these three films, further supports a similarity of chromophore association in M0 and P4. Given P2's lack of reorganization during thermal annealing, as evidenced by incomplete quenching and stable decay dynamics, the amorphous "foam-like" structures and broad diffraction rings seen in P2 films both before and after annealing may be representative of kinetically-trapped mesostructures, within which the 2-carbon tethers are not only restricting chromophore reorganization, but are also disfavoring the formation of highly crystalline domains.

However, this set of spectral and microscopic data fails to explain the lack of fluorescence intensity emitted from the P4 film prior to annealing, considering its similarities with M0 as shown in the TEM micrographs. In order to further probe any existing differences between these systems that are not visually evident, an analysis of d-spacing values extracted from the ED patterns was conducted.

2.2.4 Electron Diffraction D-Spacing Analysis

The calculated π-stack d-spacings obtained from the drop-cast films are given in Table 3.4. The crystalline structures sampled in the pristine M0 film exhibit a 5 Å d-spacing, which decreases to 4.8 angstroms after annealing.

This 0.2 Å decrease occurs as the M0 film changes from a highly fluorescent sample to almost completely quenched. This seems likely to be due to multi-chromophore thermodynamic relaxation into a tightened crystalline packing pattern. By comparison, the d-spacing from P2 films are considerably larger than those of M0, and *remain unchanged by annealing*, which correlates with its unchanging solid state TRPL relaxation behavior upon annealing. Interestingly, P4 shares not only the spectral characteristics of M0 in its annealed form, but also has the same d-spacing, both before and after annealing. Both annealed M0 and pristine or annealed P4 thus exhibit largely quenched PL and have the tightest d-spacings in this work.

Table 2.4: D-spacing values calculated from measured ring-to-center values from electron diffractograms. D-spacing values were calibrated using a gold standard.

	M0	P2	P4
Pristine Film	5.0	5.4	4.8
Annealed Film	4.8	5.4	4.8

Although the main goal of my dissertation work was to determine photophysical effects of polymer main-chain nonconjugated linker variation, the pendant chains required for solution solubility in the oPV work also appear to play a factor. Oligophenylenevinylenes that lack large side-chain substituents favor herringbone stacking, as does polyphenylenevinylene itself[56-58]. This is exemplified by the crystal structure for a 4.5-PV system without sidechains that has been reported by Van Hutten and coworkers[57], and in the crystal structure of PV3.5(OMe)$_6$ (Figure 2.15) synthesized by Rathnayake.
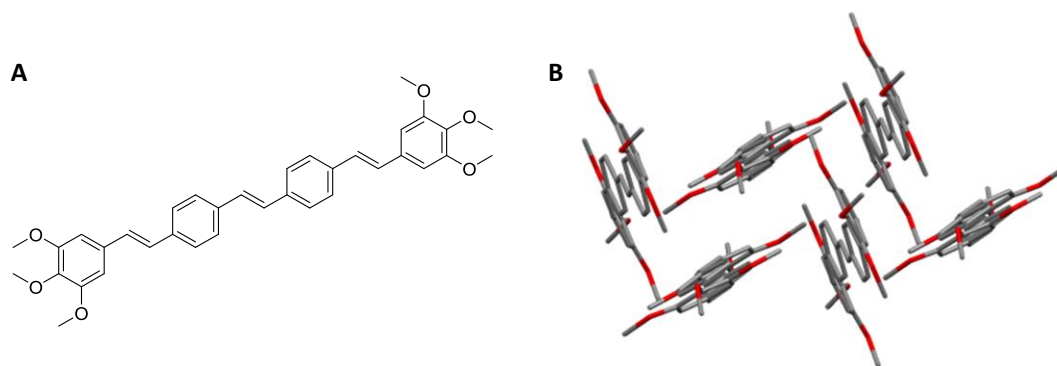
Figure 2.16: (A) Chemical structure of PV3.5(OMe)$_6$ and **(B)** crystalline structure of PV PV3.5(OMe)6 showing a herringbone-type packing pattern.

But, addition of straight-chain alkyl or alkoxy groups to the *interior* phenylene units of an oPV favor co-facial π-system stacking, as exemplified by the crystal packing analyses of dioctyl-4.5-PV reported by Brouwer and coworkers[59], by single crystal structures reported for a di-octyloxy-4.5-PV by Detert et al.[60] and a tetraoctyl-4.5-PV reported by Luping Yu's group[61]. It has not so far proven possible to obtain single crystals of M0, but the ED results show that it clearly forms crystalline domains, and it is reasonable to surmise that it favors co-facial π-stacks, given its structural similarity to these literature examples.

Assuming that M0 prefers co-facial π-stacks like di-octyl-4.5-PV, this would favor solid state exciton hopping and PL quenching mechanisms. This is quite consistent with the observed solid film behavior of M0. Pristine M0 films form with many crystalline domains, but with enough disordered domains to allow the film PL that corresponds to the "isolated chromophore" TRPL decay process (τ_2). Upon annealing, the disordered domains become better ordered (consistent with the ED results), and the previously emitting chromophores assemble into π-stacks. The fast M0 TRPL decay

36

process corresponds to rapid relaxation of excited state, π-stacked chromphores: this fast relaxation is all that remains in the annealed, more orderly morphology, with concomitant quenching of static ensemble PL.

The comparatively large d-spacing values and tendency to form largely amorphous mesostructures seen in P2 thin films is also consistent with its PL behavior. Considering that M0 chromophores are highly fluorescent with d-spacing of 5.0 Å, it is not unreasonable to assume that the persistent fluorescence seen in P2 both before and after annealing is due to P2 chromophores with even larger d-spacing. The few semicrystalline domains seen in TEM for P2 may account for the contribution of the fast PL decay process, but considering the significant contribution of fast decay τ_1 to the overall fluorescence decay, there may exists some short-range interchromophore electronic interaction even in the amorphous domains of P2, but perhaps not on a well-organized, long range scale as seen in the highly crystalline phases of M0.

Priori to annealing, P4 stacks at a distance identical to that seen in M0 after annealing, which correlates with the paucity of P4 PL emission and the relatively high contribution of the fast decay process before annealing. The longer linker in P4 restricts the spatial separation of P4 chromophores while being flexible enough to allow interchromophore stacking during film casting, rather than inhibiting stacking and inducing chromophore isolation as with the short tether in P2. Given its longer length and increased flexibility in comparison to the 2-carbon linker, the 4-carbon tether apparently possesses the appropriate length scale to *enhance* chromophore organization, possibly by allowing the formation of intramolecular π-stacks through folding events. To bolster this contention, computational modeling of the P4.5 chromophore stacking was carried out.

2.2.5 DFT Molecular Modelling Computations

As stated above, P2 has short linker groups that were suspected of hindering flexibility and folding within individual polymer chains. In order to probe this from a computational modeling standpoint, in collaboration with Jonathan Tinkham of the Lahti group, DFT geometry optimization computations were carried out, using Grimme's B97D3 functional[62] with a manually added dispersion term that, in the literature, has been reported to give accurate geometries with respect to π-π stacking interactions[63]. Using this method, ground state energies and geometries of M0, P2 and P4 chromophore dyads were obtained. The rigors of modelling the exact M0, P2 and P4 systems were beyond our available computational resources. Therefore, the pendant side-chain length was reduced from hexyloxy- to methoxy- to provide an approximation for the electronic properties and steric interactions imparted by the side chains. As shown in Figure 2.17, a 2-chromophore segment of P4 can adopt a cofacially-stacked conformation with a π-stacking distance of 3.4 Å, much like that of a M0 dyad, which was calculated to be 3.1 Å.

M0   **P4**
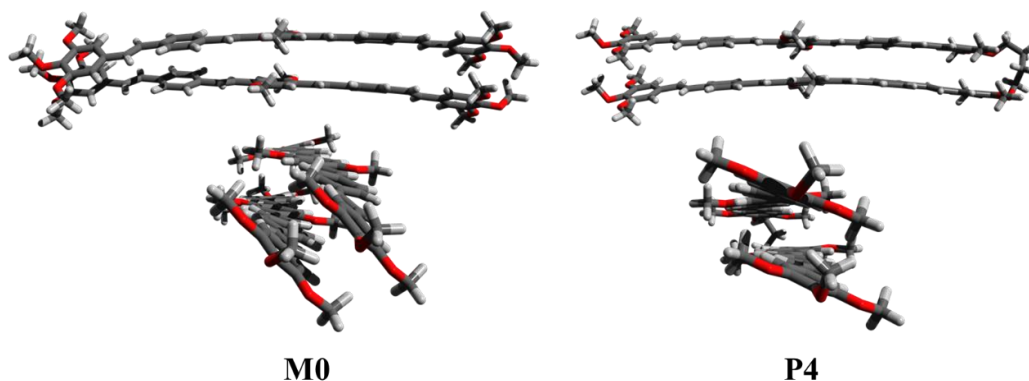
Figure 2.17: DFT calculations of M0 and P4 dyads, showing a geometrically optimized folded conformation.

This distance is moderately shorter than those that have been seen in the experimental crystalline structures[57,60,61] of similar oligo-p-phenylenevinylenes that π-stack cofacially; this disparity which may have arisen from computationally using the shortened side chains. The most critical piece of evidence relative to the experimental results is that the computations of P2 suggest that the 2-carbon linker of P2 is too short to accommodate a stacked conformation, since P2 calculations would not converge after several weeks of attempting to obtain a stable ground state geometry. Although the approximations in this model mean that the d-spacing values obtained from the calculations may not quantitatively represent cofacial π-stack distances, these theoretical experiments qualitatively support that P2 folding is less likely than M0 stacking or P4 stacking, and that cofacial stacking can indeed occur for the substituted 4.5-PV chromophores lke M0 and P4.

2.2.6 A "Big Picture" Assessment of Chromophore Aggregation (Including Folding) in the oligo-4.5-p-phenyleneinylenes.

The studies of monomeric chromophore M0 gave good supporting evidence for major amounts of chromophore ordering in the solid state, analogous to the crystallography of structurally related 4.5-PVs with similar side chains. The quenching of remnant PL in pristine M0 films after annealing indicates that mobility in M0 favors more chromophore organization. The segmented conjugated-nonconjugated P2 and P4 systems can form inter-chromophore contacts either by folding or by interchain stacking. As supported by the computational studies, P2 chromophores may not form intra-chain folds, but hypothetically, they could still form inter-chain π-stacks, even though the flexible oligomer/polymer P2 chains are not expected to crystallize as readily as molecular M0 (which is confirmed by the experimental ED results). The experimental

39

observation of static PL in pristine P2 shows that the chromophores do not all π-stack in a manner that quenches PL, although the TRPL results indicate that a substantial number stack well enough for the fast relaxation process to dominate. The annealing process has no effect on P2 d-spacing values, and annealed P2 retains significant steady-state film PL and unchanged TRPL dynamics. This indicates that already-quenched, orderly P2 domains become more orderly upon annealing, but that domains that lack inter-chromophore quenching contacts simply cannot reorganize much: as a result, the disordered, emitting domains as the major contributor to TRPL decay behavior.

Although the computations indicate P2 to be inhibited in its ability to achieve folded, intrachain, cofacial or similar quenching geometries between chromophores, they show that P4 has long enough linkers to permit chain folding. The sum of evidence indicates that this is exactly what happens. Pristine P4 has significant film crystallinity as a pristine drop-cast film which is retained upon annealing, based on ED evidence. Notably, it is only poorly photoluminescent in both pristine and annealed films. The P4 linkers are flexible enough to accommodate forming cofacial PL-quenching geometries during film casting that is favored in other 4.5-PV chromophores having similar pendant side chain functionalization. It appears to favor folding with chromophore quenching to some extent even in solution, which would explain P4 having the lowest solution phase PL quantum efficiency in the study set. Precipitation of at least partly pre-folded P4 chains would also explain the low static PL in pristine P4 films, as well as the fact that pristine P4 films already exhibit TRPL relaxation dynamics that are nearly the same as those of post-annealed (orderly) M0 films. Annealing increases the order in P4 films according to ED, and actually improves quenching somewhat. The overall set of results is

consistent with initial formation of numerous folded, intra-chain chromphore contacts that quench PL in P4, with some disordering between chains upon annealing on a long-range scale that nonetheless gives better inter-chromophore contact on a short-range local scale (both in folded chains and at local inter-chain, interchromophore contacts).

2.3 Summary

Although copolymer and monomer behaviors for the control monomeric 4.5-PV chromophore and related, segmented copolymers look nominally the same in solution based on static PL spectra, further examination clearly shows a large difference in photophysics, which can be attributed to variations in the structural and solid-state morphological behaviors of these species.

It is interesting to compare to results from Plunkett's study, although it did not include annealing or TEM/ED experiments. That study examined both shorter and longer oPV chromophores (up to 6.5-PV) that also have long, *branched* side chain substitution on every monomer unit to inhibit *either* co-facial or herringbone stacking. Most of the absorption and PL behavior in these segmented copolymers remained similar to that of the monomeric chromophores, but there was still some variation in solid state PL behavior as a function of linker. The evidence was interpreted to mean that $-O(CH_2)_nO-$ linked systems folded better than $-(CH_2)_n-$linked systems, especially for longer $-O(CH_2)_nO-$ linkers; this would give more inter-chromophore interaction *within* a chain, consistent with solid film PL spectral lineshape changes that occurred in these cases.

In the previous work by Karasz and coworkers on PV2.5 based segmented copolymers, long linker length was intended to improve processability and film formation, but$-O(CH_2)_nO-$ linkers having n = 2,4,6,8 all gave the same PL spectrum

without major quenching, and without indications of crystallinity in powder x-ray diffraction studies. If the chromophores in these studies form either intra- or inter-chain local close contacts, they seem more likely to be herringbone contacts rather than co-facial, based on comparison to the crystal structure obtained during Rathnayake's work on the closely related monomer, PV3.5(OMe)$_6$ (see Figure 2.16). The Karasz systems and PV3.5(OMe)$_6$ lack the internal side chains that appear to be crucial to forming cofacial π-stacks, where π-stacking of oligo-PVs is definitely known to occur. If chromophore contacts develop, they would not favor quenching so much as cofacial contacts: this is consistent with the known efficacy of the PV2.5 segmented copolymers as blue emitting layers in OLEDs.

This work strongly indicates that the segmented copolymer design strategy does not prevent co-facial oPV π-stacks for chromophores having straight-chain side-chain substituents for added solubility. Use of chromophores with branched side chains -- like those in Plunkett's study[46] -- avoids this problem to some extent, but even then not entirely, depending on linker chain structure. Interestingly, use of short linkers with straight chain chromophore substituents also seems to limit the problem of chromophore stacking in segmented polymer, by making intra-chain folding unlikely. The combination of possibilities allows tuning of chromophore-incorporating, segmented copolymer behavior between eliminating co-facial π-stacks that are bad for OLEDs due to exciton quenching, and encouraging them for situations like organic photovoltaics where interchromophore exciton or charge transport is desirable.

2.4 References

(1)   Liu, F.; Gu, Y.; Shen, X.; Ferdous, S.; Wang, H.-W.; Russell, T. P. Characterization of the morphology of solution-processed bulk heterojunction organic photovoltaics. *Progress in Polymer Science* **2013**, *38*, 1990-2052.

(2)   Hedley, G. J.; Ward, A. J.; Alekseev, A.; Howells, C. T.; Martins, E. R.; Serrano, L. A.; Cooke, G.; Ruseckas, A.; Samuel, I. D. W.: Determining the optimum morphology in high-performance polymer-fullerene organic photovoltaic cells. In *Nature Communications*, 2013; Vol. 4.

(3)   Giridharagopal, R.; Ginger, D. S. Characterizing Morphology in Bulk Heterojunction Organic Photovoltaic Systems. *The Journal of Physical Chemistry Letters* **2010**, *1*, 1160-1169.

(4)   Liu, F.; Zhao, W.; Tumbleston, J. R.; Wang, C.; Gu, Y.; Wang, D.; Briseno, A. L.; Ade, H.; Russell, T. P. Understanding the Morphology of PTB7:PCBM Blends in Organic Photovoltaics. *Advanced Energy Materials* **2014**, *4*, n/a-n/a.

(5)   Ray, B.; Lundstrom, M. S.; Alam, M. A. Can morphology tailoring improve the open circuit voltage of organic solar cells? *Applied Physics Letters* **2012**, *100*, -.

(6)   Günes, S.; Neugebauer, H.; Sariciftci, N. S. Conjugated Polymer-Based Organic Solar Cells. *Chemical Reviews* **2007**, *107*, 1324-1338.

(7)   Brunetti, F. G.; Kumar, R.; Wudl, F. Organic electronics from perylene to organic photovoltaics: painting a brief history with a broad brush. *Journal of Materials Chemistry* **2010**, *20*, 2934-2948.

(8)   Campoy-Quiles, M.; Ferenczi, T.; Agostinelli, T.; Etchegoin, P. G.; Kim, Y.; Anthopoulos, T. D.; Stavrinou, P. N.; Bradley, D.; Nelson, J. Morphology Evolution Via Self-organization and Lateral and Vertical Diffusion in Polymer:fullerene Solar Cell Blends. *Nature Materials* **2008**, *7*, 158-164.

(9)   Noriega, R.; Rivnay, J.; Vandewal, K.; Koch, F. P. V.; Stingelin, N.; Smith, P.; Toney, M. F.; Salleo, A. A general relationship between disorder, aggregation and charge transport in conjugated polymers. *Nature Materials* **2013**, *12*, 1038-1044.

(10)   Venkataraman, D.; Yurt, S.; Venkatraman, B. H.; Gavvalapalli, N. Role of Molecular Architecture in Organic Photovoltaic Cells. *The Journal of Physical Chemistry Letters* **2010**, *1*, 947-958.

(11)   Chen, D.; Nakahara, A.; Wei, D.; Nordlund, D.; Russell, T. P. P3HT/PCBM Bulk Heterojunction Organic Photovoltaics: Correlating Efficiency and Morphology. *Nano Letters* **2010**, *11*, 561-567.

(12)   Bounos, G.; Ghosh, S.; Lee, A. K.; Plunkett, K. N.; DuBay, K. H.; Bolinger, J. C.; Zhang, R.; Friesner, R. A.; Nuckolls, C.; Reichman, D. R.; Barbara, P. F. Controlling Chain Conformation in Conjugated Polymers Using Defect Inclusion Strategies. *Journal of the American Chemical Society* **2011**, *133*, 10155-10160.

(13)   Hu, D.; Yu, J.; Wong, K.; Bagchi, B.; Rossky, P. J.; Barbara, P. F. Collapse of Stiff Conjugated Polymers with Chemical Defects into Ordered Cylindrical Conformations. *Nature* **2000**, *405*, 1030-1033.

(14)   Grigoras, M.; Catargiu, A.-M.; Musteata, V.-E. Multi-Block Copolymers Containing Oligoaniline Pentamer as Electroactive Segment. *Soft Materials* **2011**, *11*, 90-97.

(15)   Benvenho, A. R. V.; Hummelgen, I. A. Positive Charge Transport in an Alternative Oligo-p-phenylenevinylene-derivative/aliphatic-segment Block Copolymer. *Materials Research* **2001**, *4*, 133-136.

(16)   Ignatious, F.; Lu, C.; Kantor, S. W.; Lenz, R. W. Alternating, Block, and Random Copolymers of a Triad Mesogen with Alkylene Terephthalate Flexible Segments. *Macromolecules* **1994**, *27*, 7785-7793.

(17)   Wang, H.; Sun, Q.; Li, Y.; Duan, L.; Qiu, Y.; Li, X. Synthesis and electroluminescent properties of a novel copolymer with short alternating conjugated and non-conjugated blocks. *Polymer International* **2003**, *52*, 343-346.

(18)   Husken, D.; Feijen, J.; Gaymans, R. J. Segmented Block Copolymers with Terephthalic-Extended Poly(ethylene oxide) Segments. *Macromolecular Chemistry and Physics* **2008**, *209*, 525-534.

(19)   Heun, S.; Mahrt, R. F.; Greiner, A.; Lemmer, U.; Bassler, H.; Halliday, D. A.; Bradley, D. D. C.; Burn, P. L.; Holmes, A. B. Conformational effects in poly(p-phenylene vinylene)s revealed by low-temperature site-selective fluorescence. *Journal of Physics: Condensed Matter* **1993**, *5*, 247-260.

(20)   Junkers, T.; Vandenbergh, J.; Adriaensens, P.; Lutsen, L.; Vanderzande, D. Synthesis of poly(p-phenylene vinylene) materials via the precursor routes. *Polymer Chemistry* **2012**, *3*, 275-285.

(21)   Saini, S.; Bagchi, B. Photophysics of conjugated polymers: interplay between Förster energy migration and defect concentration in shaping a photochemical funnel in PPV. *Physical Chemistry Chemical Physics* **2010**, *12*, 7427-7433.

(22)   Yu, Z.; Barbara, P. F. Low-Temperature Single-Molecule Spectroscopy of MEH-PPV Conjugated Polymer Molecules. *The Journal of Physical Chemistry B* **2004**, *108*, 11321-11326.

(23)   Kim, D. Y.; Grey, J. K.; Barbara, P. F. A detailed single molecule spectroscopy study of the vibronic states and energy transfer pathways of the conjugated polymer MEH-PPV. *Synthetic Metals* **2006**, *156*, 336-345.

(24)   Summers, M. A.; Robinson, M. R.; Bazan, G. C.; Buratto, S. K. Optical Microscopy of Polycrystalline Oligo(phenylenevinylene) Films. *Synthetic Metals* **2003**, *137*, 957-958.

(25)   Lee, Y. J.; Kim, D. Y.; Barbara, P. F. Effect of Sample Preparation and Excitation Conditions on the Single Molecule Spectroscopy of Conjugated Polymers. *The Journal of Physical Chemistry B* **2006**, *110*, 9739-9742.

(26)   Summers, M. A.; Bazan, G. C.; Buratto, S. K. Matrix-Induced Intensity Fluctuations in the Fluorescence from Single Oligo(phenylenevinylene) Molecules. *Journal of the American Chemical Society* **2005**, *127*, 16202-16206.

(27)   Bianchi, R. F.; Balogh, D. T.; Gonçalves, D.; Faria, R. M.; Irene, E. A. Photo-oxidation Phenomenon of MH-PPV Films Studied by Ellipsometry and Infrared Spectroscopy. *Molecular Crystals and Liquid Crystals* **2002**, *374*, 457-462.

(28)   Clafton, S. N.; Beattie, D. A.; Mierczynska-Vasilev, A.; Acres, R. G.; Morgan, A. C.; Kee, T. W. Chemical Defects in the Highly Fluorescent Conjugated Polymer Dots. *Langmuir* **2010**, *26*, 17785-17789.

(29)   Strobl, G. R.: *The Physics of Polymers: Concepts for Understanding Their Structures and Behavior*; Springer, 2007.

(30)   Baughman, R. H.; Chance, R. R. Point defects in fully conjugated polymers. *Journal of Applied Physics* **1976**, *47*, 4295-4300.

(31)   Nalwa, H. S.: *Handbook of Advanced Electronic and Photonic Materials and Devices*; Academic Press, 2000.

(32)   Drury, A.; Maier, S.; Ruther, M.; Blau, W. J. Investigation of different synthetic routes to and structure-property relationships of poly(m-phenylenevinylene-co-2,5-dioctyloxy-p-phenylenevinylene). *Journal of Materials Chemistry* **2003**, *13*, 485-490.

(33)   Masse, M.; Martin, D.; Thomas, E.; Karasz, F.; Petermann, J. Crystal morphology in pristine and doped films of poly (p-phenylene vinylene). *J Mater Sci* **1990**, *25*, 311-320.

(34)   Olsen, B. D.; Alcazar, D.; Krikorian, V.; Toney, M. F.; Thomas, E. L.; Segalman, R. A. Crystalline Structure in Thin Films of DEH−PPV Homopolymer and PPV-b-PI Rod−Coil Block Copolymers. *Macromolecules* **2007**, *41*, 58-66.

(35)   Nayyar, I. H.; Batista, E. R.; Tretiak, S.; Saxena, A.; Smith, D. L.; Martin, R. L. Effect of trans- and cis-isomeric defects on the localization of the charged excitations in π-conjugated organic polymers. *Journal of Polymer Science Part B: Polymer Physics* **2013**, *51*, 935-942.

(36)   Drori, T.; Utah, T. U. o.: *Optical Study of Pi-conjugated Polymers and Pi-conjugated Polymers/fullerene Blends*; The University of Utah, 2009.

(37)   Liu, D.; Yin, S.; Xu, H.; Liu, X.; Sun, G.; Xie, Z.; Yang, B.; Ma, Y. Cis- and trans-isomerization-induced transition of charge transport property in PPV oligomers. *Chemical Physics* **2011**, *388*, 69-77.

(38)   Salamone, J. C.: *Polymeric materials encyclopedia*; CRC Press, 1996.

(39)   Rissler, J. Effective conjugation length of π-conjugated systems. *Chemical Physics Letters* **2004**, *395*, 92-96.

(40)   Meier, H.; Stalmach, U.; Kolshorn, H. Effective conjugation length and UV/vis spectra of oligomers. *Acta Polymerica* **1997**, *48*, 379-384.

(41)   Khoshkhoo, M. S.; Taromi, F. A.; Kowsari, E.; Shalamzari, E. K. Contribution of chromophores with different numbers of repeat units to overall emission of MEH–PPV: An experimental and simulation study. *Polymer* **2013**, *54*, 4017-4029.

(42)   Padmanaban, G.; Ramakrishnan, S. Fluorescence Spectroscopic Studies of Solvent- and Temperature-Induced Conformational Transition in Segmented Poly[2-methoxy-5-(2'-ethylhexyl)oxy-1,4-phenylenevinylene] (MEHPPV). *The Journal of Physical Chemistry B* **2004**, *108*, 14933-14941.

(43)   Hu, D.; Yu, J.; Padmanaban, G.; Ramakrishnan, S.; Barbara, P. F. Spatial Confinement of Exciton Transfer and the Role of Conformational Order in Organic Nanoparticles. *Nano Letters* **2002**, *2*, 1121-1124.

(44)   Yang, Z.; Karasz, F. E.; Geise, H. J. Intrinsically soluble copolymers with well-defined alternating substituted p-phenylenevinylene and ethylene oxide blocks. *Macromolecules* **1993**, *26*, 6570-6575.

(45)   Yang, Z.; Sokolik, I.; Karasz, F. E. A soluble blue-light-emitting polymer. *Macromolecules* **1993**, *26*, 1188-1190.

(46)   Zhu, X.; Traub, M. C.; Vanden Bout, D. A.; Plunkett, K. N. Well-Defined Alternating Copolymers of Oligo(phenylenevinylene)s and Flexible Chains. *Macromolecules* **2012**, *45*, 5051-5057.

(47)   Zhang, Y.; Zhu, W.; Wang, W.; Tian, H.; Su, J.; Wang, W. Synthesis and nonlinear optical properties of rod-like luminescent materials containing Schiff-base and naphthalimide units. *Journal of Materials Chemistry* **2002**, *12*, 1294-1300.

(48)   Rathnayake, H. P.; Cirpan, A.; Karasz, F. E.; Odoi, M. Y.; Hammer, N. I.; Barnes, M. D.; Lahti, P. M. Luminescence of Molecular and Block Copolymeric 2,7-Bis(phenylethenyl)-fluorenones; Identifying Green-Band Emitter Sites in a Fluorene-Based Luminophore. *Chemistry of Materials* **2007**, *19*, 3265-3270.

(49)   Siddiqui, S.; Spano, F. C. H- and J-aggregates of conjugated polymers and oligomers: A theoretical investigation. *Chemical Physics Letters* **1999**, *308*, 99-105.

(50)   Spano, F. C. Emission from aggregates of oligo-phenylene vinylenes: a recipe for superradiant H-aggregates. *Chemical Physics Letters* **2000**, *331*, 7-13.

(51)   Lakowicz, J. R.: *Principles of Fluorescence Spectroscopy*; Springer, 2007.

(52)   Baghgar, M.; Labastide, J.; Bokel, F.; Dujovne, I.; McKenna, A.; Barnes, A. M.; Pentzer, E.; Emrick, T.; Hayward, R.; Barnes, M. D. Probing Inter- and Intrachain Exciton Coupling in Isolated Poly(3-hexylthiophene) Nanofibers: Effect of Solvation and Regioregularity. *The Journal of Physical Chemistry Letters* **2012**, *3*, 1674-1679.

(53)   Schweikart, K. H.; Hohloch, M.; Steinhuber, E.; Hanack, M.; Lüer, L.; Gierschner, J.; Egelhaaf, H. J.; Oelkrug, D. Highly luminescent oligo(phenylenevinylene) films: the stereochemical approach. *Synthetic Metals* **2001**, *121*, 1641-1642.

(54)   van Hutten, P. F.; Krasnikov, V. V.; Brouwer, H. J.; Hadziioannou, G. Excimer luminescence from single crystals and films of a cyano-substituted phenylene–vinylene model compound. *Chemical Physics* **1999**, *241*, 139-154.

(55)   Birckner, E.; Grummt, U. W.; Rost, H.; Hartmann, A.; Pfeiffer, S.; Tillmann, H.; Hörhold, H. H. Fluorescence spectroscopy of potential electroluminescent materials: Substituent effects on DSB and segmented PPV derivatives. *Journal of Fluorescence* **1998**, *8*, 73-80.

(56)   Gierschner, J.; Park, S. Y. Luminescent distyrylbenzenes: tailoring molecular structure and crystalline morphology. *Journal of Materials Chemistry C* **2013**, *1*, 5818-5832.

(57)   van Hutten, P. F.; Wildeman, J.; Meetsma, A.; Hadziioannou, G. Molecular Packing in Unsubstituted Semiconducting Phenylenevinylene Oligomer and Polymer. *Journal of the American Chemical Society* **1999**, *121*, 5910-5918.

(58)   Spano, F. C. Temperature dependent exciton emission from herringbone aggregates of conjugated oligomers. *The Journal of Chemical Physics* **2004**, *120*, 7643-7658.

(59)   Brouwer, H. J.; Krasnikov, V. V.; Pham, T. A.; Gill, R. E.; van Hutten, P. F.; Hadziioannou, G. Optical properties of single crystals and vacuum-deposited thin films of a substituted oligo(p-phenylene vinylene). *Chemical Physics* **1998**, *227*, 65-74.

(60)   Detert, H.; Schollmeyer, D.; Sugiono, E. Synthesis, Structure and Solvatochromism of the Emission of Cyano-Substituted Oligo(phenylenevinylene)s. *European Journal of Organic Chemistry* **2001**, *2001*, 2927-2938.

(61)   Wang, H.; Ng, M.-K.; Wang, L.; Yu, L.; Lin, B.; Meron, M.; Xiao, Y. Synthesis and Characterization of Conjugated Diblock Copolymers. *Chemistry – A European Journal* **2002**, *8*, 3246-3253.

(62)   Grimme, S. Do Special Noncovalent π–π Stacking Interactions Really Exist? *Angewandte Chemie International Edition* **2008**, *47*, 3430-3434.

(63)   Grimme, S.; Ehrlich, S.; Goerigk, L. Effect of the damping function in dispersion corrected density functional theory. *Journal of Computational Chemistry* **2011**, *32*, 1456-1465.

**PROBING OF FOLDING IN FLEXIBLY LINKED FLUORENONE-BASED
DYADS VIA EXCIMER EMISSION**

3.1 Overview

3.1.1 Introduction

The folding of complex, flexible molecules is important in biomolecules and in synthetic polymers for applications such as sensors[1,2], biomimetics[3-5] and organic electronic devices[6-8]. For example, cable polymers where core conjugated chromophores are tethered to side chains are an important class of materials whose electronic behaviors are much influenced by whether the side chains fold atop the core chromophores, or remain largely separated[9-12]. For such studies, model systems provide useful insight for folding behavior in many cases, so long as there is a sensitive probe methodology to detect folding or unfolding.
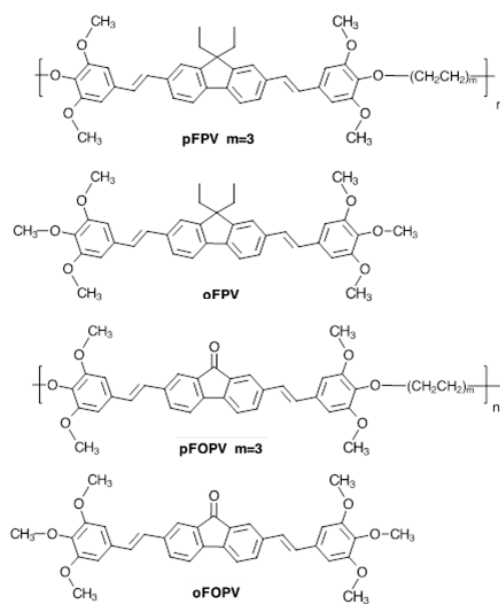
**Figure 3.1: Chemical structures of pFPV, oFPV, pFOPV and oFOPV
synthesized in a previous study by Rathnayake et al.**

During studies of organic materials with prospects for light-emitting diode (LED) behavior, Rathnayake et al.[13] studied the alternating segmented block copolymers pFPV and pFOPV, and the molecular analogues oFPV and oFOPV (Figure 3.1). They found for the molecular species that <1% of fluorenone-containing chromophores admixed into fluorene-containing solid analogues gave rise to a green-emitting band quite similar to those seen in nominally blue-emitting fully conjugated polyfluorenes. In follow-up studies, Barnes and coworkers[14] found that the molecular chromophore oFOPV gave not only monomolecular single molecule emission at about 540 nm, but also a small number of red-emitting sites at about 630 nm, which were attributed to oFOPV dyad formation. Longer wavelength emitting oFOPV dyad emission would be consistent with oFOPV's predominantly excimeric longer wavelength emission at higher solution concentrations and in the solid state. Fluorenones are known for their strong tendency to give excimer emission[15-17]. The ready formation of excimer sites in these fluorenone-containing solids prompted consideration that this process might be useful to probe folding in flexible chain systems, including segmented block copolymers.

To test the folding capacity of chromophores linked by nonconjugating tethers, a series of flexibly-linked fluorenone-based dyads was designed, synthesized and characterized to ascertain an optimal tether length that would allow folding and show evidence of enhanced intramolecular chromophore interactions in a bichromophoric system.

3.1.2 Excimers and Exciplexes

Some of the more interesting behaviors of excited state species are electronic effects caused by excited state bonding interactions occurring at close intermolecular
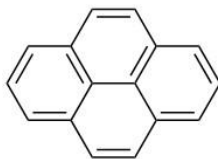
Figure 3.2: Chemical structure of pyrene.

distances, such as excimer/exciplex formation. Since the turn of the 20th century,

concentration, temperature and pH dependent fluorescence spectroscopy has sometimes

uncovered a red-shifted fluorescence band favored by increasing concentration of

chromophore in solution. Such bands were reported in the literature for decades without

suitable rationalization. The notion of a transient dimeric species that forms through the

interaction between an excited state chromophore and a neighboring ground state

chromophore was first set forth by Förster in 1955, during the investigations of the

fluorescence of a polycyclic chromophore, pyrene[18,19] (Figure 3.2). The term "excimer"

(from *exci*ted state di*mer*) was later coined by Stevens and Hutton, who examined the

effects of temperature and concentration on the red-shifted fluorescence band seen in

solutions of pyrene in cyclohexane[20].

Excimeric emission requires the bimolecular formation of a weak interaction

between an excited state luminophore and a neighboring ground state luminophore of the
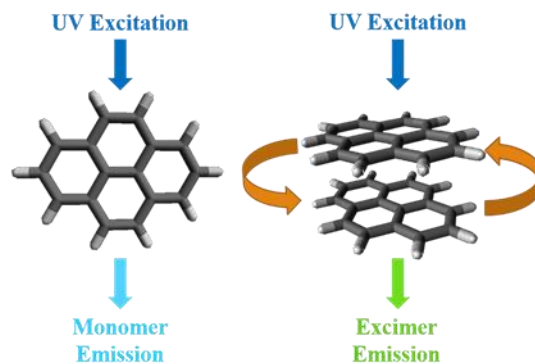
Figure 3.3: Schematic depicting monomer and excimer emission of pyrene.

51

same species[20]. This interaction involves overlap between the lowest unoccupied

molecular orbital (LUMO) of the excited molecule and the highest occupied molecular

orbital (HOMO) of the ground state chromophore, giving a weakly-bound dimer (Figure

3.3). The formation of the excimer results in net stabilization of an excited state

molecular dyad with a red-shifted emission relative to monomer emission[18]. As

hypothesized by Förster, the red-shift could in principle be due to a photochemical

reaction that occurs upon radiating the test sample, but a key factor in his explanation of

the excimer is that the red-shifted band must occur without the appearance of new

absorption characteristics. If irradiation of the sample formed a new compound in

solution that was stable after relaxation, new features in the absorbance spectrum would

be expected. In the absence of such changes, Förster concluded that the photochemical

product must exist only in the excited state, which undergoes dissociation of the two

associated molecules after excimer emission.

Since then, numerous aromatic hydrocarbons, such as benzene[21], naphthalene[22],

anthracene[23], pentacene[24] and perylene[25] have all been shown to form excimers, although

these interactions are weaker than those seen in pyrene, and the occurrence of the telltale

excimeric spectral signature is far more dependent on temperature and substitution in

these cases. Minor substitution on pyrene and other aromatic hydrocarbons tends to

disrupt or eliminate eximer formation[24]. In the process of examining these species,

fluorescence lifetime has been shown to be a defining characteristic of the excimer[26]. For

stronger excimeric bonds, emission occurs with lifetimes that are greater than ~25 ns,

while weaker excimer association produces lifetimes on the order of 10 ns. Molecular

modeling calculations have been done for simple examples of excimers, and the values

obtained for the theoretical emission mission bands are in reasonable agreement with experimental results of the photophysical studies[27], but due to the rigors and time demands of modeling larger molecules, more complex examples have yet to be computationally studied[28].

3.1.3 Fluorenone Excimers
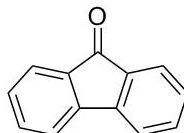
Figure 3.4: Chemical structure of fluorenone.

More recently, several studies of the rigid, fused-ring biphenyl chromophore, fluorenone (Figure 3.4), have also yielded concentration dependent excimeric behavior. Interestingly, solutions of fluorenone form excimers at room temperature, a characteristic that makes fluorenone excimers easily studied without the need for elaborate cooling or
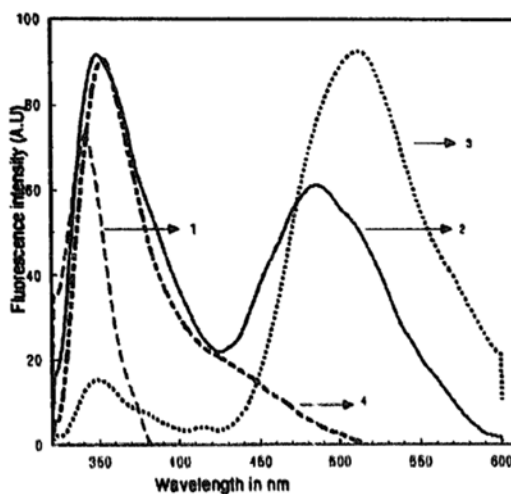
Figure 3.5: Solution-phase fluorescence spectra of fluorenone in chloroform showing the transition from monomer to excimer emission with increasing concentration. (1) 1.1×10-3 M, (2) 1.1×10-4 M, (3) 1.1×10-5 M, (4) 1.1×10-6 M. See Rani et al[15]. (permission license number 3402711432322).

matrix isolation methodologies. A study of unsubstituted fluorenone by Arathi Rani and coworkers[15] showed monomeric emission in a band centered at about 350 nanometers (Figure 3.5). However, as the concentration of fluorenone in solution increases, an excimer emission band centered at about 500 nanometers appears at the expense of the monomeric emission band. Since excimer formation requires bimolecular collision of an excited state monomer and a ground state monomer, excimer formation quenches monomer emission. Since the monomeric emission band is reduced with an increased intensity of the red-shifted band without the appearance of new absorption characteristics, the emission at increased concentration fits excimeric behavior. Unlike substituted pyrenes, fluorenones have been proven to form excimers with numerous different substituents and in a variety of solvent systems[16,17,29-32]. Interestingly, the lifetimes of fluorenone excimers seem unique amongst excimer-forming species reported to date; fluorenone excimer decay lifetimes are on the order of 0.5-10 nanoseconds, which is much shorter than the typical 10-25 ns range seen for polycyclic benzenoid species[17,29,30]. Furthermore, when compared to the associated monomeric singlet fluorescent decay, the fluorenone excimer lifetime can, in some cases, be the faster of the two processes[17,29,30].

3.1.4 Intramolecular Excimers

As mentioned above, concentration and temperature dependent excimer formation has been observed in several different species of π-conjugated organic molecules. However, fifteen years after the initial study by Förster, a study by Dempster et al. attempted to determine intrinsic excimeric formation variation in a series of tethered naphthalenes linked together by varying lengths of flexible polymethylene chains (Figure

3.6). By limiting the distance between the chromophores to a few angstroms, excimer

formation independent of concentration was induced in several naphthalene derivatives[33].
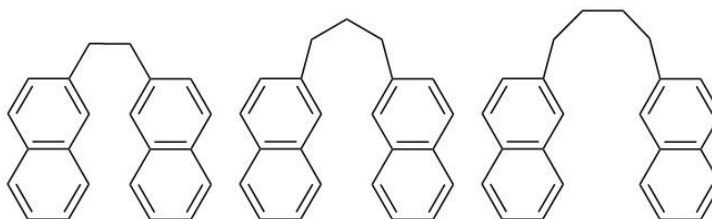
Figure 3.6: Chemical structures of α,ω-dinaphthylalkanes synthesized in a previously published study by Chandross and Dempster[33].

Naphthalene dyads tethered by ethylene, propylene and butylene linkers were

studied in solution by the Dempster group and later in thin films by Mathauer and

Frank[34]. Their findings suggest that the tetramethylene linker has too much freedom of

movement to favor π-stacking between chromophores, while the tethered naphthalenes in

the ethylene-linked derivative are held apart at a greater distance than is optimal for

excimer formation, and the required deformations are too unfavorable in the sp^3 carbon-

carbon bonds to reach the needed close inter-ring distances required. In this study with

two linked naphthalenes, a three carbon trimethylene chain provided the best balance

between chain flexibility and imposed chromophore proximity.

Since the original studies of tethered naphthalene, projects aimed at controlling

excimer formation have been few in number, but recently, interest in the topic has been

rekindled due to possible applications of tethered excimeric systems in the chemical

sensing of DNA and electron transfer materials[35], such as organic photovoltaic (OPV)

devices[36]. In the case of OPV materials and chromophoric materials for other electron

transfer applications, excimer formation may help in converting higher-energy photons

into lower-energy electrons, and may serve to streamline the electron transfer process between traditional electron-donating materials and electron accepting materials.
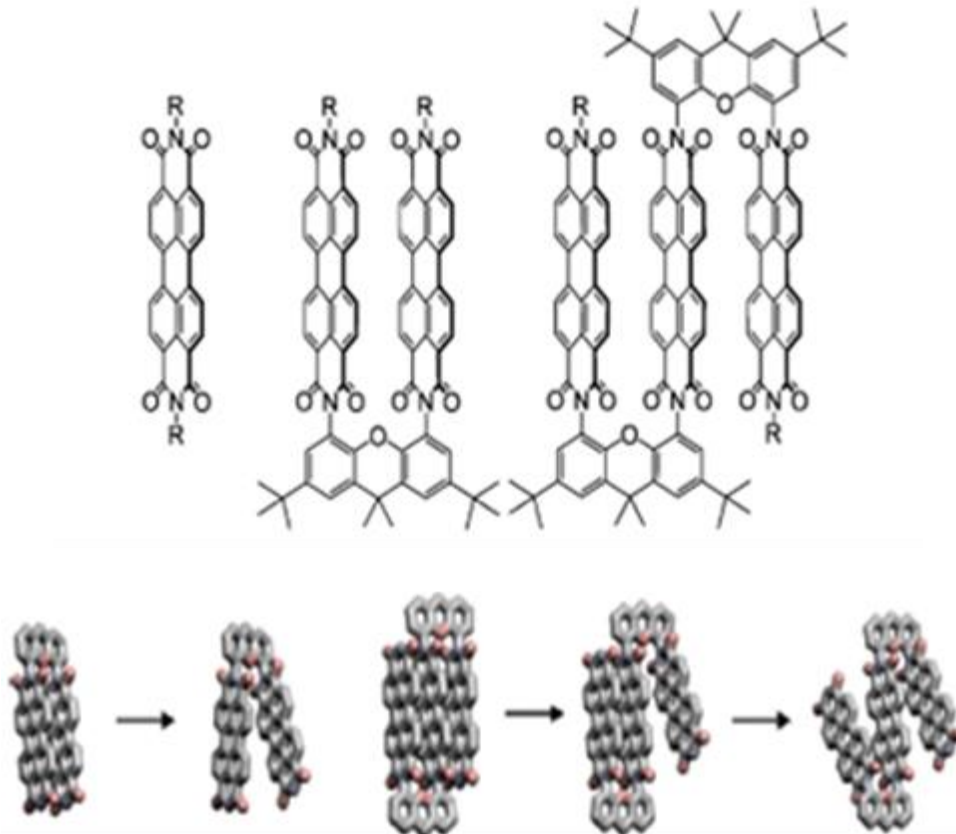
Figure 3.7: Chemical structures of perylenediimide monomer together with dyad and triad linked with rigid xanthene bridges, and possible conformational isomers contributing to concentration-independent excimer fluorescence. Reprinted (adapted) with permission from Kim et al.[37], *Journal of the American Chemical Society* **2010,** *132***, 3939-3944. Copyright 2012 American Chemical Society.**

One of the most recent studies was conducted by Wasielewski and Kim[37]. In this work, perylenediimides were forced into a π-stacking organization by connection to rigid tricyclic xanthene bridging units, and a finite population of the molecules was shown by fluorescence spectroscopy to form excimers at any concentration (Figure 3.7). As expected, the amount of excimer formation is determined by the flexibility of the

structure in studies of related systems. The trimeric form of the reticulated PDI

derivatives -- also shown in Figure 3.7 -- undergoes fluorescence relaxation with a time

constant of 29.8 ns. Deviations from parallel plane geometric constraints, which are

proposed to be more common in the dimer, broaden the fluorescence excimer band width

and reduce the fluorescence lifetime to 9 ns, which is suggestive of a less-stable, non-

ideal excimeric geometry or interaction[37].

3.1.5 Design of New, Fluorenone-Based Intramolecular Excimer Systems

In the following portions of this chapter, I describe the synthesis and electronic

spectral characterization of flexibly-linked dyads of 1,*n*-(2,6-dimethoxy-4-(2-

fluorenoneethenyl)diphenoxy)-oligomethylenes, where *n* = 2,4,8, (Figure 3.8) for

structures FOSFx2, FOSFx4, and FOSFx8, respectively. The photoluminescent behaviors

of these dyad chromophores show a strong dependence upon tether length. In particular,

FOSFx2 showed behavior indicating that it alone in this series of compounds folds in a

manner that gives substantial intramolecular excimer emission.
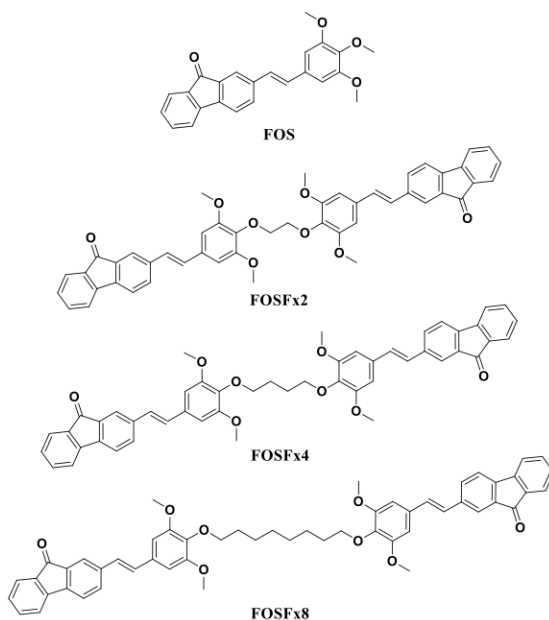
Figure 3.8: Chemical structures of dyads FOSFx2, FOSFx4, FOSFx8, and FOS.

3.2 Results and Discussion

3.2.1 Molecular Design

As shown in Scheme 3.1, I synthesized FOSFx4, and FOSFx8 by adapting a literature procedure[38] to link syringaldehyde with an appropriate α,ω-dibromoalkane through potassium carbonate promoted Williamson ether synthesis.
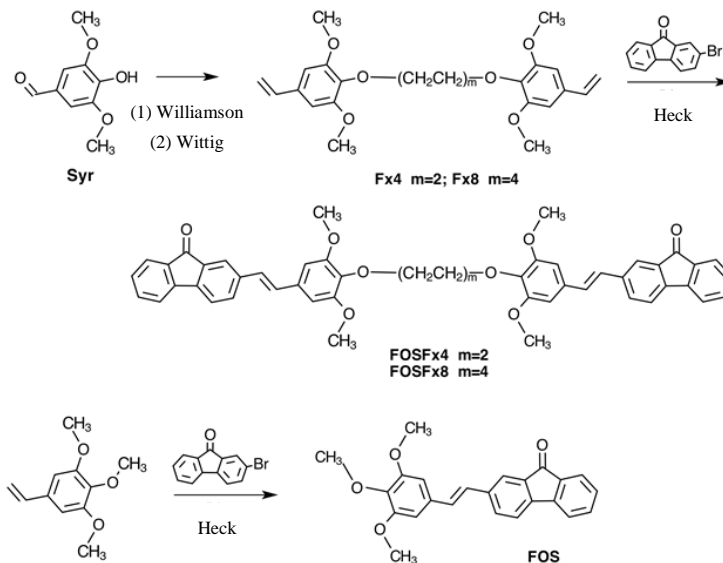
Scheme 3.1: Synthetic route to make fluorenone-based FOSFx4 and FOSFx8 dyads, and a monomeric control system FOS.

These reactions were comparatively straight forward, and required only an aqueous workup and recrystallization from ethanol to produce both FX4 and FX8 in pure form. These were then functionalized by Wittig vinylation of end-group carbaldehyde units. The base utilized in these Wittig reactions, n-butyllithium, is highly reactive and pyrophoric, so this reaction must be done with extreme care and under an inert atmosphere. Despite the hazards of this reaction, the strength of the base aided in producing a nearly quantitative conversion. Purification consisted of an aqueous workup followed by column chromatography to separate the product from a small amount of unreacted dialdehyde and the triphenylphosphine oxide byproduct. The large difference

in polarity between the desired product and the other components of the crude mixture made for a relatively easy separation. The products resulting from these vinylation reactions are typically yellow oils that are slow to crystallize. In order to produce purer, crystalline products that are easier to work with, the oil can be dissolved in a minimal amount of diethyl ether, then poured into cold hexanes to produce white, microcrystalline flexibly-linked segments (flexors).

The fluorenone moiety, 2-bromofluoren-9-one, was then appended on the ends of the flexors using Heck-type coupling adapted from a literature procedure[13]. This reaction is yield-limiting in these synthetic routes, as it results in a relatively low yield (~30% on average), and involves time-consuming workup and purification of the multi-component crude mixture by column chromatography. But, the final products show excellent purity by ^{1}H NMR. The un-tethered monomeric model control chromophore system, FOS, was made following previously published procedure[39] by vinylating 3,4,5-trimethoxybenzaldehyde and then performing a similar Heck coupling procedure with 2-bromofluoren-9-one.
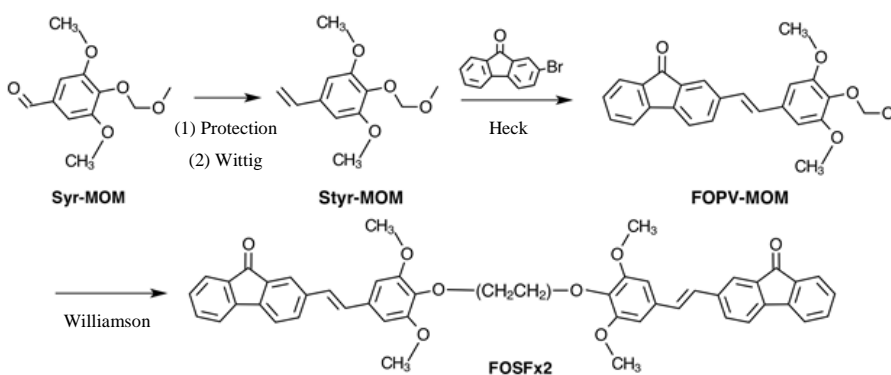
Scheme 3.2: Synthetic route to FOSFx2.

FOSFx2 was not formed in useful amounts by this procedure due to very low synthetic yield and difficulties with purification. To combat this issue, I designed an alternate synthetic route (Scheme 3.2) starting with methoxymethyl protection of syringaldehyde to protect the phenolic group from undesired reaction in the following Wittig vinylation step, which involves the highly reactive base, n-butyllithium. The protection step must be conducted with extreme care, due to the highly toxic and volatile nature of the chloromethyl methyl ether protecting reagent. After achieving successful vinylation with a similar procedure to that described above, I used a Heck coupling reaction with 2-bromofluoren-9-one that was analogous to that used to synthesize the other dyads, and then deprotected the methoxymethyl protecting from the phenolic group with concentrated hydrochloric acid. In the final step, two of the deprotected phenols were coupled with 1,2-dibromoethane via Williamson etherification. At first, this final Williamson reaction was troublesome, and resulted in low yield using a similar method to that used in Scheme 3.1, possibly due to a slower deprotonation step by potassium carbonate. This may be because potassium carbonate for the Williamson reaction is only modestly soluble in suitable organic solvents. After attempting use of several other bases, I found that organic-soluble tetra-n-butylammonium hydroxide performed much better than other bases tested. The tetra-n-butylammonium cation can also act as a phase transfer catalyst in shuttling the highly polar hydroxide anion into the organic solvent reaction environment. The difference in reactivity was visually evident; upon adding the base to the reaction mixture, the color of the solution instantaneously turned from a pale red to a deep, opaque brown color. Furthermore, conducting this reaction using microwave irradiation rather than conventional thermal heading techniques gave similar

yields, but with much-decreased reaction times. This improved synthetic modification

gave the desired FOSFx2 in yields comparable to those that I obtained for FOSFx4 and

FOSFx8. Full synthetic details and structural characterization data are given in Chapter 5.

3.2.2 Steady State Spectral Properties

After fully establishing the identities of the fluorenone dyads and the control
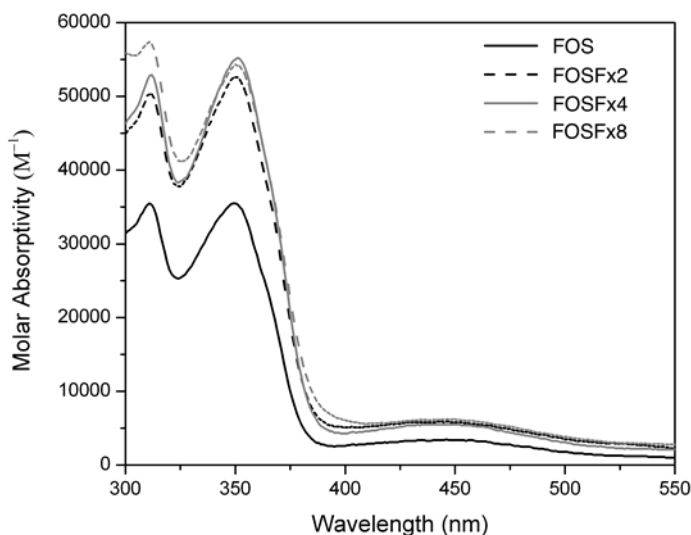
**Figure 3.9: Solution-phase absorption spectra of
FOS, FOSFx2, FOSFx4 and FOSFx8 in
chloroform.**

molecule, FOS, I characterized the four species via steady state solution phase absorption

and photoluminescence to identify any spectral differences between the fluorenone

dyads. Figure 3.9 shows the room temperature absorption spectra for all of the dyads and

for the model system FOS in chloroform, a solvent in which all four analytes are highly

soluble. The spectra are essentially identical in shape, with two major bands in the high

energy region and a broad, weaker band at about 450 nm. There are no lineshape

variations that indicate inter-chromophore interaction for the dyads by comparison to the

monomeric FOS. The spectral shapes do not change at higher concentrations up to 100

mM, so there is also no evidence of strong intermolecular aggregation. There is a small

solvatochromic effect on the low energy absorption maximum of FOS, a red shift from 432 nm in hexane to 442 nm in acetonitrile (65 meV). Analogous solvatochromic shifts in fluorenone have been much discussed in the literature, and have been attributed to $\pi \rightarrow \pi^*$ versus $n \rightarrow \pi^*$ excited state transitions that give the lowest energy band under conditions of different polarity[40].

The situation is more complex for static photoluminescence (PL). The strongest absorption band at 350 nm for each of the four species can be attributed to a π-π^* transition, and it was therefore chosen as the wavelength of excitation for initial experiments. FOS in chloroform at 10^{-6} M concentrations excited at 350 nm shows monomeric emission with poorly resolved fine-structure over 400-550 nm (Figure 3.10).
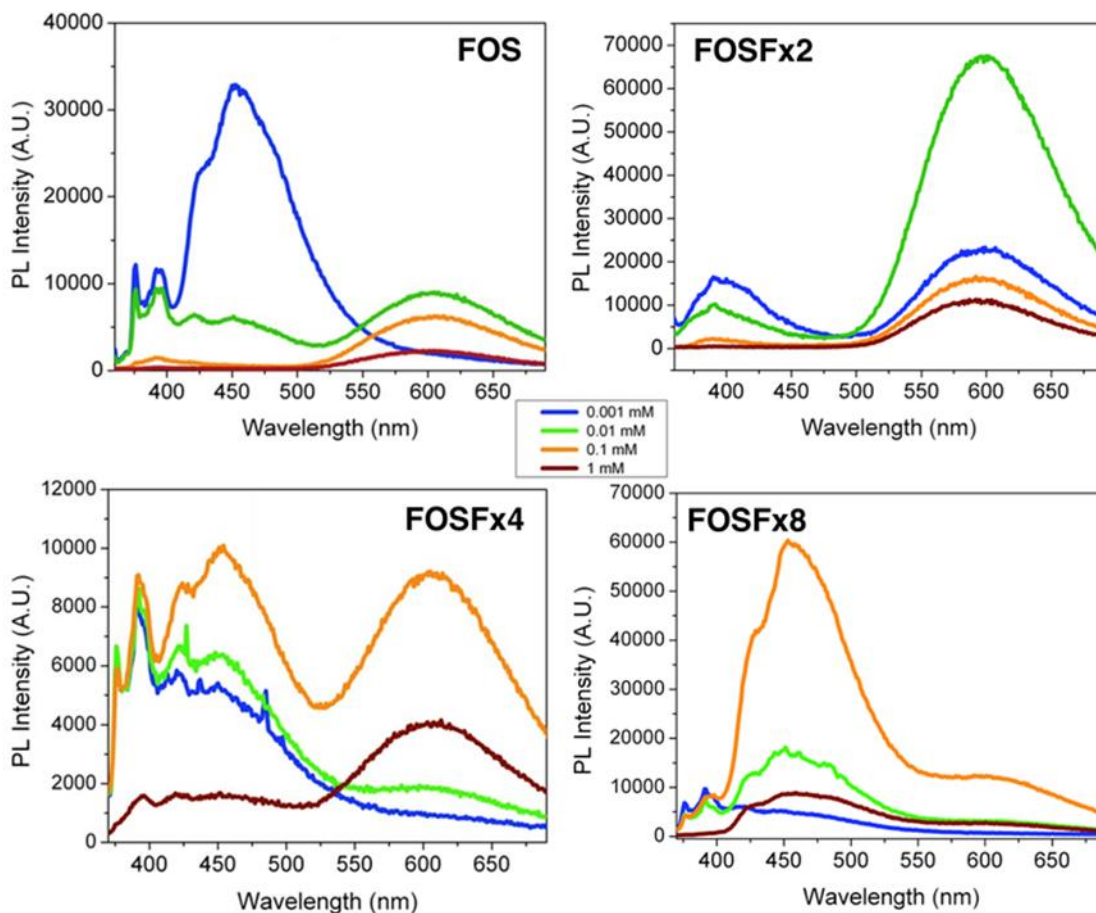
Figure 3.10: Steady-state photoluminescence spectra for FOS, FOSFx2, FOSFx4 and FOSFx8 in chloroform solutions at different concentrations.

As concentration increases, this PL band in FOS is quenched at the expense of a weaker, broad, featureless, presumptively excimeric band centered at 610 nm; this is the only band seen for FOS concentrations above 10^{-3} M in chloroform. This behavior is qualitatively similar to that observed by Rathnayake et al.[13] for oFOPV, and is even obvious to the naked eye as the emission color changes from blue to orange at high concentration of the analyte.

Table 3.1: Fluorescence maxima of monomer and excimer fluorescence for FOS, FOSFx2, FOSFx4 and FOSFx8 excited at 350 nm in toluene (PhMe), dichloromethane (DCM), chloroform (CHCl₃) and acetonitrile (MeCN).

		Monomer Peak Intensity [nm]	Excimer Peak Intensity [nm]
FOS	PhMe	391 (weak)	550
	DCM	411	602
	CHCl₃	391	602
	MeCN	442	620 (weak)
FOS2FX	PhMe	400 (weak)	544
	DCM	389	600
	CHCl₃	392	604
	MeCN	414	N/A
FOS4FX	PhMe	401 (weak)	554
	DCM	409	584
	CHCl₃	392	597
	MeCN	460	N/A
FOS8FX	PhMe	461 (weak)	562
	DCM	403	604 (weak)
	CHCl₃	450	604 (weak)
	MeCN	461	N/A

The tethered dyads FOSFx8 and FOSFx4 show solvent effects quite similar to those of FOS at the same 20×10^{-6} M concentration, although their spectral shapes can be different at the same concentration. They show multiple emission bands in dichloromethane and chloroform, strongly favor emission at 550 nm in toluene, and almost exclusively favor emission at about 460 nm in acetonitrile (Table 3.1). Figure 3.11 displays the spectral curvature of FOS and the three dyads in toluene, dichloromethane (DCM), chloroform (CHCl₃) and acetonitrile (MeCN).
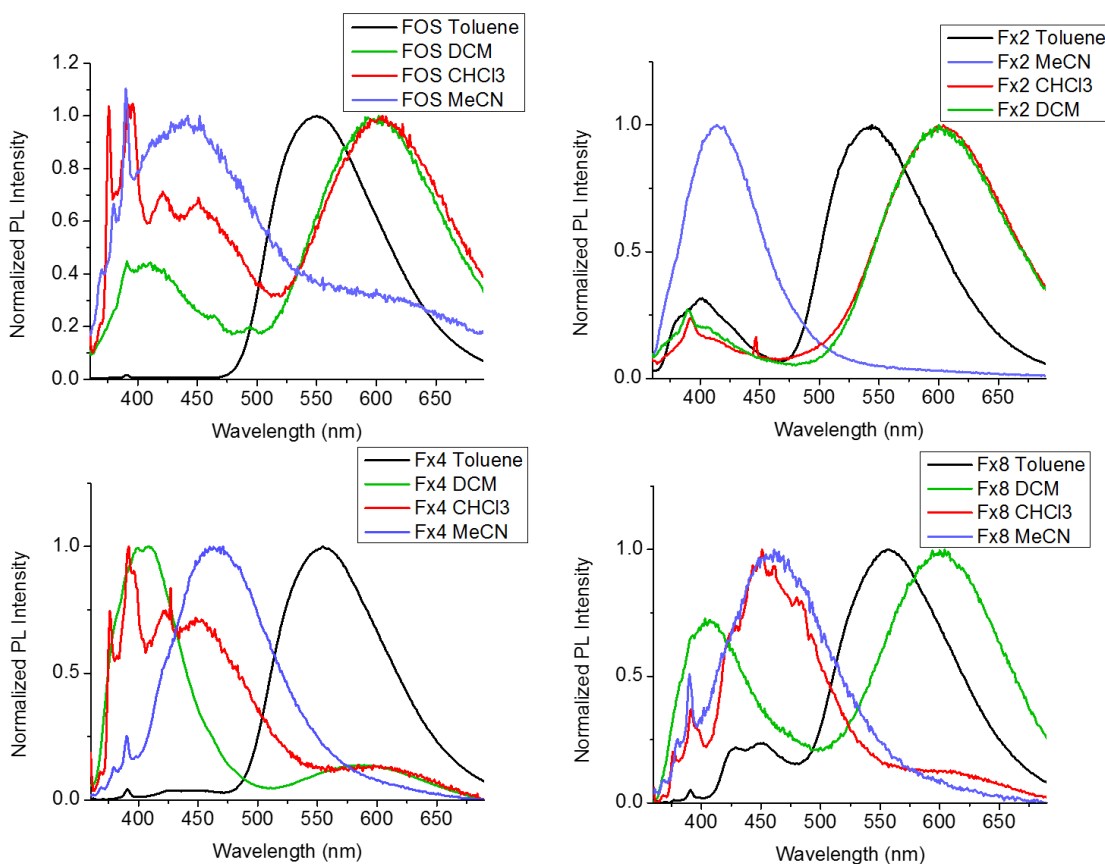
Figure 3.11: Normalized photoluminescence spectra for FOS, FOSFx2, FOSFx4 and FOSFx8 in toluene (black), dichloromethane (DCM, green), chloroform (CHCl₃, red) and acetonitrile (MeCN, blue). All concentrations are 10⁻⁵ M.

Based on peak positions and concentration dependence of intensities for 350 nm excitation, the bands at <500 nm are attributed to monomer emission and those at >500 nm are attributed to excimer emission. In chlorinated solvents, FOSFx8 gives less excimer emission relative to monomer than is seen in FOSFx4. But, FOSFx2 favors excimer emission in all solvents tested except for acetonitrile, in which it shows only monomeric emission at 414 nm. As is seen in FOS, monomer emission in FOSFx8 and FOSFx4 is blue shifted in dichloromethane relative to chloroform: FOSFx2 shows a blue shifted monomer band at about 400 nm in all solvents where the band appears. In acetonitrile, FOS shows only a broad, shoulder of excimer emission at about 620 nm,

with most of the (relatively weak) spectrum dominated by monomer emission at $\lambda_{max} =$ 450 nm. In toluene, FOS shows emission only at 550 nm, attributed to excimers by comparison to the behaviors of the tethered systems. Fluorenone and a number of substituted variants, like FOS, show analogously significant solvent effects on excimer band position, intensity, shape, and relative ratio of excimer to monomer emission[15-17,41].

As seen in Table 3.1, the variations in monomer peak position between solvents and between species make it difficult to extract conventional trends in solvatochromism for these systems. The shape of the monomer emission in Figure 3.11 varies from species to species, and different bands at about 410 nm and/or about 450 nm contribute to the emission seen in the 400-500 nm range. However, the effects of solvent polarity on excimer versus monomer emission are quite clear. In non-polar toluene, excimer emission dominates the spectra for all species. As the solvent polarity increases, the monomer emission intensity at lower wavelengths appears and becomes favored. This suggests that a more polar solvent interacts with the FOS-type carbonyl functionalities, thus forcing a separation between neighboring FOS moieties, whether they are in separate molecules or within the same dyad.

For more detailed study of concentration effects in the tethered systems, chloroform was chosen because it dissolved all of the studied compounds very well. Like FOS, FOSFx4 and FOSFx8 show primarily monomeric emission at wavelengths <500 nm at 10^{-6} M. In all three, raising concentration favors the longer wavelength, broad excimer band at 610 nm, but comparatively higher concentrations of FOSFx4 are required to give roughly the same ratio of excimer to monomer emission that is seen for FOS. FOSFx8 in chloroform does *not* give predominant excimer emission intensities at

any concentration. The behavior of FOSFx8 could mean that the long linker disfavors π-stacking interactions between adjacent FOS pendants, but the exact origin of this phenomenon is unclear. Perhaps the relatively large number of conformers possible for FOSFx8 makes it very unlikely to fold or for FOS groups on the end of the chain to approach one another in an excimer-favoring geometry. Uniquely in this study, a vastly different situation is seen for FOSFx2. At all concentrations, excimer emission is favored by comparison to monomer emission, to a much greater extent than is seen for FOS or for the tethered species with longer linker units. In FOSFx2, excimer emission is seen down to lowest concentration tested in chloroform. Figure 3.12 compares the ratios of
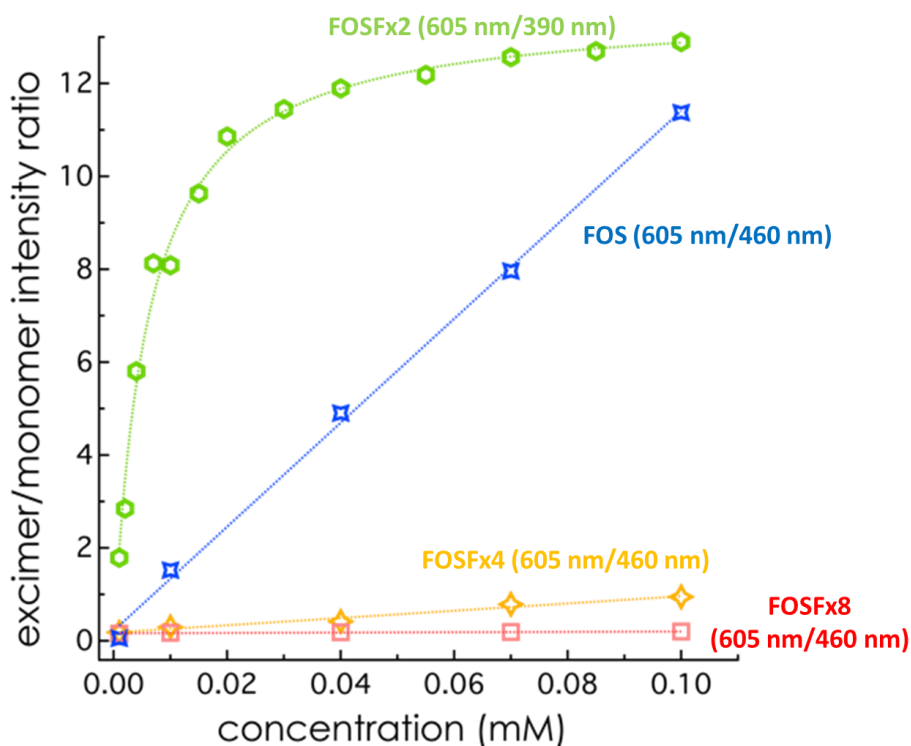
Figure 3.12: Excimer/monomer emission ratio plotted versus concentration for FOS, FOSFx2, FOSFx4 and FOSFx8. Wavelengths used to determine the ratios are labeled appropriately.

excimer/monomer emission intensities at λ_{max} for each compound, plotted as functions of concentration in chloroform. The plots all extrapolate *linearly* to an excimer/monomer

ratio of about zero at limiting low concentration in the concentration range used, *except* for FOSFx2. The excimer/monomer ratio is 20-fold higher in FOSFx2 than the other three species at the lowest concentration tested in this experiment, below which emission detection was too noisy for useful peak intensity determination. This behavior can be explained by favorable folding in FOSFx2 to give intramolecular excimeric interactions at the lowest concentration studied. The presence of overlapping intramolecular and intermolecular excimer formation would account for the higher excimer/monomer ratio seen for the 2-carbon-linked dyad.

Although the monomer, and the 4- and 8-carbon tethered systems show differences in the concentrations where any given excimer/monomer fluorescence ratio is observed, the data obtained for FOS, FOSFx4 and FOSFx8 can all be fit to a linear relationship. Again, FOSFx2 is unique in this study, as the data shows strongly nonlinear behavior in the concentration range studied. In the 0.001 mM to 0.02 mM regime, the excimer/monomer ratio for FOSFx2 increases very quickly, and then gradually seems to saturate at higher concentrations. At approximately the 0.02 mM concentration threshold, nearly all emission is from excimeric interactions, and the monomeric fluorescence is quenched to a minimum. At higher concentrations than this threshold, no additional excimers are formed due to limitations on monomeric excited state formation (self-filtering at high concentration) needed to yield excimers through bimolecular processes: this phenomenon has been documented in the literature[42]. It is not unreasonable to assume that at higher concentrations of FOS, FOSFx4 and FOSFx8, similar saturation behavior would occur, but due to the limits imposed on the study by a lack of solubility at concentrations higher than those studied in this experiment, this could not be examined.

Overall, FOSFx8 and FOSFx4 have significantly lower excimer/monomer emission ratios

than FOS at the same concentrations, while FOSFx2 has a much higher ratio. The 4-

carbon and 8-carbon linkers *disfavor* excimer compared to monomer emission, with

opposite behavior for the 2-carbon linker. The trend disfavoring excimer formation in

solution is strongest for the longest linker chain. The fact that the FOSFx2 curve reaches

saturation very quickly upon increasing concentration could be rationalized by

considering that intermolecular excimer formation may simply be more allowed than for

the monomer.   The FOSFx2 curve did not plateau at lower concentrations, for purely

intramolecular excimer formation. However, a hypothetical model that excludes

intramolecular excimer formation through folding of the 2-carbon linker leaves the

unique solid state time-resolved photoluminescence behavior (discussed later in the text)

of FOSFx2 unexplained.

For each dyad, an intramolecular excimer could in principle form, which is

influenced by the number of possible conformations that the dyad can thermally populate.

Since the number of possible conformations increases by the cube of the number of
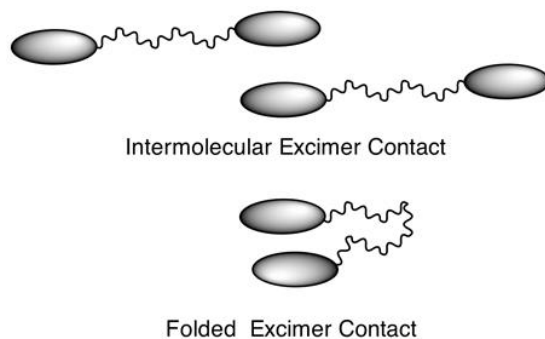
**Figure 3.13: Schematic depicting intermolecular
excimer emission and folded excimer emission.**

saturated atoms in the linker, this simple statistical probability of folding is much lower

for the 4- and 8-carbon systems in comparison to FOSFx2. Assuming for simplicity that

69

only the parallel and anti-parallel π-stacked conformations can result in intramolecular excimer formation for all the dyads -- although is not necessarily true, as will be described below -- the probability of folded, *intramolecular* excimer formation should be intrinsic to a particular species, and not dependent on the species concentration. It is, therefore, unclear why excimer/monomer ratio increases so abruptly for the 2-carbon linked system in comparison to the other species in this study, but, as described above, the favoring of excimer emission in FOSFx2 at *all* concentrations seems likely to arise from overlapping contributions to its broad excimer emission band from both intermolecular and intramolecular inter-chromophore contacts (Figure 3.13). In this scenario, FOSFx2 would always exhibit at least intramolecular (folded FOS dyad) excimer emission, even as intermolecular excimer emission decreases at low concentrations.

3.2.3 Solid State Time-resolved Photoluminescence Studies

To assist with understanding this complex PL behavior, time-resolved photoluminescence (TRPL) decay studies in the solid state, where excimer emission seemed likely to dominate based on the previously reported behavior of oFOPV[13]. This work was done in collaboration with Joelle A. Labastide of the Barnes group -- she did the actual TRPL experiments. We hoped that the differences in solution PL summarized in Figure 3.10 would be clarified in glassy solid state studies where a static set of inter-chromophore contacts would form, including folded dyads that would give excimer emission. Glassy states are expected, because multiple efforts failed to yield x-ray diffraction quality crystals of the dyads, and I found powder x-ray diffraction to indicate that the compounds are essentially amorphous. As will be described in detail below, the

TRPL experiments *did* show variations as a function of structure, and were carried out without worries about solution phase PL variations like those that have made fluorenone simultaneously fascinating and difficult to use as a bellwether for similar but non-identical molecules like FOS and its dyads. In addition, the solid state studies are more germane than solution studies for linking the this research to electronic materials behavior, given the strong effects of solid state inter-chromphore contacts on OLED and organic photovoltaic materials.
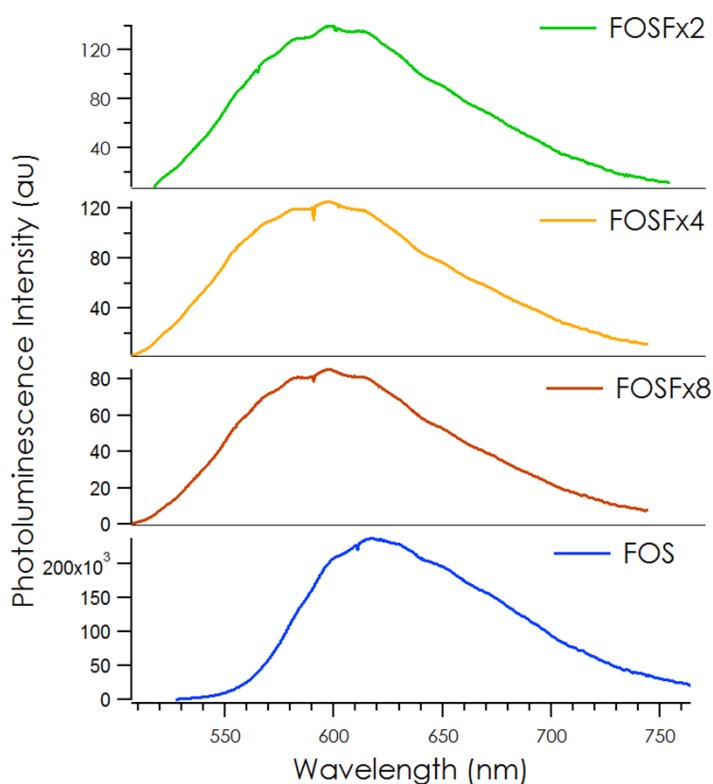
Figure 3.14: Steady state photoluminescence spectra of FOS, FOSFx2, FOSFx4 and FOSFx8 melt films.

The (TRPL) studies were carried out on neat films of FOS and the dyads, made by melting small amounts of compound on glass slides with a hot-block heater on the benchtop: the melts give optically transparent films that were convenient for optical analysis of the condensed solid state. As expected, only low energy emission bands were

seen in the solid samples (Figure 3.14), so TRPL was done using an excitation

wavelength of 405 nm, and detection at the peak of emission at 610 nm. The TRPL decay

curves (Figure 3.15) show that FOS, FOSFx4, and FOSFx8 all have TRPL decay

behavior that fits well to biexponential functions, while a tri-exponential function was

necessary to provide a reasonable fit for FOSFx2.
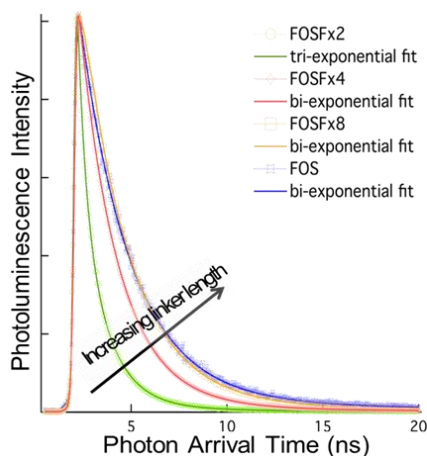
Figure 3.15: Time-resolved photoluminescence decay curves for FOS, FOSFx2, FOSFx4 and FOSFx8 obtained from melt films with excitation at 405 nm and decay monitoring at 605 nm. Arrow indicates the trend in fluorescence decay curves with an increase in dyad linker length.
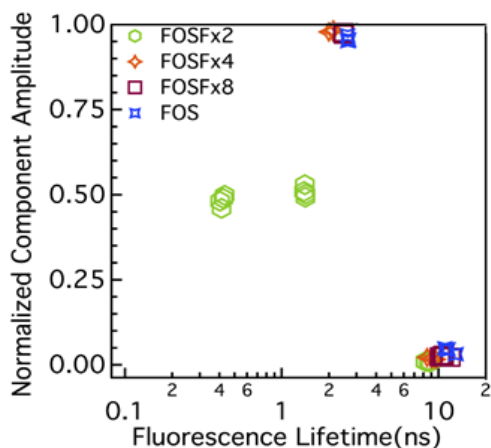
Figure 3.16: Plot of fluorescence lifetime contribution to overall fluorescence versus decay constant for FOS, FOSFx2, FOSFx4 and FOSFx8.

Figure 3.16 correlates the fitted decay constants with their percent contributions to overall TRPL decay. All showed a small component (<5%) with a long decay constant of 8-10 ns, and a major component with a faster decay constant of 1-3 ns. The triexponential decay of FOSFx2 has a longest lifetime process with nearly the same decay constant and percent contribution as was seen for the other systems; ~8 ns for 5% of the total decay trace. The remainder of the decay process arises from nearly equal amounts of *two* faster processes with decay constants of 0.3 ns and 1.2 ns.

The slow decay process seen in all of the systems in solid films (Table 2) may be associated with a particularly stable excimer state. Since this process is a small component of the overall excimer decay curve and does not vary between the species, the following discussion focuses on the primary decay processes. FOS, FOSFx4, and FOSFx8 all undergo excimer decay at one type of exciton trap site with $\tau \sim$ 1-3 ns. This decay constant is consistent with results seen for luminescent decay of fluorenone in solution[17,29,30] and in thin-films[43,44]. As stated above, emission from a less stable excimer decays with a faster time constant than that from a more stable excimer. Given the similarity of the primary decay constants for the linked dyads and for FOS, their solid-melt film excimer sites are likely to be of similar geometry and stability. But, FOSFx2 has a unique set of trap sites giving half of its excimer emission, in addition to the decay process from trap sites that are similar to those in the other systems. These results are consistent with the overall picture derived from the static PL spectral results, *i.e.*, by assuming that FOSFx2 has a special tendency to give a folded geometry that contributes to overall excimer emission, along with any intermolecular inter-chromophore contacts that also contribute.

3.2.4 Molecular Modeling Computations

All three dyad systems are expected to conformationally equilibrate in solution among folded, fully extended, and intermediate geometries. For intramolecular excimer emission, folded geometries could bring FOS groups into stacked proximity with fluorenone carbonyl groups in *syn* or *anti* carbonyl orientation (Figure 3.17).
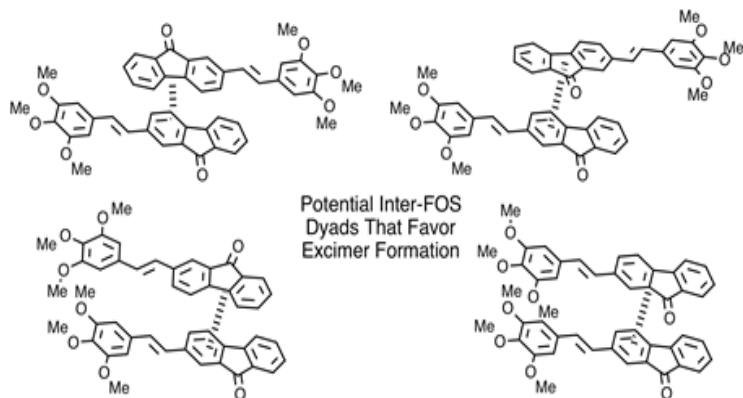
Figure 3.17: Schematic depicting the possible intermolecular conformations that could presumably lead to excimer emission for FOS.

Molecular mechanics calculations using the Merck Force Field (MFF) show that all of the dyad systems can form folded conformers with FOS dyad π-stacking as well as fully extended conformers. Geometry optimization of FOSFx2 using the B3LYP/6-31G(d) hybrid density functional method gives a folded energy minimum a mere 1.2 kJ/mol above the fully extended all-anti conformer, with fluorenone C=O groups stacked antiparallel at a distance of 3.3 Å (Figure 3.18).
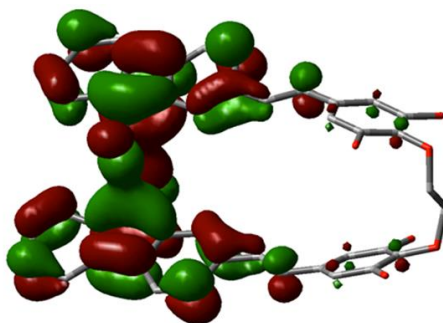
Figure 3.18: Electron density map of the LUMO of FOSFx2 as calculated using density functional theory.

The close approach between FOS units allows orbital overlap between the fluorenone carbonyl regions in the FOSFx2 lowest occupied molecular orbital (LUMO), as shown in Figure 3.18: this favors forming an excimer when an electron is promoted into this LUMO. These results do not fully sample the conformational energy surface of FOSFx2, but they show a reasonable possibility for dyad folding that should allow intra-dyad excimer formation upon photo-irradiation.

As pointed out above, FOSFx2 has fewer total conformers that the linked dyads with longer tethers, and so should have a greater probability to fold, where folded conformers can be energetically reached. While the evidence does not prove this picture unequivocally, there does not seem to be a clear alternative intramolecular geometry or intermolecular process that is special to just one of the linked dyad systems, other than formation of a folded conformer. The effects of different solvents, and especially the retention of solution excimer emission at low concentrations for FOSFx2 (Figure 3.10), also are consistent with this model operating dynamically in solution.

3.2.5 Steady State Spectral Properties at 440 nm Excitation

Along with monomeric emission and excimeric emission, fluorenone derivatives with extended π-systems have been shown to emit from twisted intramolecular charge

transfer (TICT) states when excited with the lowest energy transition seen in the absorbance spectrum[31]. To probe further relationship between linker length and excimer emission, Joelle Labastide and I characterized the four species by steady state solution phase photoluminescence when excited at 440 nm.
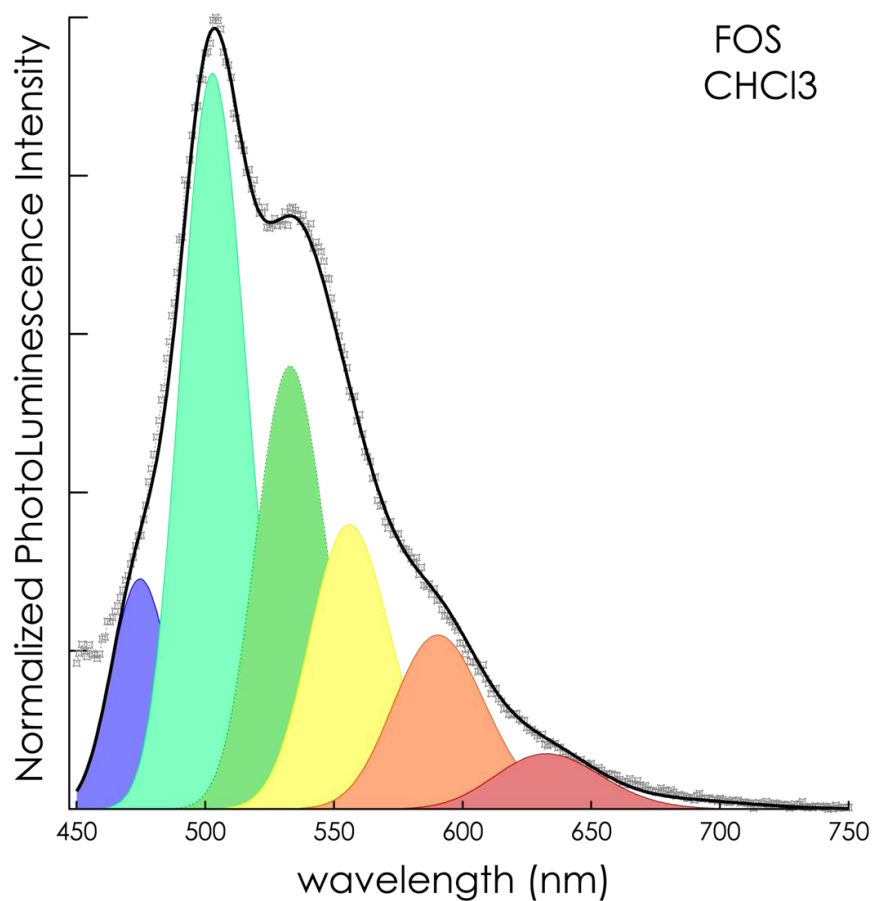
Figure 3.19: Normalized photoluminescence spectrum of FOS at 0.001 mM in chloroform. The colored Gaussian curves represent fitted multipeak contributions to the overall fluorescence profile.

Again, the situation is even more complex when using a 440 nm excitation wavelength in comparison to the aforementioned fluorescence data obtained with a 350 nm excitation wavelength (Figure 3.10). Figure 3.19 shows the normalized photoluminescence intensity plotted versus transition energy to compare the spectral

curvature of FOS in chloroform solution of low concentration (0.001 mM).   The area-

filled peaks underneath the fluorescence profile represent the line widths and amplitudes

of the individual spectral components that were modeled by manually fitting the

fluorescence spectra to six Gaussian functions using IGOR PRO graphing software. This

procedure has been used in other work aimed at deconvoluting multiple contributions to a

broader spectral transition envelope[45-47]. The choice of six functions was arbitrary, but

was the minimum needed to model the observed spectral lineshape reasonably well. The

FOS fluorescence spectrum (Figure 3.19) can be fitted to a combination of multiple

fluorescent transitions, with a maximum intensity at ~500 nm, and transitions of lower

intensity at ~530, ~560, ~590 and ~610 nm. The band at ~500 nm is similar to the energy

region of the TICT band reported by Shigeta and coworkers[31], while the longer

wavelength emission band (590-610 nm) lies in the same wavelength range as the

excimer band seen when exciting to the FOS at 350 nm. However, the yellow

fluorescence band seen at 550 nm is unique fluorescence spectra obtained from 440 nm

excitation: its assignment will be discussed later, below. The different fluorescence bands

are evenly spaced by ~160 meV, an energy that is strikingly close to the energy of the

ring breathing mode of benzene. At first, it was therefore unclear whether the

fluorescence bands >500 nm were resulting from separate fluorescent processes, or if

they were vibronic bands of the TICT state.
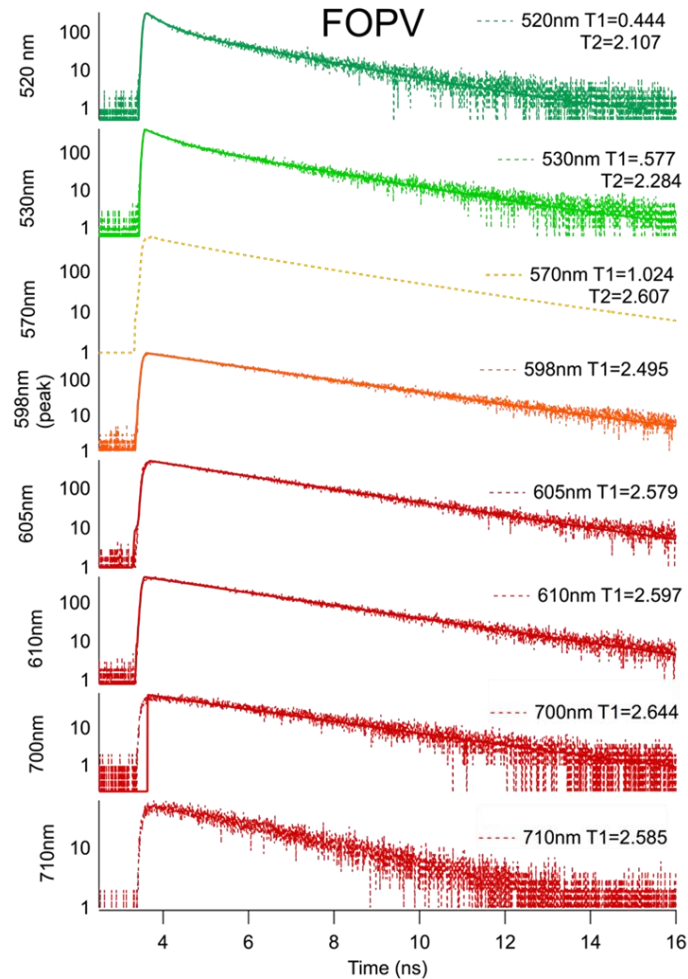
Figure 3.20: Time-resolved photoluminescence decay profiles of FOS in 0.001 mM chloroform solutions at 7 different wavelengths.

process or an ensemble emission from multiple processes, Joelle Labastide carried out

fluorescence lifetime measurements for my samples of FOS (0.001 mM in chloroform

solution) with emission decay monitored at wavelength intervals from 500 nm to 710 nm

(Figure 3.20). At 520 and 530 nm, the fluorescence decay profiles fit to a biexponential

function with relatively fast decay constants (~0.4 ns and ~2 ns): the 0.4 ns time constant

dominates the decay, with the ~2 ns time constant contributing only 5%. At 570 nm, the

contribution of the 0.4 ns time constant is minimal, and a different process with a 1 ns

decay constant dominates the fluorescence decay. At lower energy (605, 610, 700 and 710 nm), the fluorescence decay profiles are monoexponential, with a longer decay constant of 2.5 ns. The varying time constants and contributions, is strong evidence that more than one fluorescent process is responsible for the overall fluorescence spectrum of FOS under 440 nm excitation conditions. Additionally, according to Fermi's Golden Rule[48], when exciting a single transition, the lifetimes recorded at different wavelengths within the fluorescence envelope will be proportional to the cube of the wavelength. As shown in Appendix 1 (Figure A.1), the lifetimes of FOS reported in Figure 3.20 do not fit the Fermi criterion for a single transition, which provides further evidence of emission from multiple states.
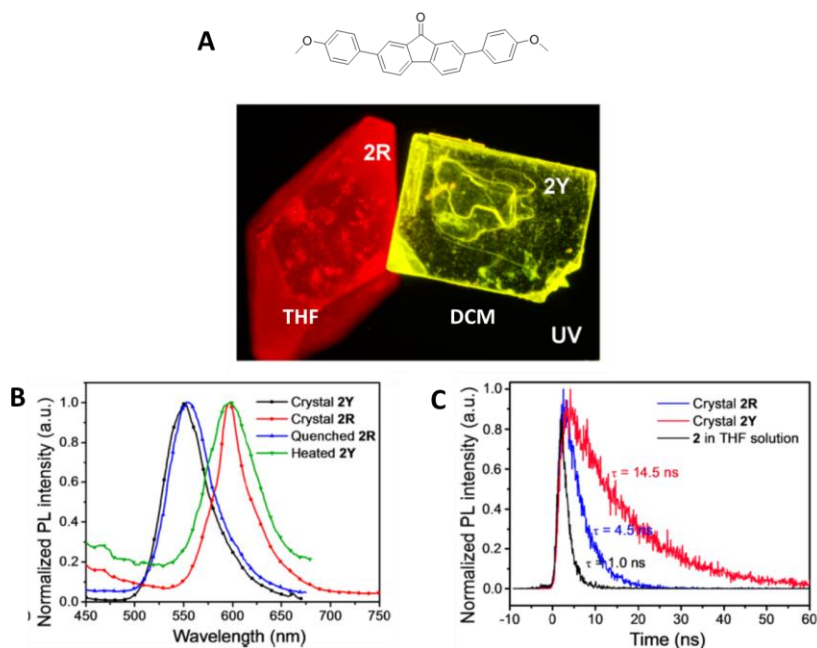
Figure 3.21: (A) Chemical structure of diphenylfluorenone derivative studied by Yuan et al. and its two crystalline polymorphs, (B) steady state photoluminescence and (C) time resolved photoluminescence of the crystalline samples. Reprinted (adapted) with permission from Yuan *et al*., *Chemistry of Materials*, 2014, 26, 2467. Copyright 2014 American Chemical Society.

Although the precise identity of each fluorescent process under these conditions is still unclear, a 2014 article by Yuan and coworkers[49] provides a reasonable explanation for the behavior that FOS exhibits upon excitation with a 440 nm source. In that study, a series of substituted 1,8-diphenylfluorenone compounds was synthesized and crystallized into two distinct crystalline polymorphs by varying the recrystallization solvent. Like FOS, the diphenylfluorenones give a combination of both monomer and excimer emission in solution, but upon characterizing the crystals by solid state fluorescence spectroscopy, it was found that the two polymorphs exhibit two distinct excimer processes, one that fluoresces at 550 nm, and the other that fluoresces at 610 nm (Figure 3.21). The root cause of the photophysical differences between the two polymorphs was revealed in the X-ray crystallographic data of the two crystalline samples; the 60 nm shift in excimer fluorescence between the two species arises from very different crystalline packing patterns. The red-fluorescent polymorph gives anti-*parallel* π-stacking interactions with a fluorenone-fluorenone distance of 3.47 Å, while the yellow-fluorescent crystal forms a herringbone (cross-hatched) packing pattern with weak π-π interactions in comparison to the red fluorescent polymorph. Furthermore, the red and yellow excimeric crystals give very different fluorescence lifetimes (14.5 ns and 4.5 ns, respectively), which supports that there are two structurally different excimers that are quite different in both emission wavelength and stability[49].

The study by Yuan and coworkers is very germane to my work on FOS and the FOSFx dyads, as it provides clear evidence that different π-stacking interactions between fluorenone derivatives can result in different excimers with different fluorescence wavelength and decay dynamics. When excited at 440 nm, FOS shows multiple

fluorescence bands, which likely arise from a combination of TICT fluorescence at about

540 nm and emission from several different excimeric trap states at longer wavelengths.

The actual conformations leading to different types of excimers remains unclear, but

Figure 3.22 shows four different possible conformations that might produce excimers of

varying energies, without even considering herringbone dyads like those in Yuan's work.
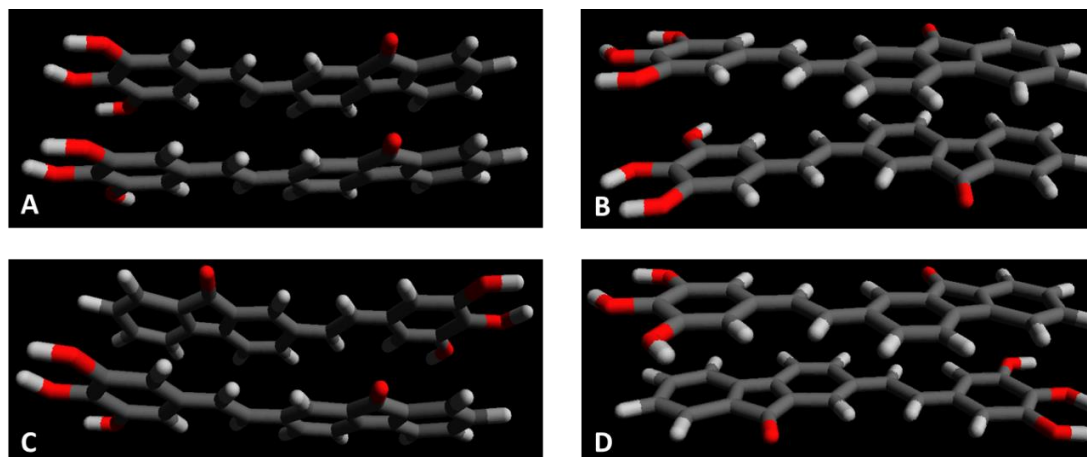
Figure 3.22: Possible excimeric interactions of FOS modeled using Avogadro molecular visualization software (A) syn-parallel, (B) anti-parallel, (C) syn-antiparallel, and (D) anti-antiparallel.

In the case of FOS, it is not unreasonable to suggest that variations between syn-

and anti- carbonyl overlap (Figure 3.22, A versus B, respectively) and parallel and anti-

parallel chromophore stacking (Figure 3.22, A versus C, respectively) may lead to

excimers with considerable differences in energy. Polycyclic aromatic hydrocarbons such

as pyrene do not show multiple excimer bands because of their high level of symmetry:

any energy differences between minor variations in excimer geometry are relatively

minute[18]. However, this dissertation work presents additional direct evidence of a

relatively new research area; unsymmetrical conjugated systems have the potential to

form multiple excimers with different interchromophore conformations, giving rise to

discernable structural features in the excimer emission envelope, as opposed to the typically broad, featureless excimer spectrum seen for pyrene.
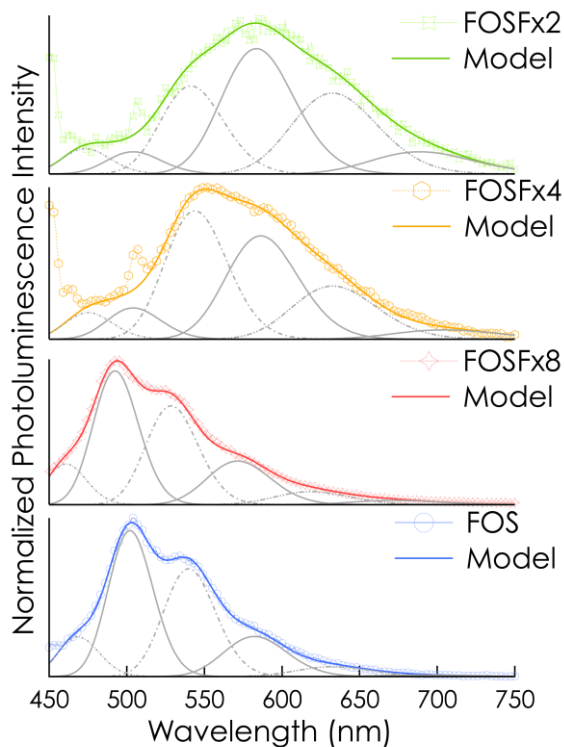
Figure 3.23: Normalized photoluminescence spectra of FOS, FOSFx2, FOSFx4 and FOSFx2 in 0.001 mM chloroform solution. The Gaussian curves below the fluorescence profiles represent the manually modeled components and their amplitudes that contribute to the overall fluorescence spectrum.

The multi-peak fitting procedure used for FOS can be extrapolated to the photoluminscence spectra observed for the FOSFx dyads under 440 nm excitation conditions. Figure 3.23 shows FOSFx2, FOSFx4 and FOSFx8 excited at 440 nm in chloroform solution (0.001 mM) with the FOS data for comparison. The figure also shows manual multipeak fitting contributions. FOSFx8 behaves much like the FOS monomer, with a small blue-shift (~10 nm) in the fluorescence maximum component in comparison to the monomer. Also like FOS, FOSFx8 shows minimal fluorescence from

560-610 nm, suggesting that at this concentration, the monomeric TICT state is favored, and excimer formation is minimal for these two species. FOSFx4 shows a much smaller amount of the presumed TICT emission and favors lower energy excimer emission in comparison to the monomer. This effect is even greater for FOSFx2; the TICT emission band is very small, and the processes at 550 nm and 610 nm are strongly favored. This behavior suggests that excimer relaxation and the monomeric TICT relaxation are in competition, and once again, the two carbon linker seems to favor excimer formation over monomeric emission, presumably through folding to form intramolecular excimers. Even the different shape of the FOSFx2 440 nm excited photoluminescence spectrum favors the view that its photophysics are fundamentally different from the others.

3.3 Summary

This chapter has given a report of the synthesis, steady state and time resolved spectral properties, and theoretical geometry optimization computations of a series of tethered, fluorenone-based dyads. The work described herein assembles a variety of consistent results indicating that a larger amount of inter-chromophore communication is exhibited by the shorter, 2-carbon linked dyad. This work provides provides a specific assay procedure to evaluate the folding capacity of the flexible linkers used in this study, which could find use in various areas of chemical research. If a particular application requires electronic communication between tethered moieties, results indicate that a shorter linker would provide the necessary distance control, while if a lack of electronic coupling is required, shorter linkers should be avoided. Furthermore, this set of experiments suggests that the incorporation of short flexible tethers into segmented alternating copolymers with chromophores that have been conventionally utilized in organic electronic devices may yield a greater amount of inter-chromophore

communication, *if fluorenone chromophores are involved*. However, the linker length

that will enhance these interactions is dependent upon the thermodynamically favored

intermolecular distance between the tethered species, or at least upon the ability of that

geometry to achieve other geometries that give inter-chromophore geometries with

different photophysics (like excimer formation). According to geometry optimization

computations, the fluorenone-based chromophores used in this study tend to stack at a

closer distance than is typical for conjugated systems conventionally utilized in organic

electronics. Therefore, if molecular folding is desired, the length of the linker may require

fine-tuning to accommodate the stacking of other chromophores to fit the particular

system.

3.4 References

(1)   Heidarsson, Pétur O.; Otazo, Mariela R.; Bellucci, L.; Mossa, A.; Imparato, A.; Paci, E.; Corni, S.; Di Felice, R.; Kragelund, Birthe B.; Cecconi, C. Single-Molecule Folding Mechanism of an EF-Hand Neuronal Calcium Sensor. *Structure*, *21*, 1812-1821.

(2)   Oh, K. J.; Cash, K. J.; Plaxco, K. W. Beyond molecular beacons: optical sensors based on the binding-induced folding of proteins and polypeptides. *Chemistry* **2009**, *15*, 2244-2251.

(3)   Titov, A. V.; Wang, B.; Sint, K.; Král, P. Controllable Synthetic Molecular Channels: Biomimetic Ammonia Switch. *The Journal of Physical Chemistry B* **2009**, *114*, 1174-1179.

(4)   Maayan, G.; Albrecht, M.: Metallofoldamers: Supramolecular Architectures from Helicates to Biomimetics. Wiley: Weinheim, Germany, 2013.

(5)   Bruzewicz, D. A.; Boncheva, M.; Winkleman, A.; St. Clair, J. M.; Engel, G. S.; Whitesides, G. M. Biomimetic Fabrication of 3D Structures by Spontaneous Folding of Tapes. *Journal of the American Chemical Society* **2006**, *128*, 9314-9315.

(6)   Notestein, J. M.; Canlas, C.; Siegfried, J.; Moore, J. S. Covalent Grafting of m-Phenylene-Ethynylene Oligomers to Oxide Surfaces. *Chemistry of Materials* **2010**, *22*, 5319-5327.

(7)   Singh, K. A.; Sauvé, G.; Zhang, R.; Kowalewski, T.; McCullough, R. D.; Porter, L. M. Dependence of field-effect mobility and contact resistance on nanostructure in regioregular poly(3-hexylthiophene) thin film transistors. *Applied Physics Letters* **2008**, *92*, -.

(8)   Jonkheijm, P.; van Duren, J. K. J.; Kemerink, M.; Janssen, R. A. J.; Schenning, A. P. H. J.; Meijer, E. W. Control of Film Morphology by Folding Hydrogen-Bonded Oligo(p-phenylenevinylene) Polymers in Solution. *Macromolecules* **2005**, *39*, 784-788.

(9)   Mohamad, D. K.; Fischereder, A.; Yi, H.; Cadby, A. J.; Lidzey, D. G.; Iraqi, A. A novel 2,7-linked carbazole based "double cable" polymer with pendant perylene diimide functional groups: preparation, spectroscopy and photovoltaic properties. *Journal of Materials Chemistry* **2011**, *21*, 851-862.

(10)   Li, Q.: *Self-Organized Organic Semiconductors: From Materials to Device Applications*; Wiley, 2011.

(11)   Cravino, A.; Zerza, G.; Maggini, M.; Bucella, S.; Svensson, M.; Andersson, M. R.; Neugebauer, H.; Sariciftci, N. S. A novel polythiophene with pendant fullerenes: toward donor/acceptor double-cable polymers. *Chemical Communications* **2000**, 2487-2488.

(12)   Mohamad, D. K.; Chauhan, S. S.; Yi, H.; Cadby, A. J.; Lidzey, D. G.; Iraqi, A. A regioregular head to tail thiophene based "double-cable" polymer with pendant anthraquinone functional groups: Preparation, spectroscopy and photovoltaic properties. *Solar Energy Materials and Solar Cells* **2011**, *95*, 1723-1730.

(13)   Rathnayake, H. P.; Cirpan, A.; Karasz, F. E.; Odoi, M. Y.; Hammer, N. I.; Barnes, M. D.; Lahti, P. M. Luminescence of Molecular and Block Copolymeric 2,7-Bis(phenylethenyl)-fluorenones; Identifying Green-Band Emitter Sites in a Fluorene-Based Luminophore. *Chemistry of Materials* **2007**, *19*, 3265-3270.

(14)   Odoi, M. Y.; Hammer, N. I.; Rathnayake, H. P.; Lahti, P. M.; Barnes, M. D. Single-Molecule Studies of a Model Fluorenone. *ChemPhysChem* **2007**, *8*, 1481-1486.

(15)   Rani, S. A.; Sobhanadri, J.; Prasada, R. Solvent and Concentration Effects on the Steady State Fluorescence of Fluorenone. *Journal of Photochemistry and Photobiology A: Chemistry* **1996**, *94*, 1-5.

(16)   Heldt, J. R.; Heldt, J.; Józefowicz, M.; Kamiński, J. Spectroscopic Studies of Fluorenone Derivatives. *Journal of Fluorescence* **2001**, *11*, 65-73.

(17)   Jozefowicz, M.; Heldt, J. R.; Heldt, J. The Red-edge Effect in the Spectra of Fluorenone and 4-Hydroxyfluorenone Alcohol Solutions. *Verlag der Zeitschrift für Naturforschung Tübingen* **2002**, *57 a*, 787-796.

(18)   Birks, J. B. Excimers. *Reports on Progress in Physics* **1975**, *38*, 903-974.

(19)   Lowry, T. H.; Richardson, K. S.: *Mechanism and Theory in Organic Chemistry*; Harper and Row Publishers: New York, 1987.

(20)   Stevens, B.; Hutton, E. Radiative Life-time of the Pyrene Dimer and the Possible Role of Excited Dimers in Energy Transfer Processes. *Nature* **1960**, *186*, 1045-1046.

(21)   Christophorou, L. G.; Abu-Zeid, M. E. M.; Carter, J. G. Emission and Decay of Liquid-Benzene and Naphthalene Derivatives Excited by Electron Impact. *The Journal of Chemical Physics* **1968**, *49*, 3775-3782.

(22)   Selinger, B. The photoassociation of some substituted naphthalenes. I. Rate constants and thermodynamic data for excited dimer formation. *Australian Journal of Chemistry* **1966**, *19*, 825-834.

(23)   Perkampus, H.; Pohl, L. Uber die Fluoreszenzspektren dunner Filme aromatischer Kohlenwasserstoffe. *Zeitschrift für Physikalische Chemie* **1964**, *40*, 162-188.

(24)   Birks, J. B.; Christophorou, L. G. `Excimer' Fluorescence. I. Solution Spectra of 1:2-Benzanthracene Derivatives. *Proceedings of the Royal Society of London. Series A. Mathematical and Physical Sciences* **1963**, *274*, 552-564.

(25)   Chu, N. Y. C.; Kearns, D. R. Monomer Emission from Excimer Forming Crystals: Pyrene and Perylene. *Molecular Crystals and Liquid Crystals* **1972**, *16*, 61-74.

(26)   Forster, T. Formation and Dissociation of Excited Dimers. *Pure and Applied Chemistry* **1963**, *7*, 73-78.

(27)   Birks, J. B. Higher Excited States of Benzene and Toluene Excimers. *Chemical Physics Letters* **1968**, *1*, 625-626.

(28)   Wolfbeis, O.; Berberan-Santos, M.: Fluorescence of Supermolecules, Polymers and Nanosystems. Springer: Verlag Berlin Heidelberg, 2008.

(29)   Nayak, M. K.; Dogra, S. K. Photophysics of 1-hydroxy- and 1-methoxy-9-fluorenone: II. Non-radiative deactivation. *Journal of Photochemistry and Photobiology A Chemistry* **2005**, *169*, 299-307.

(30)   Murphy, R. S.; Moorlag, C. P.; Green, W. H.; Bohne, C. Photophysical Characterization of Fluorenone Derivatives. *Journal of Photochemistry and Photobiology A Chemistry* **1997**, *110*, 123-129.

(31)   Shigeta, M.; Morita, M.; Konishi, G.-i. Selective Formation of Twisted Intramolecular Charge Transfer and Excimer Emissions on 2,7-bis(4-Diethylaminophenyl)-fluorenone by Choice of Solvent. *Molecules* **2012**, *17*, 4452-4459.

(32)   Scott, J. L.; Yamada, T.; Tanaka, K. Guest specific solid-state fluorescence rationalised by reference to solid-state structures and specific intermolecular interactions. *New Journal of Chemistry* **2004**, *28*, 447-450.

(33)   Chandross, E. A.; Dempster, C. J. Intramolecular excimer formation and fluorescence quenching in dinaphthylalkanes. *Journal of the American Chemical Society* **1970**, *92*, 3586-3593.

(34)   Mathauer, K.; Frank, C. W. Naphthalene chromophore tethered in the constrained environment of a self-assembled monolayer. *Langmuir* **1993**, *9*, 3002-3008.

(35)   Geddes, C. D.; Lakowicz, J. R.: *Advanced Concepts in Fluorescence Sensing: Part B: Macromolecular Sensing*; Springer, 2010.

(36)   Anslyn, E. V.; Dougherty, D. A.: *Modern Physical Organic Chemistry*; University Science Books: Sausalito, California, 2006.

(37)   Yoo, H.; Yang, J.; Yousef, A.; Wasielewski, M. R.; Kim, D. Excimer Formation Dynamics of Intramolecular π-Stacked Perylenediimides Probed by Single-Molecule Fluorescence Spectroscopy. *Journal of the American Chemical Society* **2010**, *132*, 3939-3944.

(38)   Yang, Z.; Karasz, F. E.; Geise, H. J. Intrinsically soluble copolymers with well-defined alternating substituted p-phenylenevinylene and ethylene oxide blocks. *Macromolecules* **1993**, *26*, 6570-6575.

(39)   Homnick, P. J.; Tinkham, J. S.; Devaughn, R.; Lahti, P. M. Engineering Frontier Energy Levels in Donor–Acceptor Fluoren-9-ylidene Malononitriles versus Fluorenones. *The Journal of Physical Chemistry A* **2013**, *118*, 475-486.

(40)   Aihara, J. Anomalous Solvatochromism of Charge-Transfer Absorption Bands. *Bulletin of the Chemical Society of Japan* **1981**, *54*, 1561-1562.

(41)   Homnick, P. J.; Lahti, P. M. Modular electron donor group tuning of frontier energy levels in diarylaminofluorenone push-pull molecules. *Physical Chemistry Chemical Physics* **2012**, *14*, 11961-11968.

(42)   Yu, C.; Yam, V. W.-W. Glucose sensing via polyanion formation and induced pyrene excimer emission. *Chemical Communications* **2009**, 1347-1349.

(43)   Ananthakrishnan, S. J.; Varathan, E.; Ravindran, E.; Somanathan, N.; Subramanian, V.; Mandal, A. B.; Sudha, J. D.; Ramakrishnan, R. A solution processable fluorene-fluorenone oligomer with aggregation induced emission enhancement. *Chemical Communications* **2013**, *49*, 10742-10744.

(44)   Yan, D.; Zhao, Y.; Wei, M.; Liang, R.; Lu, J.; Evans, D. G.; Duan, X. Regular assembly of 9-fluorenone-2,7-dicarboxylate within layered double hydroxide and its solid-state photoluminescence: a combined experiment and computational study. *RSC Advances* **2013**, *3*, 4303-4310.

(45)   Baghgar, M.; Labastide, J.; Bokel, F.; Dujovne, I.; McKenna, A.; Barnes, A. M.; Pentzer, E.; Emrick, T.; Hayward, R.; Barnes, M. D. Probing Inter- and Intrachain Exciton Coupling in Isolated Poly(3-hexylthiophene) Nanofibers: Effect of Solvation and Regioregularity. *The Journal of Physical Chemistry Letters* **2012**, *3*, 1674-1679.

(46)   Labastide, J. A.; Baghgar, M.; Dujovne, I.; Venkatraman, B. H.; Ramsdell, D. C.; Venkataraman, D.; Barnes, M. D. Time- and Polarization-Resolved Photoluminescence of Individual Semicrystalline Polythiophene (P3HT) Nanoparticles. *The Journal of Physical Chemistry Letters* **2011**, *2*, 2089-2093.

(47)   Labastide, J. A.; Baghgar, M.; McKenna, A.; Barnes, M. D. Time- and Polarization-Resolved Photoluminescence Decay from Isolated Polythiophene (P3HT) Nanofibers. *The Journal of Physical Chemistry C* **2012**, *116*, 23803-23811.

(48)   Zereg, M.; Durand, P.; Paidarová, I. About the Fermi golden rule and the computation of lifetimes of quantum resonances. *Physics Letters A* **1992**, *169*, 71-76.

(49)   Yuan, M.-S.; Wang, D.-E.; Xue, P.; Wang, W.; Wang, J.-C.; Tu, Q.; Liu, Z.; Liu, Y.; Zhang, Y.; Wang, J. Fluorenone Organic Crystals: Two-Color Luminescence Switching and Reversible Phase Transformations between π–π Stacking-Directed Packing and Hydrogen Bond-Directed Packing. *Chemistry of Materials* **2014**, *26*, 2467-2477.

CHAPTER 4

CONCLUSION, WITH PROSPECTS FOR FUTURE WORK: DONOR-ACCEPTOR DYADS, AND FLEXIBLE THIOPHENE-BASED ALTERNATING COPOLYMERS

4.1 Introduction

Understanding from a physical chemical standpoint the light-matter interactions that arise from inter- and intra-chromophore electronic communication has long been a goal of the scientific community[1-3]. With modern advances in optical spectroscopy, the ability to probe this behavior on the single-molecular level[4] and on the femtosecond timescale[5] has shed light on interactions that were previously beyond measurement. The design of novel systems that are engineered to probe poorly-understood processes has the potential to equip chemists with methods by which the next generation of conjugated materials can brought from theory to application.

As detailed in Chapters 2 and 3, the study of flexibly-linked bichromophoric dyads and segmented, alternating copolymers with flexible conjugation-interrupting units provides a range of photophysical behavior, whose study is valuable to understanding effects of solution-phase conformations and solid state morphological packing patterns of chromophores. This dissertation work shows that the inclusion of short but flexible tethers to link chromophores in segmented copolymers may provide a method to produce organic electronic devices with long-term performance stability and resistance to device degradation due to morphological changes, especially for OLED work. The results outlined in Chapter 3 also relate to the "green band" OLED impurity seen in oFPV and pFPV synthesized by Rathnayake et al[6-8]. As described in that chapter, green band emission is a major issue in fluorene-based OLED work, and the Chapter 3 results

showed the suppression of excimer emission by using longer linkers in fluorenone-incorporating dyads. A similar strategy may be effective in fluorene-incorporating, blue-emitting polymer-based OLEDs related to Rathnayake's pFPV.

In a further example of a class of materials that is particularly important in recent electronic materials development, polythiophene (PT) derivatives have been shown have several distinct excited state relaxation pathways in solution[9] and thin films[10], as well as in nanoparticle[11-13] and nanofiber[14-17] assemblies. Studies examining synthetically elaborated analogs of PT have the potential to isolate and identify the spectroscopic signatures of these different photophysical processes, and would be valuable in efforts to characterize and further improve the efficiency of organic electronic devices that utilize PT materials.

This chapter describes the design, some preliminary results, and proposed future work to extend further the study of photophysical processes in solution and in aggregates or the solid state. First, the design, preliminary proof of concept, and proposed synthesis and photophysical characterization of a fluorene-fluorenone-based dyad linked by flexible tethers will be discussed. Utilizing the folding capacity of the 2- and 8-carbon tethers reported in Chapters 3, such dyads would have the potential to extend elucidation of the source of "green band" emission reported in polyfluorene derivatives. Secondly, in an effort to expand the study described in Chapter 2 to the PT family of electronic materials, the synthesis and characterization of a septithiophene chromophore will be described, with proposed future extension of the work to segmented copolymers of the sort used Chapters 2-3. By employing the different degrees of flexibility of the tethers reported in Chapters 2-3, these copolymers may produce varying photophysical behavior

that helps deconvolute ensemble fluorescence spectra of polythiophene homopolymers, and as well as to identify stable and reproducible PT-based microstructures that favor particular fluorescent processes.

4.2 Fluorene-Fluorenone Donor-Acceptor Dyads -- Do Fluorene-fluorenone Dyads Contribute to Green Band Emission?

4.2.1 "Green Band" Emission in Poly(fluorene) Derivatives

As reported in Chapter 2, the appearance of a green fluorescence emission band (g-band) in thermally-stressed light emitting diodes based on the normally blue-fluorescent fluorene-incorporating polymers and their derivatives has been the subject of several studies during the past few decades[6-8,18-21]. Rathnayake in the Lahti group found[8] that OFPV and pFPV OLEDS gave a g-band that varied with differences in purifying the fluorene derivatives used on that OLED work.
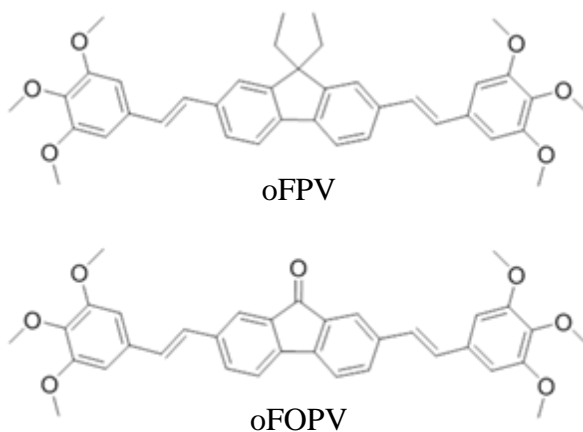
oFPV

oFOPV

Figure 4.1: Chemical structures of oFPV and oFOPV studied in Rathnayake et al.[8]

The purification of oFPV (Figure 4.1) -- the monomeric analogue of pOFPV -- by room temperature column chromatography gave a highly efficient blue-fluorescent (400-440 nm) species, but purification of the same compound by recrystallization from boiling organic solvents gave oFPV showing a mixture of expected blue fluorescence along with

a broad g-band emission having a maximum at ~560 nm. The appearance of the g-band was hypothesized to result from a small amount of oxidation of fluorene units to fluorenone, thus giving rise to fluorenone-based emission. In subsequent collaborative work between the Barnes and Lahti groups[6] it was noted that OFOPV excimer emission arising in solution and in single-molecule spectroscopy matched the long wavelength tail of the oFPV g-band but that the *main* g-band maximum region at around 560 nm matched monomeric oFOPV emission *in a non-solvated environment*. This is very reminiscent of the present findings for FOS and related dyads in Chapter 2 of this dissertation.
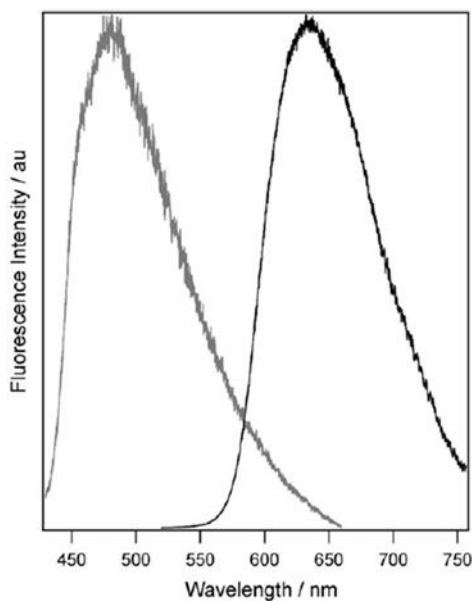
Figure 4.2: Bulk thin film emission spectra of oFOPV (black) compared to that of oFPV (gray). See Odoi et al.[6] (permission license number 3403101111149).

Solution-phase measurements of FOS in solution seem inconsistent with OFPV and pFPV g-band photoluminescence from a homo-molecular fluorenone excimer, since high concentrations give emission only at 600 nm or higher wavelength, not the 560 nm region of the g-band. FOS does give emission in the g-band region *in toluene*, however.
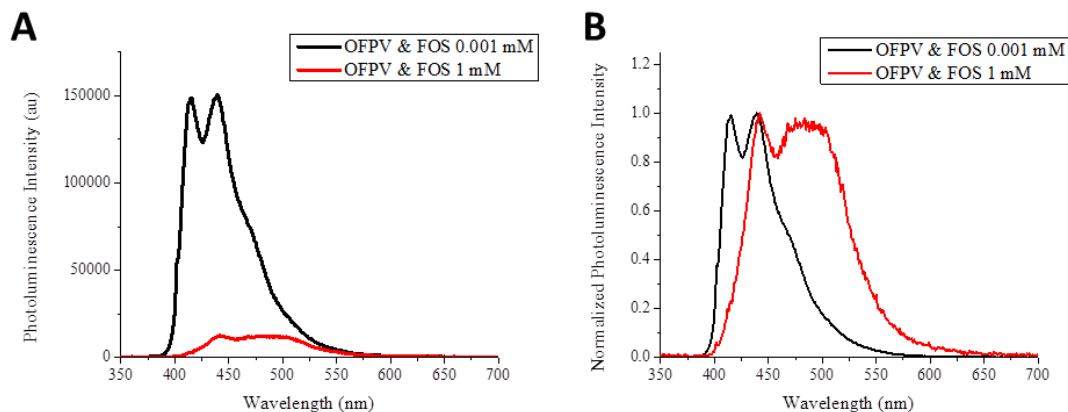
Figure 4.3: Fluorescence spectra of oFPV and FOS co-solutions in chloroform solution excited at 405 nm displayed in both absolute (A) and normalized (B) intensity.

This solvent-dependent result caused me to consider whether the g-band fluorescence and at least some of the other related emission behavior arises due to emission from solvent-influenced energy transfer events. Fluorene-fluorenone interactions are considered to be g-band sources based on other studies involving materials having deliberate incorporation of both fluorenone and fluorenone units[22,23]. This is not unreasonable for oFPV (and, by extention, pFPV) emision, since the amount of fluorenone required to give the g-band in oFPV is only 0.5-1%[8], making direct fluorenone-fluorenone contacts rare in the nearly immobilized solid state. As a simple test for an energy transfer fluorene-fluorenone based g-band, I measured the solution PL spectra of co-dissolved equimolar amounts of FOS and OFPV at different concentrations in chloroform. As shown in Figure 4.3, at a concentration of 0.001 mM of *both* OFPV and FOS, only the blue fluorescent signal typical of oFPV is seen (400-440 nm). As the concentration of both species is increased by a factor of 10^3, a longer wavelength g-band like fluorescence becomes quite prevalent while the oFPV emission spectrum is quenched. Since the concentration of FOS in the 1 mM sample is quite high, it is remarkable that there is no sign of the 600 nm fluorenone

excimer in this situation: the 600 nm band is readily seen in the FOS-only solutions at this concentration. This indicates that the proposed energy transfer event between fluorene and fluorenone is a faster and easier process than fluorenone excimer formation. Additionally, given that any oFPV-FOS exciplex emission should occur with a fundamentally lower intensity than the monomeric fluorescence[24], the decreased absolute intensity of the "g-band" seen in Figure 4.3A (relative to low concentration oFPV emission intensity) gives credence to the possibility that a g-band emission arises from fluorene-fluorenone exciplex emission here. Given other evidence for emission from fluorene-fluorenone mixtures and possibly from exciplexes between them based on behavior in other systems[22,23], it is not unreasonable to consider that the g-band in Figure 4.3 results from this type of bimolecular relaxation pathway caused by interaction between fluorene and fluorenone encounters leading to direct molecular orbital overlap.

Considering the above information, the g-band in oFPV and pFPV seems to result from a hetero-bimolecular process. To date, there have been no studies probing synthetic systems that exclusively exhibit g-band emission in solution at lower concentration, but utilizing the research presented in Chapter 3, a test system composed of a fluorenone pendant and a fluorene pendant linked by a short tether may provide a method of examining this bimolecular process in a single molecule under dilute conditions to learn whether the g-band can be assigned to a single structure. The following subsection describes a possible synthetic approach to such a system.

4.2.2 Proposed Experimental Design and Preliminary Results for Fluorene-Fluorenone Interaction Photophysics

Figure 4.4 displays potential target donor-acceptor dyads for the proposed fluorene-fluorenone exciplex study. As I learned during the studies reported in Chapter 3,

the two-carbon tether allows the dyad to occupy a folded conformation, while the 8-carbon tether inhibits intramolecular excimer formation. The two- and eight-carbon tethers are therefore recommended for this study.

FFOFx2

FFOFx8
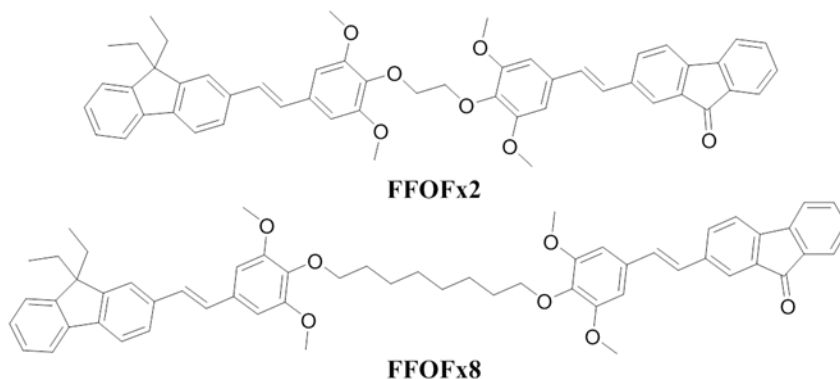
Figure 4.4: Chemical structures of proposed fluorene/fluorenone-based dyads.

Since these systems are asymmetrical, utilizing the exact synthetic approach of Chapter 2 used to make the FOSFx series would not be effective. However, using similar synthetic processes to extend the dyad systematically should work, starting with the fluorene-based chromophore and finishing by attaching a fluorenone-based chromophore previously reported in Chapter 3 in a step-wise fashion. The proposed syntheses of FFOFx2 and FFOFx8 are displayed in Scheme 4.1.
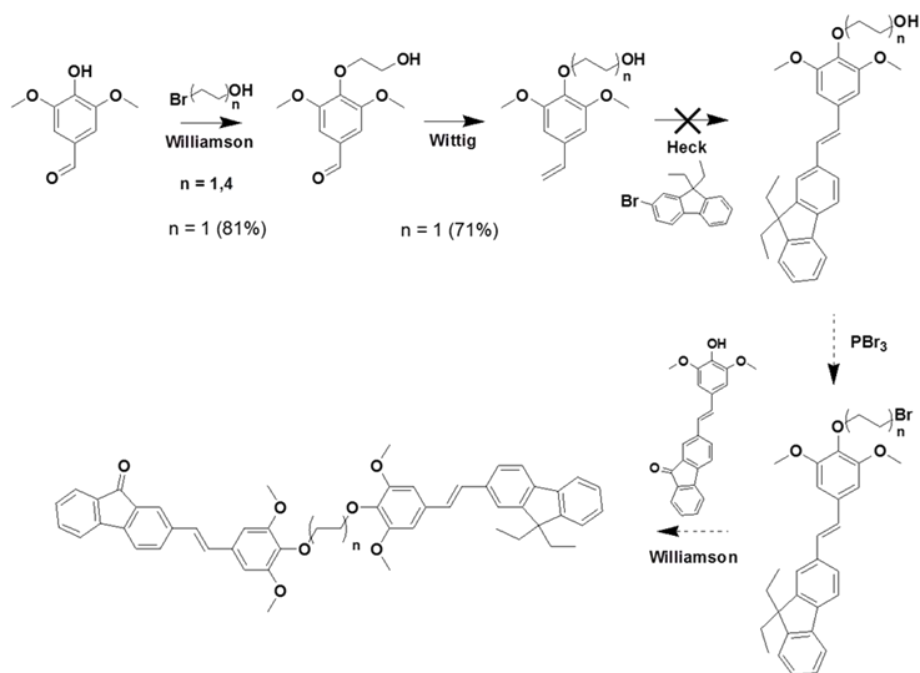
Scheme 4.1: Proposed synthetic route to FFOFx2 and FFOFx8.

During my preliminary efforts to synthesize FFOFx2, the first two steps
(Williamson and Wittig reactions) gave yields comparable to those obtained in the
synthesis of the FOSFx series described in Chapter 3. Full details describing the synthesis
of these two precursors from the figure are given in Chapter 5. However, the Heck
coupling reaction of 2-bromo-9,9-diethyl fluorene and 2-(2,6-Dimethoxy-4-vinyl-
phenoxy)-ethanol gave no amount of usable product due to low yields and difficulties
with purification. Still, the presence of trans-vinylene protons in the preliminary ^{1}HNMR
spectrum and the visibly blue fluorescent color of the crude reaction mixture suggest that
some amount of the desired product was formed. Utilizing other cross-coupling catalysts,
ligands, additives and solvents in a microwave-assisted reaction should produce the
fluorene-based pendent in usable amounts. If this challenge can be overcome, the
remaining two synthetic steps should be comparatively straightforward. If not, an
alternate synthetic route to FFOFx2 and FFOFx8 is shown in Scheme 4.2, which involves

preparation of the chromophore pendants separately by methods similar to those utilized

in the synthesis of FOSFx2 in Chapter 3. Considering the success of the Heck reaction
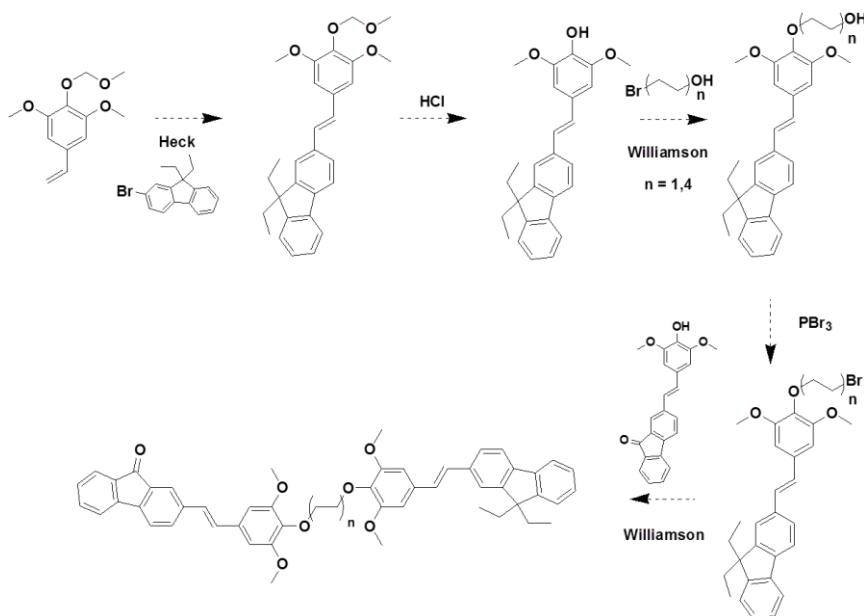
Scheme 4.2: Alternate synthetic route to FFOFx2 and FFOFx8.

between the MOM-protected syringyl unit and 2-bromofluorenone described in Chapter

3, should Scheme 4.1 fail, Scheme 4.2 would be a logical alternative.

If these target molecules can be made analytically pure, solution-phase

photoluminescence studies should provide previously unprobed results concerning the

identity of the g-band. As learned from the FOSFx series, the 2-carbon flexible linker

allows excimer formation through dyad folding, while the 8-carbon flexible unit renders

pendent chromophores unlikely to form excimeric interactions. At high concentrations

(~1 mM), the g-band should be quite prevalent in the mixed dyad systems, because at that

concentration, *intermolecular* encounters that lead to g-band emission should be common

(by analogy to the results of Figure 4.3). Taking into account that intermolecular energy

transfer can occur at distances of 10-100 nm[2], while exciplex formation requires intimate

molecular orbital overlap between chromophores[26], if both dyads produce the g-band at low concentrations (<0.001 mM), the g-band can be attributed to an energy transfer process. If, however, only FFOFx2 is capable of producing the g-band, energy transfer can be ruled out as the cause of the green emission band, and exciplex formation becomes the more-likely g-band emitter.

4.3 Flexible Septihiophene-based Segmented Copolymers

4.3.1 Background on Polythiophene Photophysics

Crystalline aggregates of PT derivatives, such as poly(3-hexylthiophene) (P3HT), show complex and varied internal electronic environments that are acutely sensitive to polymer properties (molecular weight, polydispersity and regioregularity)[14], as well as processing conditions (annealing, solvent composition, speed of crystallite formation)[27-29]. The further development of nanostructured P3HT as a more efficient photovoltaic material has proven critical in organic photovoltaic development, to promote exciton dissociation and charge transport while inhibiting competing processes by which excitons recombine[12,30-33]. By utilizing systems with flexible linkages as demonstrated in this dissertation, finding and manipulating structural parameters that control the electronic communications in P3HT structures to optimize exciton dissociation and charge transport could be much improved.

Considerable effort has been put into identifying and characterizing excitonic processes important to photovoltaic function[32,33]. A combination of x-ray diffraction measurements and spectroscopic techniques, which provide spectral wavelength, process timescale, and polarization resolution, has helped to further our understanding of the structural origins of these processes on the molecular scale[11,12,14,16]. In crystalline P3HT, lamellar sheets of polymer chains assemble into cofacial π-stacks[34]. In other equilibrium

nanostructures, such as extended nanofibers, the polymer backbones are oriented

transverse to the π-stack axis, and are approximately planar[14,16]. The electronic

environment that results from this collection of closely spaced, planar polymer chains is

an HJ-aggregate: a structure in which excitonic processes take place in both the

interchain (H) and intrachain (J) directions[35]. However, current extended P3HT

nanostructures are inefficient photovoltaic materials due in part to the fact that J–type

coupling dominates the excitonic environment. To improve the functionality of P3HT

nanostructures, radiative intrachain processes should be inhibited, and interchain

communication enhanced[11-14,16,17,35].

These two coupling mechanisms should be sensitive to the spacing of cofacial

thiophene ring alignment in π-stacked structures. It should be possible to manipulate

intrachain versus interchain interaction parameters through structural design. Specifically,

connecting oligothiophene chains in ways that allow or forbid them to assemble into

intrachain π-stacked conformations should provide fundamental insight into the

geometric requirements for H-aggregation. In the proposal for future work given below to

probe these requirements, intrachain J-aggregation will be minimized by utilizing specific

oligomers of 7 thiophene units long, which is below the effective conjugation length for

PT[36], yet long enough to be considered a reasonable mimic of polymeric analogs.

4.3.2 Proposed Molecular Design and Preliminary Results for Oligothiophene Interaction Photophysics

By analogy to the Chapter 2 work, installing flexible linkers of appropriate

lengths provides a test to diminish or enhance the H-aggregate relaxation processes for

oligothiophenes. Chemical structures of the proposed septithiophene-based, segmented

alternating copolymers are given in Figure 4.5.
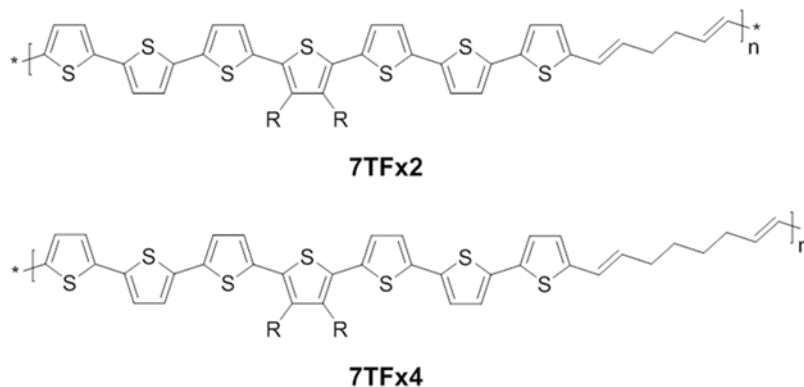
7TFx2

7TFx4

Figure 4.5: Chemical structures of 7TFx2 and 7TFx4.

Scheme 4.3 displays a synthetic route to form 7TDA, a septithiophene chromophore with solubilizing hexyl chains attached to the center thiophene ring and terminal aldehydes to facilitate Wittig polymerization.
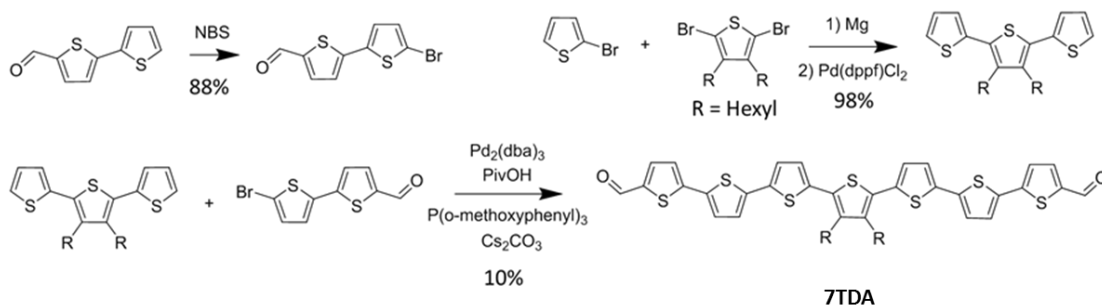
Scheme 4.3: Synthetic route to 7TDA.

In my hands, NBS bromination of bithiophene-carbaldehyde followed by Kumada coupling resulted in high yields of 88% and 98%, respectively, with relatively easy purification, although completion of the Kumada reaction requires utmost care in maintaining a completely anhydrous reaction environment, which includes flame drying of not only all reaction glassware, but the reactant magnesium turnings as well. In initial efforts to carry out the final step, direct hetero-arylation (DHA) coupling of the terthiophene and bithiophene monomers was fairly straightforward, but gave an average yield of 10% after purification, and required a difficult and time-consuming column

101

chromatography to isolate the pure product. However, considering the small amounts of polymer required for spectroscopy, ensuring a high yield polymerization will make this low yield step an acceptable method of producing the monomer, if future use remains inherently low-yield.
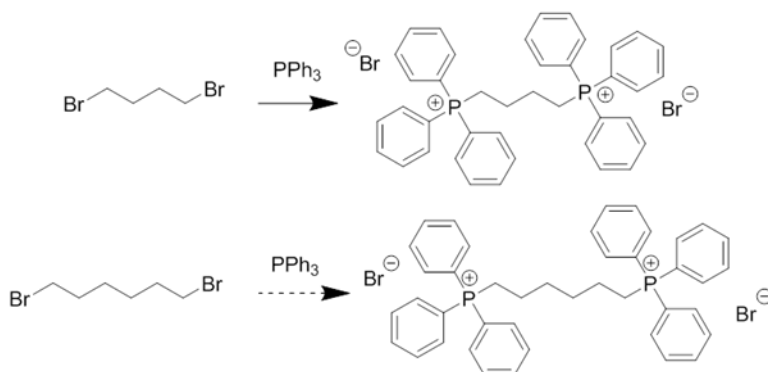
Scheme 4.4: Synthesis of aliphatic 4-carbon and 6-carbon monomers.

Scheme 4.4 displays the proposed synthesis of triphenylphosphonium bromide-functionalized linkers that could be Wittig-polymerized with 7TDA to form 7TFx2 and 7TFx4, using methods adapted from the literature[37].

7TFx2 (n = 1)
7TFx4 (n = 2)
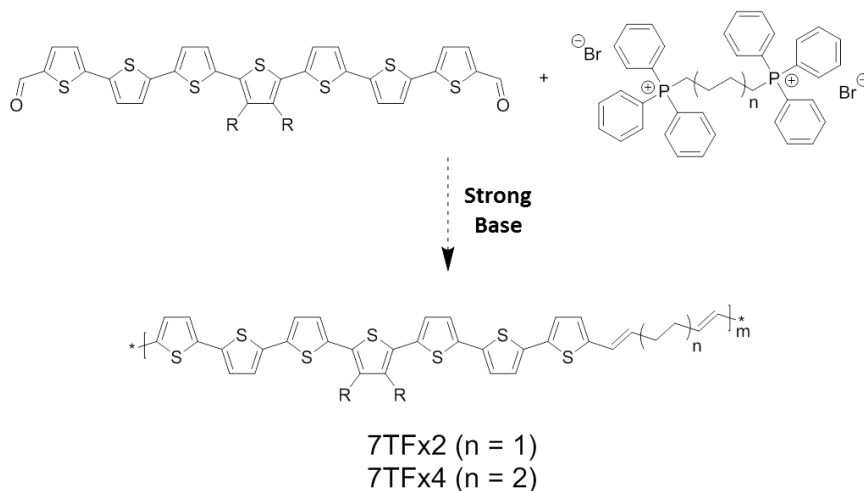
Scheme 4.5: Proposed synthetic route to 7TFx2 and 7TFx4.

Scheme 4.5 displays the proposed synthetic route to make 7TFx2 and 7TFx4 via Wittig

polymerization. While using conventional methods to complete this reaction would

require n-butyllithium to be used as the base due to the low acidity of the alkylated

phosphonium bromide, utilizing microwave synthesis to run the polymerization at a high

temperature and pressure may allow the use of a less powerful base, such as sodium t-

butoxide.
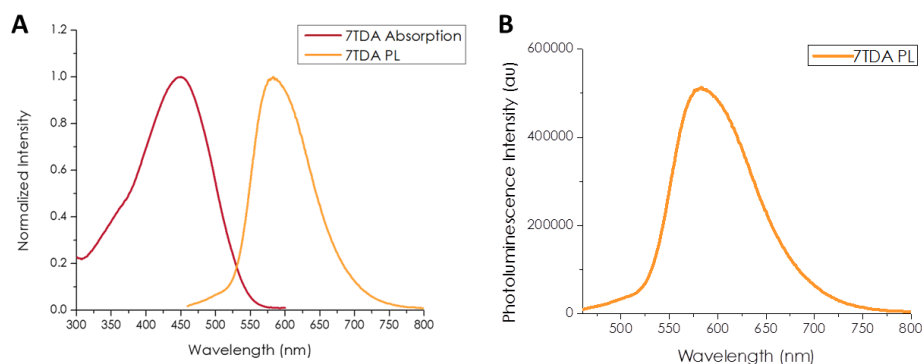
Figure 4.6: (A) Normalized absorption (red) and photoluminescence (orange) spectra of 7TDA (normalized with respect to peak maxima), and (B) absolute photoluminescence intensity of 7TDA (0.01 mM in chloroform). Photoluminescence was obtained using a 450 nm excitation.

Figure 4.6 shows preliminary spectroscopy done for 7TDA in chloroform. In

solution, the primary absorption peak occurs at 450 nm, with a fluorescence maximum at

~580 nm. Neither curve shows resolved vibronic structure, which suggests that any

aggregates that may be present in solution are not well-organized. .

In collaboration with Joelle Labastide of the Barnes spectroscopy lab, solution

versus solid phase PL spectra of 7TDA were obtained (Figure 4.7) for a single droplet of

0.01 mM 7TDA chloroform solution, compared to the spectrum of the same sample as a

dried solid film after solvent evaporation. The droplet emits broadly at ~550 nm while

still wet, but after drying, the peak at ~550 is replaced by a vibronic progression from

~550-700 nm. Interestingly, the presumptive 0-0 transition at 610 nm is lower in intensity than the presumptive 0-1 transition at ~655 nm, which strongly indicates that 7TDA forms of H-aggregates as it precipitates under these conditions.
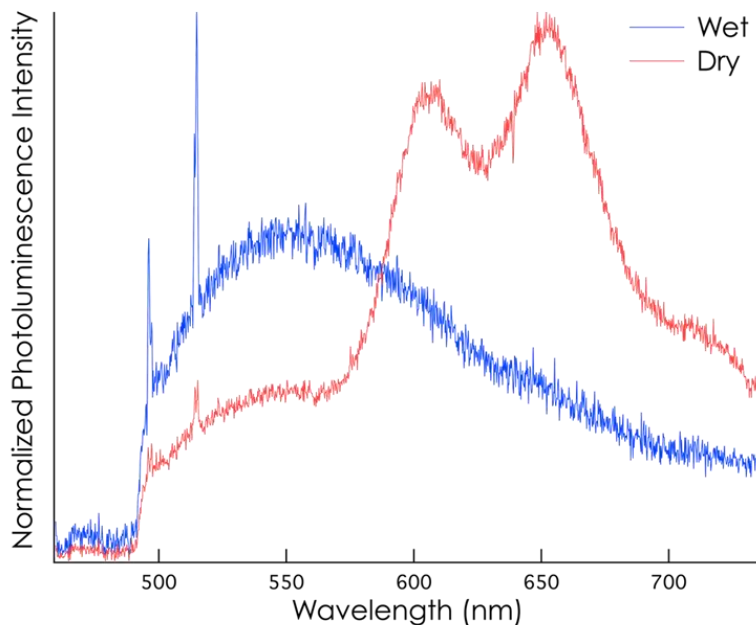
Figure 4.7: Photoluminescence spectra of 7TDA excited at 455 nm in chloroform before (wet, blue) and after drying (dry, red).

After sampling many areas of the dropcast film, the ratio of the 0-0 and 0-1 transitions was shown to be highly reproducible (Figure 4.8), which suggests that in this case, 7TDA can be used as an experimental control to gauge any enhancement (or attenuation) of aggregation-induced processes that manifest in segmented copolymers such as 7TFx2 or 7TFx4.
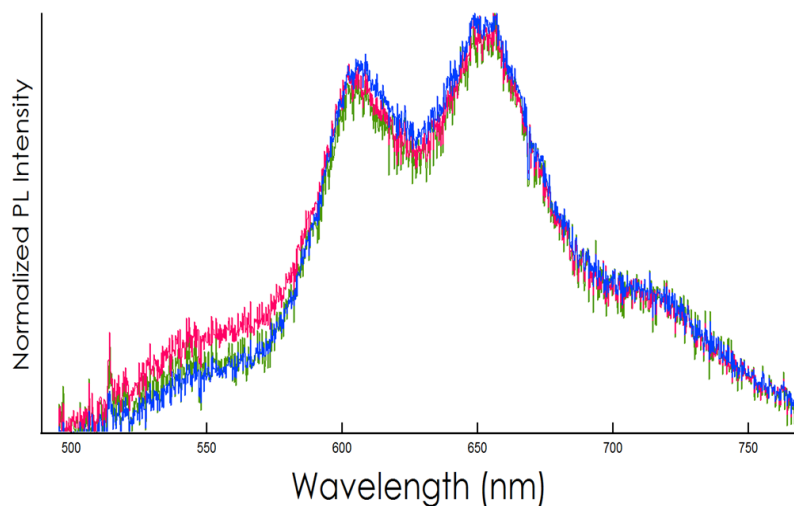
Figure 4.8: Photoluminescence spectra of 7TDA from 3 separate areas of a dropcast film, showing the reproducibility of the 0-0 to 0-1 transition intensity ratio.
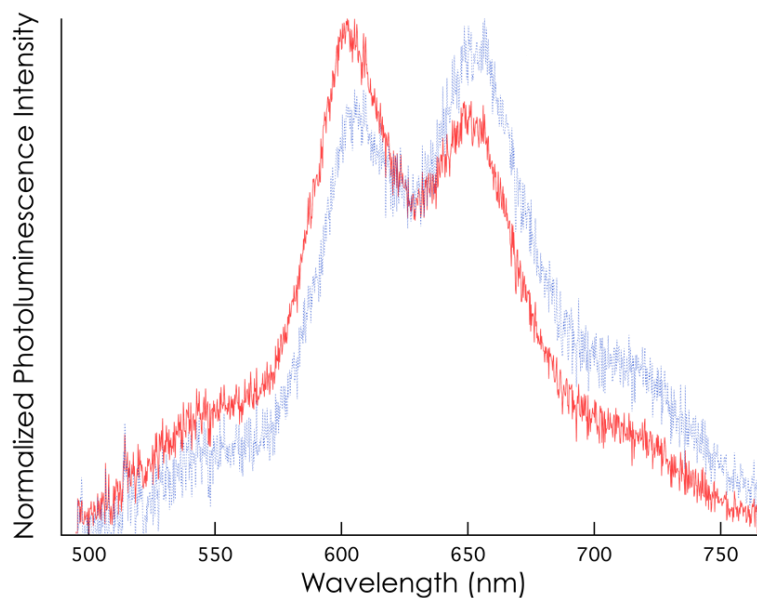
Figure 4.9: Photoluminescence spetra of 7TDA from 2 separate dropcast films, showing a reversal of the 0-0 to 0-1 transition intensity ratio.

One area of the 7TDA dropcast film did show some variation in 0-0 to 0-1 intensity ratio. Figure 4.9 shows the PL spectrum of this area (Figure 4.9, red) normalized along with one PL spectrum from an area reported in Figure 4.8 (Figure 4.9, blue) for

comparison. This area showed a reversal in the intensity of the 0-0 and the 0-1 transitions, which is a typical indication of J-aggregation. However, only a single area on the film exhibited this reversal, and attempts to find another area with matching spectral curvature were unsuccessful. This suggests that H-aggregation is favored by 7TDA, but that J-aggregation might be achieved by varying film deposition conditions (for example, by varying the surface on which deposition occurs).

As in Chapters 2-3, time-resolved photoluminescence measurements will be well suited to investigate the relative contributions of multi-chromophore radiative events, which will manifest as an increase (or decrease) in the amount of any fast decay rate (τ_1) relative to isolated chromophore decay results. Changes in the relative contribution of J- and H-type vibronic couplings should be apparent in the relative ratios of 0-0 to 0-1 vibronic bands in the emission spectra, which can be used as to evaluate changes in the ratio of inter-and intrachain coupling as a function of copolymer flexibility. TEM and electron diffraction measurements may also be of use in defining the general form and degree of crystallinity of any morphological features these systems display in the solid state. The steady state and time-resolved photophysical data could then be correlated with morphological features to develop structure-property relationships relating H-aggregation to structure and morphology in PT derivatives. Additionally, as was the case for the oligophenylenevinylene derivatives described in Chapter 2, the photophysics of dropcast films of 7TFx2 and 7TFx4 may show resistance to thermal annealing, offering a solution to the problems that plague PT derivatives in their applications as organic electronic materials.

4.4 Concluding Remarks

The proposed work on donor-acceptor dyads may play a defining role in clarifying the mystery of the g-band fluorescence seen in oxidatively degraded polyfluorenes. The proposed study on flexibly linked, septithiophene-based segmented alternating copolymers should provide additional answers to critical questions concerning control and understanding of the photophysical behavior of polythiophenes in solid state applications, and may provide a method by which PT's and other polymers can be made more photophysically stable in thin films. If proven successful, these logical extensions of my work have the potential to provide structure-property relationships between photophysics and assembly, which will aid in developing a better understanding of solid state organic photophysics as a function of interchromophore interactions.

4.5 References

(1)   Geddes, C. D.; Lakowicz, J. R.: *Advanced Concepts in Fluorescence Sensing: Part B: Macromolecular Sensing*; Springer, 2010.

(2)   Lakowicz, J. R.: *Principles of Fluorescence Spectroscopy*; Springer, 2007.

(3)   Lowry, T. H.; Richardson, K. S.: *Mechanism and Theory in Organic Chemistry*; Harper and Row Publishers: New York, 1987.

(4)   Moerner, W. E.; Fromm, D. P. Methods of single-molecule fluorescence spectroscopy and microscopy. *Review of Scientific Instruments* **2003**, *74*, 3597-3619.

(5)   Gadermaier, C.; Lanzani, G. Photophysics of conjugated polymers: the contribution of ultrafast spectroscopy. *Journal of Physics: Condensed Matter* **202**, *14*.

(6)   Odoi, M. Y.; Hammer, N. I.; Rathnayake, H. P.; Lahti, P. M.; Barnes, M. D. Single-Molecule Studies of a Model Fluorenone. *ChemPhysChem* **2007**, *8*, 1481-1486.

(7)   Rathnayake, H. P.; Cirpan, A.; Delen, Z.; Lahti, P. M.; Karasz, F. E. Optimizing OLED Efficacy of 2,7-Diconjugated 9,9-Dialkylfluorenes by Variation of Periphery Substitution and Conjugation Length. *Advanced Functional Materials* **2007**, *17*, 115-122.

(8)   Rathnayake, H. P.; Cirpan, A.; Karasz, F. E.; Odoi, M. Y.; Hammer, N. I.; Barnes, M. D.; Lahti, P. M. Luminescence of Molecular and Block Copolymeric 2,7-Bis(phenylethenyl)-fluorenones; Identifying Green-Band Emitter Sites in a Fluorene-Based Luminophore. *Chemistry of Materials* **2007**, *19*, 3265-3270.

(9)   Cook, S.; Furube, A.; Katoh, R. Analysis of the excited states of regioregular polythiophene P3HT. *Energy & Environmental Science* **2008**, *1*, 294-299.

(10)   Fichou, D.; Horowitz, G.; Xu, B.; Garnier, F. Low temperature optical absorption of polycrystalline thin films of α-quaterthiophene, α-sexithiophene and α-octithiophene, three model oligomers of polythiophene. *Synthetic Metals* **1992**, *48*, 167-179.

(11)   Labastide, J. A.; Baghgar, M.; Dujovne, I.; Venkatraman, B. H.; Ramsdell, D. C.; Venkataraman, D.; Barnes, M. D. Time- and Polarization-Resolved Photoluminescence of Individual Semicrystalline Polythiophene (P3HT) Nanoparticles. *The Journal of Physical Chemistry Letters* **2011**, *2*, 2089-2093.

(12)   Labastide, J. A.; Baghgar, M.; Dujovne, I.; Yang, Y.; Dinsmore, A. D.; G. Sumpter, B.; Venkataraman, D.; Barnes, M. D. Polymer Nanoparticle Superlattices for Organic Photovoltaic Applications. *The Journal of Physical Chemistry Letters* **2011**, *2*, 3085-3091.

(13)   Nagarjuna, G.; Baghgar, M.; Labastide, J. A.; Algaier, D. D.; Barnes, M. D.; Venkataraman, D. Tuning Aggregation of Poly(3-hexylthiophene) within Nanoparticles. *ACS Nano* **2012**, *6*, 10750-10758.

(14)   Baghgar, M.; Labastide, J.; Bokel, F.; Dujovne, I.; McKenna, A.; Barnes, A. M.; Pentzer, E.; Emrick, T.; Hayward, R.; Barnes, M. D. Probing Inter- and Intrachain Exciton Coupling in Isolated Poly(3-hexylthiophene) Nanofibers: Effect of Solvation and Regioregularity. *The Journal of Physical Chemistry Letters* **2012**, *3*, 1674-1679.

(15)   Hammer, B. A. G.; Bokel, F. A.; Hayward, R. C.; Emrick, T. Cross-Linked Conjugated Polymer Fibrils: Robust Nanowires from Functional Polythiophene Diblock Copolymers. *Chemistry of Materials* **2011**, *23*, 4250-4256.

(16)   Labastide, J. A.; Baghgar, M.; McKenna, A.; Barnes, M. D. Time- and Polarization-Resolved Photoluminescence Decay from Isolated Polythiophene (P3HT) Nanofibers. *The Journal of Physical Chemistry C* **2012**, *116*, 23803-23811.

(17)   Barnes, M. D.; Baghar, M. Optical probes of chain packing structure and exciton dynamics in polythiophene films, composites, and nanostructures. *Journal of Polymer Science Part B: Polymer Physics* **2012**, *50*, 1121-1129.

(18)   He, B.; Li, J.; Bo, Z.; Huang, Y. Studies of Green Emission in Polyfluorenes Using a Model Polymer. *Polymer* **2007**, *39*, 1345-1350.

(19)   Gamerith, S.; Gadermaier, C.; Scherf, U.; List, E. J. W.: The Origin of the Green Emission Band in Polyfluorene Type Polymers. In *Physics of Organic Semiconductors*; Wiley-VCH Verlag GmbH & Co. KGaA, 2006; pp 153-181.

(20)   Ferenczi, T.; Sims, M.; Bradley, D. D. C. On the nature of the fluorenone-based emission in oxidized poly(dialkyl-fluorene)s. *Journal of Physics: Condensed Matter* **2008**, *20*.

(21)   Liu, L.; Lu, P.; Wang, H.; Tang, S.; Wang, Z.; Zhang, W.; Ma, Y. Role of nonemissive quenchers for the green emission in polyfluorene. *Journal of Physical Chemistry B* **2007**, *111*, 10639-10644.

(22)   Kulkarni, A. P.; Kong, X.; Jenekhe, S. A. Fluorenone-Containing Polyfluorenes and Oligofluorenes: Photophysics, Origin of the Green Emission and Efficient Green Electroluminescence†. *The Journal of Physical Chemistry B* **2004**, *108*, 8689-8701.

(23)   Romaner, L.; Pogantsch, A.; Scandiucci de Freitas, P.; Scherf, U.; Gaal, M.; Zojer, E.; List, E. J. W. The Origin of Green Emission in Polyfluorene-Based Conjugated Polymers: On-Chain Defect Fluorescence. *Advanced Functional Materials* **2003**, *13*, 597-601.

(24)   Gordon, M.; Ware, W. R.: *The Exciplex*; Academic Press: New York, 1975.

(25)   Gebler, D. D.; Wang, Y. Z.; Fu, D.-K.; Swager, T. M.; Epstein, A. J. Exciplex emission from bilayers of poly(vinyl carbazole) and pyridine based conjugated copolymers. *The Journal of Chemical Physics* **1998**, *108*, 7842-7848.

(26)   Birks, J. B. Excimers. *Reports on Progress in Physics* **1975**, *38*, 903-974.

(27)   Chen, D.; Nakahara, A.; Wei, D.; Nordlund, D.; Russell, T. P. P3HT/PCBM Bulk Heterojunction Organic Photovoltaics: Correlating Efficiency and Morphology. *Nano Letters* **2010**, *11*, 561-567.

(28)   Liu, F.; Gu, Y.; Shen, X.; Ferdous, S.; Wang, H.-W.; Russell, T. P. Characterization of the morphology of solution-processed bulk heterojunction organic photovoltaics. *Progress in Polymer Science* **2013**, *38*, 1990-2052.

(29)   Liu, F.; Zhao, W.; Tumbleston, J. R.; Wang, C.; Gu, Y.; Wang, D.; Briseno, A. L.; Ade, H.; Russell, T. P. Understanding the Morphology of PTB7:PCBM Blends in Organic Photovoltaics. *Advanced Energy Materials* **2014**, *4*, n/a-n/a.

(30)   Lanzani, G.: *Photophysics of Molecular Materials: From Single Molecules to Single Crystals*; Wiley, 2006.

(31)   Pandit, B.; Gautam, B. R.; Basel, T. P.; Vardeny, Z. V. Correlation between ultrafast transient photomodulation spectroscopy and organic photovoltaic solar cell efficiency based on RR-P3HT/PCBM blends. *Organic Electronics* **2014**, *15*, 1149-1154.

(32)   Morfa, A. J.; Barnes, T. M.; Ferguson, A. J.; Levi, D. H.; Rumbles, G.; Rowlen, K. L.; van de Lagemaat, J. Optical characterization of pristine poly(3-hexyl thiophene) films. *Journal of Polymer Science Part B: Polymer Physics* **2011**, *49*, 186-194.

(33)   Reid, O. G.; Malik, J. A. N.; Latini, G.; Dayal, S.; Kopidakis, N.; Silva, C.; Stingelin, N.; Rumbles, G. The influence of solid-state microstructure on the origin and yield of long-lived photogenerated charge in neat semiconducting polymers. *Journal of Polymer Science Part B: Polymer Physics* **2012**, *50*, 27-37.

(34)   Sirringhaus, H.; Brown, P. J.; Friend, R. H.; Nielsen, M. M.; Bechgaard, K.; Langeveld-Voss, B. M. W.; Spiering, A. J. H.; Janssen, R. A. J.; Meijer, E. W.; Herwig, P.; de Leeuw, D. M. Two-dimensional charge transport in self-organized, high-mobility conjugated polymers. *Nature* **1999**, *401*, 685.

(35)   Spano, F. C.; Silva, C. H- and J-Aggregate Behavior in Polymeric Semiconductors. *Annual Review of Physical Chemistry* **2014**, *65*, 477-500.

(36)   Wohlgenannt, M. Confind and delocalized polarons in pi-conjugated oligomers and polymers: A study of the effective conjugation length. *Physical Review B* **2004**, *69*.

(37)   Kolodiazhnyi, O. I.: *Phosphorus Ylides: Chemistry and Applications in Organic Synthesis*; Wiley, 2008.

CHAPTER 5

EXPERIMENTAL METHODS

5.1 Materials, General Synthetic Methods, Sample Preparation and Instrumental Procedures

Solvents and reagents were purchased from Fisher Scientific or Sigma-Aldrich and used as received unless stated otherwise. Tetrahydrofuran was distilled from sodium-benzophenone under nitrogen just before use. Spectroscopic grade solvents were used as received without further purification. Reported melting points are uncorrected.

All reactions were heated with a heating mantle controlled by a variable rheostat unless otherwise stated. Microwave assisted synthesis was carried out using a CEM START SYNTH microwave reactor, using CEM disposable microwave reaction vessels capped with CEM silicone/PTFE caps. Microwave pressure limits were set to 300 PSI, and the MAX POWER cooling option was used in all reactions.

Melt-cast films of some solid organic sample were made by placing a small amount of analyte powder onto a borosilicate glass plate and heating the substrate on a hot plate until melting was complete. The melt-cast film was then cooled on a metal plate. Drop-cast films were cast by dropping the analyte solution (0.01 mM in chloroform) onto a borosilicate glass plate. The films were then allowed to dry slowly under a bell jar flushed with nitrogen gas. Annealing of drop-cast films was conducted by placing on a pre-heated hot plate at 120 °C for two minutes.

^{1}H NMR spectra were obtained at 400 MHz in solution using a Bruker Avance 400 instrument: peak positions are reported in ppm downfield of tetramethylsilane.

Polymer molecular weight and dispersity (Đ) analysis was carried out by gel-permeation chromatography (GPC) in 1,2,4-trichlorobenzene at 135 °C using a Polymer Laboratories PL-220 high-temperature GPC instrument calibrated against polystyrene standards. Dynamic light scattering (DLS) measurements were obtained on a Malvern Nano Zetasizer using 0.01 mM polymer solutions in acetonitrile that were passed through a 0.45 μm PTFE filter disk. UV-vis absorption and photoluminescence (PL) spectra were obtained in quartz cuvettes (solution) or on borosilicate glass plates (solid films), using a Shimdazu UV-2600PC spectrometer and a PTI QM-30 fluorimeter, respectively. Mass spectral analyses were carried out at the University of Massachusetts Amherst Mass Spectrometry Center using either electron ionization (EI) or fast atom bombardment (FAB). Emission quantum yields in spectrograde chloroform were determined at an excitation wavelength of 420 nm using external standard coumarin-6 (ethanol, quantum yield = 0.78): a solvent refractive index correction was made as part of the determination[1].

Time-resolved photoluminescence measurements were carried out by Joelle Labastide of the M. D. Barnes group, using a fluorescence microscope outfitted with a 100×/1.4 N.A. immersion oil objective, configured for epi-illumination. A pulsed photodiode laser (PicoQuant PDL LDH-P-C-440B) with a 10 MHz repetition rate provided a 440 nm excitation source. Data were collected through a 480 nm long pass filter using a precision avalanche photodiode (IDquantique) that was registered to the microscope confocal spot, and a time-correlated single photon counting (TCSPC) module (PicoQuant PicoHarp 300). TCSPC histograms were analyzed using the SymPhoTime

program from PicoQuant, and normalized to their respective maxima for easy

comparison[2].

Transmission electron microscopy (TEM) images were obtained by Dr. Lang Wei

of the Lahti group, using a JEOL JEM-2000FX transmission electron microscope. The

typical procedure is that one drop of freshly prepared polymer dispersion (0.01 mM

chloroform solution) was deposited on a carbon-coated copper grid (Electron Microscopy

Sciences, carbon film on 400 square mesh copper grid) and left to dry overnight. Some

samples were subjected to an additional annealing process of 2 min at 120 °C.

Subsequent sample investigations were performed at room temperature using an

accelerating voltage of 200 kV.

5.2 Synthetic Methods, Purification Procedures and Characterization Data
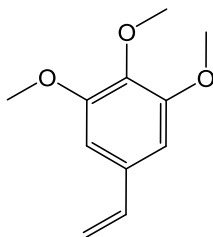
5.2.1 Trimethoxystyrene (1,2,3-trimethoxy-5-vinylbenzene).

Adapted from a literature procedure[3]. Methyltriphenylphosphonium bromide

(2.35 g, 6.6 mmols) was suspended in 40 mL of dry tetrahydrofuran in a 3-neck round

bottom flask under a nitrogen atmosphere. The suspension was cooled to 0 °C and 2.5 M

n-butyllithium (3.0 mL in hexanes, 7.5 mmol) was injected dropwise by syringe. The

color of the suspension slowly changed from white to orange. After stirring for 30 min,

the solution was allowed to warm to 20 °C. A solution of 3,4,5-trimethoxybenzaldehyde

(0.98 g, 5 mmol) in 10 mL of dry tetrahydrofuran was then added via cannula to the

stirring ylide solution. After stirring at room temperature for 24 h, the reaction was

114

carefully poured into 100 mL of water. The aqueous layer was extracted with diethyl ether (3×30-mL). The combined organic layers were dried over anhydrous magnesium sulfate, filtered and concentrated onto silica gel for column chromatography. The product was then purified by elution with diethyl ether, yielding a yellow oil (0.85 g, 88% yield). FT-IR (liquid, cm^{-1}): 3086 (w), 2958 (s), 2935 (s), 1724 (s), 1692 (m), 1630 (s), 1582 (s), 1505 (s), 1462 (s), 1408 (s), 1326 (s), 1275 (m), 1239 (s), 1184 (m), 1112 (s), 1073 (m), 1007 (m), 943 (w), 838 (m), 777 (m), 744 (w), 707 (w). ^{1}H NMR (CDCl$_3$, 400 MHz): δ (ppm) = 3.84 (s, 3H), 3.88 (s, 6H), 5.21 (d, 1H, J = 12 Hz), 5.66 (d, 1H, J = 20 Hz), 6.63 (t, 3H, J = 4 Hz).
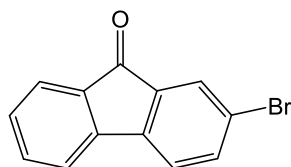
5.2.2 2-Bromofluorenone

Adapted from literature procedure[4]. 2-Bromo-9H-fluorene (3.0 g, 0.012 mol) was dissolved in acetic anhydride (100 mL). Chromium trioxide (3.0 g, 0.03 mol) was added carefully in portions, and the reaction was stirred overnight. After pouring into an ice/water mixture (1:1) and allowing precipitation to occur for 15 min, the resulting yellow solid was collected by vacuum filtration and rinsed with water. The precipitate was then recrystallized with 95% ethanol, giving yellow needles (3.0 g, 95%). ^{1}H-NMR (400 MHz, CDCl$_3$): δ (ppm) 7.31 (s, 1H), 7.40-7.42 (d, 1H, J = 8 Hz), 7.50-7.52 (m, 2H), 7.61-7.63 (dd, 1H, J = 8 Hz, 2 Hz), 7.66-7.68 (d, 1H, J = 8 Hz), 7.77 (d, 1H, J = 2 Hz). Mp = 147-149 °C.
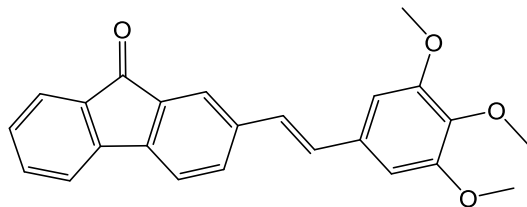
5.2.3 FOS ((*E*)-2-(3,4,5-trimethoxystyryl)-9*H*-fluoren-9-one).

Adapted from a literature procedure[5]. 3,4,5-Trimethoxystyrene (0.78 g, 4 mmol) and 2-bromofluorenone (1.14 g, 4.4 mmol) were combined with palladium acetate (0.06 g, 0.28 mmol) and tris(2-methylphenyl)phosphine (0.24 g, 0.80 mmol) in a 3-neck, 100-mL round bottom flask under nitrogen atmosphere. Then, 80 mL of dry dimethylformamide was added by syringe, and the solution was heated to 105 °C. Then, 4 mL of triethylamine was added, and the solution was allowed to stir for 24 h. The reaction was cooled to room temperature and poured into 200 mL of distilled water. The aqueous suspension was then extracted with dichloromethane (3×50 mL). The organic layers were combined, washed with distilled water (3×100 mL), dried over anhydrous magnesium sulfate, filtered and concentrated onto silica gel. The product was purified by column chromatography using dichloromethane as the eluent, yielding an orange powder (0.32 g, 21%). ATR-IR (neat, cm-1) 1703 (s, C=O str). ^{1}H-NMR (400 MHz, CDCl$_3$): δ (ppm) 3.88 (s, 3H), 3.93 (s, 6H), 6.75 (s, 2H), 6.99-7.03 (d, 1H, J = 16 Hz), 7.10-7.14 (d, 1H, J = 16 Hz), 7.30-7.31 (td, 1H, J = 16 Hz, J' = 8 Hz, J'' = 1.6 Hz), 7.48-7.53 (m, 3H), 7.56-7.57 (dd, 1H, J = 16 Hz, J' = 8 Hz), 7.66-7.68 (d, 1H, J = 8 Hz), 7.87 (s, 1H). MS (FAB, m/z): found *m/z* = 372.1362, calculated for C$_{24}$H$_{20}$O$_4$ *m/z* = 372.1362. Mp 147-149 °C.
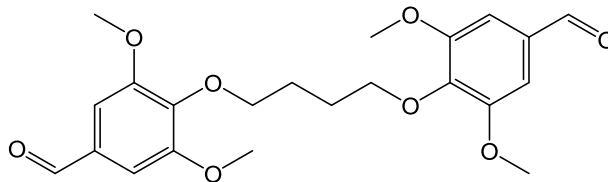
5.2.4 1,4-Bis(2,6-dimethoxy-4-formylphenoxy)butane.

Adapted from a literature procedure[6]. Syringaldehyde (9.1 g, 50 mmol) and 7.5 g of anhydrous potassium carbonate were combined in a 3-neck round bottom flask under a nitrogen atmosphere. Then, 250 mL of dry dimethylformamide was injected and the solution was heated to 100 °C. 1,4-Dibromobutane (3.76 mL, 25 mmol) was then added dropwise by syringe, and the reaction stirred for 24 h. The reaction was cooled to room temperature and poured into 400 mL. After precipitation for 4 h, an off-white solid was isolated by vacuum filtration and was allowed to dry overnight. The solid was then recrystallized from absolute ethanol to give tan needles (8.67 g, 83% yield). ^{1}H NMR (400 MHz, CDCl$_3$): δ (ppm) = 1.99 (br s, 4H), 3.91 (s, 12H), 4.16 (br s., 12H), 7.14 (s, 4H), 9.87 (s, 2H). Mp = 154 – 155 °C.
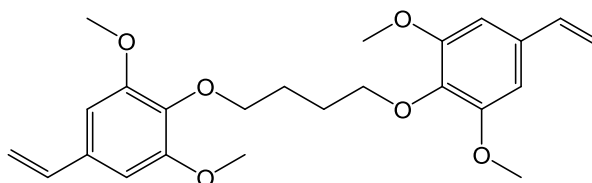
5.2.5 1,4-Bis(2,6-dimethoxy-4-vinylphenoxy)butane.

Adapted from a literature procedure[6]. Methyltriphenylphosphonium bromide (7.64 g, 21.4 mmol) was suspended in 50 mL of dry tetrahydrofuran in a 3-neck round bottom flask under a nitrogen atmosphere. The suspension was cooled to 0 °C and 2.5 M n-butyllithium (8.6 mL in hexanes, 21.4 mmol) was injected dropwise. The solution was

allowed to stir and warm to 20 °C. Next, a solution of 1,4-bis(2,6-dimethoxy-4-

formyloxy)butane (2.09 g, 5 mmol) in 25 ml of dry tetrahydrofuran was added via

cannula to the stirring ylide solution. After heating at reflux for 24 h, the reaction was

reduced to room temperature and poured into 100 mL of water. The aqueous layer was

then extracted with diethyl ether (3×75-mL). The combined organic layers were dried

over anhydrous magnesium sulfate, filtered and concentrated onto silica gel for column

chromatography using diethyl ether as the eluent. The resultant yellow oil was then

washed with cold hexanes to give a white powder (1.94 g, 93% yield). 1H NMR (400

MHz ,CDCl$_3$): δ (ppm) = 1.95 (m, 4H), 3.84 (s, 12H), 4.04 (br m, 4H), 5.21 (d, 2H, J =

10.8 Hz), 5.66 (d, 2H, J = 18 Hz), 6.63 (s, 4H), 6.64 (dd, 2H, J$_1$ = 10 Hz, J$_2$ = 6.4 Hz). Mp

= 42 – 43 °C.
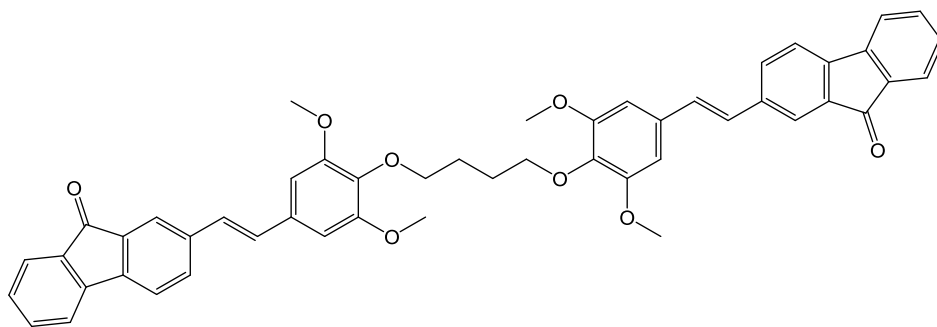
5.2.6 FOSFX4 (1,4-Bis(4-oxy-3,5-dimethoxyphenyl-1-(*E*-1-ethen-2-yl-(fluoren-9-one-2-yl)))butane).

2-Bromofluoenone (1.32 g, 5 mmol) and 1,4-bis(2,6-dimethoxy-4-

vinylphenoxy)butane (1.05 g, 2.5 mmol) was combined with palladium acetate (0.015 g,

0.05 mmol) and tris(2-methylphenyl)phosphine (0.04 g, 0.175 mmol) in a three-neck

round bottom flask under a nitrogen atmosphere. Next, 30 mL of dry dimethylformamide

was added by syringe and the solution was heated to 100 °C. Next, 2.5 mL of

triethylamine was added and the reaction was allowed to stir for 72 h. The reaction was

then cooled to room temperature and poured into 200 mL of ice water, 5 mL of 1M

aqueous hydrochloric acid was added dropwise, and the resultant precipitate was isolated

by vacuum filtration. The crude solid was dissolved in chloroform and filtered through

Celite. The filtrate was then concentrated in vacuo, dissolved in minimal hot chloroform,

and poured into excess cold methanol to give an orange powder (0.45 g, 30 % yield).

ATR-IR (neat, cm-1) 1707 (s, C=O str). ^{1}H-NMR (400 MHz, CDCl$_3$): δ (ppm) = 1.95-

2.00 (pseudo quint, 4H, J ~ 4 Hz), 3.90 (s, 12H), 4.06-4.10 (br t, 4H, J ~ 4 Hz), 6.74 (s,

4H), 6.98-7.01 (d, 2H, J = 16 Hz), 7.01-7.14 (d, 1H, J = 16 Hz), 7.46-7.57 (m, 8H), 7.65-

7.68 (d, 2H, J = 8 Hz), 7.86 (br s, 2H). MS (EI) found m/z = 770.70, calculated for

C$_{50}$H$_{42}$O$_8$ m/z = 770.2878. Mp 190-192 °C.

### 5.2.7 1,8-Bis(2,6-dimethoxy-4-formylphenoxy)octane.

Adapted from a literature procedure[7]. Syringaldehyde (3.64 g, 20 mmol) and 3.0 g

of anhydrous potassium carbonate were combined in a 3-neck round bottom flask under a

nitrogen atmosphere. Then, 150 mL of dry dimethylformamide was injected and the

solution was heated to 100 °C. 1,8-Dibromooctane (1.85 mL, 10 mmol) was then added

dropwise by syringe, and the reaction was allowed to stir for 24 h. After cooling to room

temperature, the reaction was poured into 200 mL of distilled water and was allowed to

precipitate for 4 h. The resulting white solid was isolated by vacuum filtration and was

allowed to dry overnight. The solid was then recrystallized from absolute ethanol to give an off-white powder (3.74 g, 79 % yield). ^{1}H NMR (400 MHz, CDCl$_3$): δ (ppm) = 1.36 (m, 4H), 1.46 (m, 4H), 1.76 (m, 4H), 3.90 (s, 12H), 4.06 (m, 4H), 7.12 (s, 4H), 9.86 (s, 2H). MP = 87-88 °C.
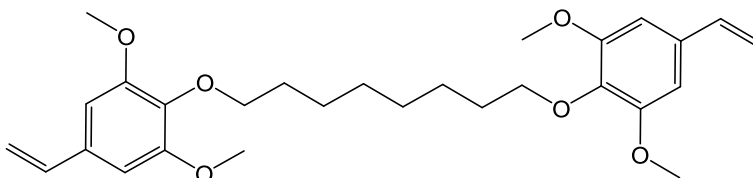
5.2.8 1,8-Bis(2,6-dimethoxy-4-vinylphenoxy)octane.

Adapted from a literature procedure[6]. Methyltriphenylphosphonium bromide (7.64 g, 21.4 mmol) was suspended in 50 mL of dry tetrahydrofuran in a 3-neck round bottom flask under a nitrogen atmosphere. The suspension was cooled to 0 °C and 2.5 M n-butyllithiu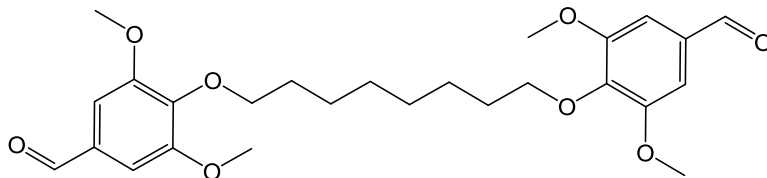m (8.6 mL in hexanes, 21.4 mmol) was added dropwise by syringe. The solution was allowed to stir and warm to room temperature, then a solution of 1,8 bis-(2,6-dimethoxy-4-formylphenoxy)octane (2.37 g, 5 mmol) in 25 mL of dry tetrahydrofuran was added via cannula to the stirring ylide solution. The reaction was then heated to reflux and was allowed to stir for 24 h. The reaction was then cooled to room temperature and poured into 100 mL distilled water. The aqueous layer was extracted with diethyl ether (3×75-mL). The combined organic layers were dried over anhydrous magnesium sulfate, filtered and concentrated onto silica gel for column chromatography. The product was purified by elution with diethyl ether, yielding a white powder (1.66 g, 71% yield). ^{1}H NMR (400 MHz, CDCl$_3$): δ (ppm) = 1.38 (br m, 4H), 1.45 (br m, 4H), 1.76 (m, 4H), 3.87 (s, 12H), 3.97 (t, 4H, J = 7 Hz), 5.22 (d, 2H, J = 11

Hz), 5.66 (d, 2H, J = 18 Hz), 6.64 (s, 4H), 6.64 (dd, 2H, J_1 = 10 Hz, J_2 = 6.4 Hz). Mp = 48 – 50 °C.
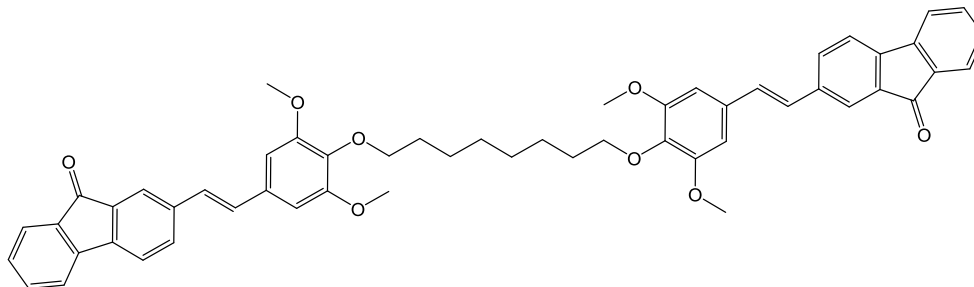
5.2.9 FOSFX8 (1,8-Bis(4-oxy-3,5-dimethoxyphenyl-1-(*E*-1-ethen-2-yl-(fluoren-9-one-2-yl)))octane).

2-Bromofluorenone (3.10g, 12 mmol), 1,8-bis(2,6-dimethoxy-4-vinylphenoxy)octane (2.35 g, 5 mmol), tri-orthotolyl phosphine (0.30 g, 1 mmol) and palladium acetate (0.08 g, 0.36 mmol) were combined in 2-neck round bottom flask under nitrogen atmosphere. Then, 150 mL of dry dimethylformamide was added, and the reaction mixture heated to 80 °C for 30 min. Next, 5.0 mL of triethylamine was added, and the reaction was allowed to stir for 2 days. The reaction mixture was allowed to cool to room temperature and was poured into 400 mL of water, then neutralized by addition of 2 M aqueous hydrochloric acid. The suspension was stirred for 15 min, extracted with chloroform, dried over anhydrous magnesium sulfate, and concentrated in vacuo. The product was purified by flash chromatography on silica using 35% ethyl acetate/hexanes. The column-purified material was dissolved in dichloromethane:methanol, and hexanes was added to force precipitation. Collection of the resultant solid by vacuum filtration yielded 0.87 g of orange/red product (21% yield). ATR-IR (neat, cm-1) 1707 (s, C=O str). ^{1}H-NMR (400 MHz, CDCl$_3$): δ (ppm) = 1.36-1.44 (br s, 4H), 1.45-1.54 (br s, 4H), 1.74-1.84 (pseudo quint, 4H, J ~ 8 Hz), 3.92 (s, 12H), 3.97-4.05 (br t, 4H, J ~ 8 Hz), 6.76

(s, 2H), 6.97-7.04 (d, 2H, J = 16 Hz), 7.09-7.17 (d, 2H, J = 16 Hz), 7.45-7.59 (br m, 8H),

7.65-7.71 (br m, 2H), 7.86 (br d, 2H, J ~ 3 Hz). MS (EI) found m/z = 826.2, calculated for

$C_{54}H_{50}O_8$ m/z = 826.3503. Mp 210 – 212 ºC.
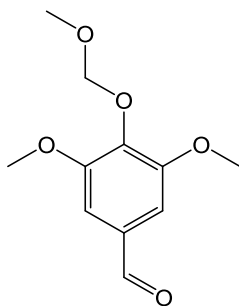
5.2.10 3,5-Dimethoxy-4-methylmethoxybenzaldehyde.

Adapted from a literature procedure[8]. Syringaldehyde (0.91 g, 5 mmols) and

anhydrous? potassium carbonate (4 g, 29 mmol) was added to a 3-neck 50-mL round

bottom flask. The flask was flushed with nitrogen and 25 mL of dry acetone was added

by syringe. The solution was cooled to 0 °C and 0.57 mL of chloromethyl methyl ether

was added dropwise by syringe. The solution was slowly warmed to reflux and was

stirred with heating for 2 h. The reaction was cooled to room temperature and filtered.

The acetone was removed by rotoevaporation to give a white solid (0.90 g, 80% yield).

This product was used in the next synthetic step without further purification. ^{1}H NMR

(400 MHz, CDCl$_3$): δ (ppm) = 3.59 (s, 3H), 3.92 (s, 6H), 5.22 (s, 2H), 7.13 (s, 2H), 9.87

(s, 1H). Mp = 51 – 52 °C.
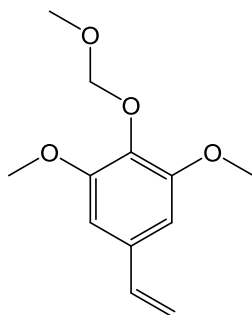
5.2.11 3,5-dimethoxy-4-methylmethoxystyrene.

Adapted from a literature procedure[9]. Methyltriphenylphosphonium bromide (2.86 g, 8 mmol) was added to a 3-neck round bottom flask under a nitrogen atmosphere, follwed by 50 mL of dry tetrahydrofuran. The suspension was cooled to 0 °C with stirring, and 2.5 M n-butyllithium (3.2 mL in hexanes, 8 mmol) was added slowly by syringe over the course of 30 min. The solution was allowed to warm to room temperature, and a solution of 3,5-dimethoxy-4-methylmethoxy benzaldehyde (0.9 g, 4 mmol) in 25 mL of dry tetrahydrofuran was added. After stirring at room temperature for 16 h, the reaction was poured into 300 mL of water and extracted with diethyl ether (3×100mL). The organic layers were combined, dried over anhydrous magnesium sulfate, and filtered. The ether was removed from the filtrate by rotoevaporation to give a yellow oil (0.89g, 97% yield). MS (EI) molecular ion peak m/z = 224.15, calculated for $C_{12}H_{16}O_4$ m/z = 224.25. ^{1}H NMR (400 MHz, CDCl$_3$): δ (ppm) = 3.61 (s, 3H), 3.88 (s 6H), 5.13 (s, 2H), 5.22 (d, 1H, J = 10 Hz), 5.67 (d, 1H, J = 18 Hz), 6.65 (s, 2H), 6.65 (dd, 1H, J_1 = 10.8 Hz, J_2 = 6.4 Hz).
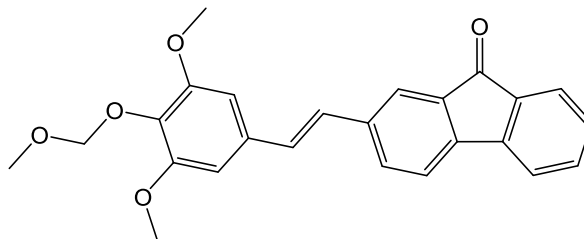
5.2.12 2-[2-(3,5-Dimethoxy-4-methoxymethoxyphenylvinylene]fluorenone.

Adapted from a literature procedure[10]. 3,5-Dimethoxy-4-methylmethoxystyrene (0.45 g, 2 mmol), 2-bromofluorenone (0.57 g, 2.2 mmol), palladium acetate (0.03 g, 0.14 mmol), and tris(2-methylphenyl)phosphine (0.13 g, 0.4 mmol) were added to a 3-neck 100 mL round bottom flask under a nitrogen atmosphere. Then, 40 mL of dry dimethylformamide was added and the solution was heated to reflux. Next, 2 mL of triethylamine was added by syringe and the reaction was allowed to stir for 48 h. The reaction was allowed to cool to room temperature and poured into 200 mL of distilled water. The resulting aqueous suspension was extracted with dichloromethane (3×100 mL). The organic layers were combined, dried over anhydrous magnesium sulfate, and filtered through Celite. The filtrate was evaporated, and the resulting residue was dissolved in minimal hot chloroform. The dark red solution was then poured into excess cold hexanes and filtered to give an orange powder (0.30 g, 37 % yield). This product was used in the next step without further purification. MS (EI) molecular ion peak $m/z =$ 402.0, calculated for $C_{25}H_{22}O_5$ $m/z = 402.44$; ^{1}H NMR (400 MHz, CDCl$_3$): δ (ppm) = 3.63 (s, 3H), 3.92 (s 6H), 5.17 (s, 2H), 6.76 (s, 2H), 7.01 (d, 1H, J = 16 Hz), 7.13 (d, 1H, J = 16 Hz), 7.30 (m, 1H), 7.50 (m, 3H), 7.57 (m, 1H), 7.68 (m, 1H), 7.87 (d, 1H, J = 2 Hz). Mp = 137-138 °C.
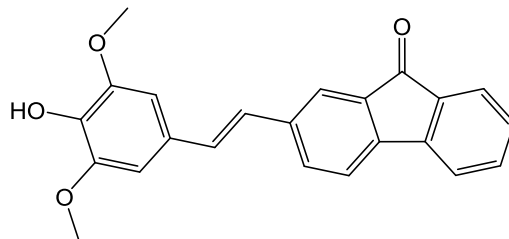
5.2.13 2-[2-(3,5-Dimethoxy-4-hydroxyphenylvinylene]fluorenone.

2-[2-(3,5-Dimethoxy-4-methoxymethoxyphenylvinylene]fluorenone (0.25 g, 0.622 mmol) was added to a 100-ml round bottom flask. Then, 50 ml of methanol was added and the solution was heated to 80 °C. Next, 15 drops of concentrated hydrochloric acid was added, and the reaction was allowed to stir for 16 h. The reaction was allowed to cool to room temperature and was poured into 200 ml of water. The resulting precipitate was filtered and dried in vacuo to give an orange powder (0.19 g, 83% yield). MS (EI) molecular ion peak m/z = 358.1, calculated for $C_{23}H_{18}O_4$ m/z = 358.39; ^{1}H NMR (400 MHz, CDCl$_3$): δ (ppm) = 3.96 (s, 6H), 5.63 (s, 1H), 6.76 (s, 2H), 7.03 (d, 1H, J = 16 Hz), 7.10 (d, 1H, J = 16 Hz), 7.29 (m, 1H), 7.30 (d, 1H, J = 2.4 Hz), 7.48 (m, 3H), 7.53 (d, 1H, J = 1.6 Hz), 7.55 (d, 1H, J = 1.6 Hz), 7.65 (s, 1H), 7.67 (m, 1H), 7.84 (m, 1H); Mp = 150 − 152 °C.
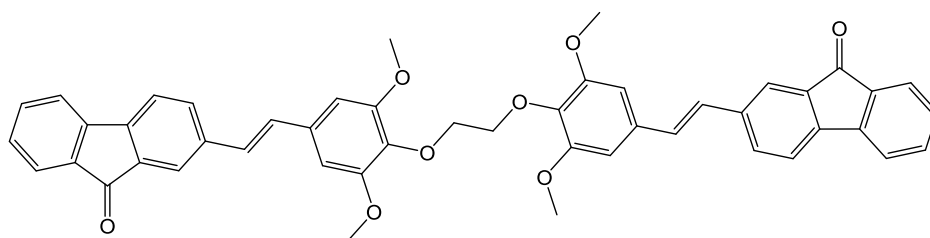
5.2.14 FOSFX2 (1,2-Bis(4-oxy-3,5-dimethoxyphenyl-1-(*E*-1-ethen-2-yl-(fluoren-9-one-2-yl)))ethane).

2-[2-(3,5-Dimethoxy-4-hydroxyphenylvinylene]fluorenone (1.00 g, 2.8 mmols) was added to a 25-ml round bottom flask under a nitrogen atmosphere. Then, 10 mL of

dry dimethylformamide was added and the solution was heated to 100 °C. Next, 2 mL of tetraethylammonium hydroxide solution (52% in water) was added by syringe, and the resulting dark brown solution allowed to stir for 10 min. 1,2-Dibromoethane (120 µL, 1.4 mmols) was then added by syringe, and the reaction was allowed to stir for 48 h. The reaction was then allowed to cool to room temperature and was poured into 50 mL of water. The resulting orange precipitate was filtered, dissolved in chloroform, dried over anhydrous magnesium sulfate, filtered and concentrated onto silica gel. The product was purified via column chromatography using chloroform as the eluent to give an orange solid (0.81g, 78% yield). ATR-IR (neat, cm^{-1}): 1707 (s, C=O str). ^{1}H-NMR (400 MHz, CDCl$_3$): δ (ppm) = 3.90 (s, 12H), 4.39 (s, 4H), 6.73 (s, 4H), 6.98-7.02 (d, 2H, J = 16 Hz), 7.10-7.14 (d, 2H, J = 16 Hz), 7.30 (m, 2H), 7.48-7.51 (m, 6H), 7.54-7.57 (dd, 2H, J = 8 Hz, J' ~ 1 Hz), 7.65-7.67 (d, 2H, 8H, J = 8 Hz), 7.85 (d, 2H J' ~ 1 Hz). MS (EI) found *m/z* =742.10, calculated for C$_{48}$H$_{38}$O$_8$ *m/z* = 742.2565. Mp 223 – 225 °C.
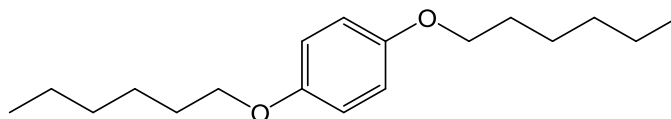
5.2.15 1,4-Dihexyloxybenzene.

Adapted from a literature procedure[11]. A suspension of hydroquinone (5.50 g, 0.05 mol) and anhydrous potassium carbonate (21 g, 0.150 mol) in acetonitrile was heated to reflux. 1-Bromohexane (16.2 mL, 0.150 mol) was then added dropwise. After stirring at reflux for 48 hours, the reaction was allowed to cool to room temperature, and was poured into 400 mL of ice water. The resulting off-white precipitate was collected by

filtration and recrystallized in ethanol twice to give large, white platelets (11.80 g, 85%

yield). ^{1}H NMR (400 MHz, CDCl$_3$): δ (ppm) = 0.90 (t, J = 5.7 Hz, 6H, CH$_3$), 1.47–1.30

(m, 12H, CH$_2$), 1.80–1.73 (m, 4H, CH$_2$), 3.90 (t, J = 6.6 Hz, 4H, CH$_2$), 6.82 (s, 4H, Ar).

Mp = 55-56 °C
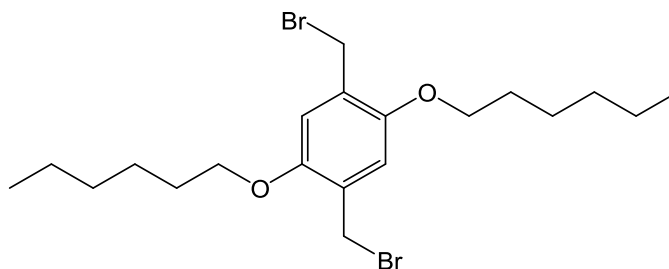
5.2.16 1,4-Bis(bromomethyl)-2,5-dihexyloxybenzene.

Adapted from a literature procedure[11]. To a solution of 1,4-bis(hexyloxy)benzene

(5.60 g, 0.02 mol) in acetic acid was added paraformaldehyde (2.50 g, ?? mmol) and

concentrated hydrobromic acid (21 mL). The reaction was heated at 65 °C for 3 h, after

which a white crystalline precipitate began to form. After cooling to room temperature,

the resulting suspension was poured into 300 mL of ice water. The resulting white

precipitate was filtered, dissolved in minimal hot chloroform and poured into cold

methanol. The resulting a white powder was collected and air-dried (7.13 g, 77%).

^{1}HNMR (400 MHz, CHCl$_3$): δ (ppm) = 0.88 (t, 6H, J = 8 Hz), 1.28 (m, 12H), 1.48 (m,

4H), 1.81 (m, 4H), 3.98 (t, 4H, J = 8 Hz), 4.52 (s, 4H), 6.85 (s, 2H). Mp = 81-82 °C.
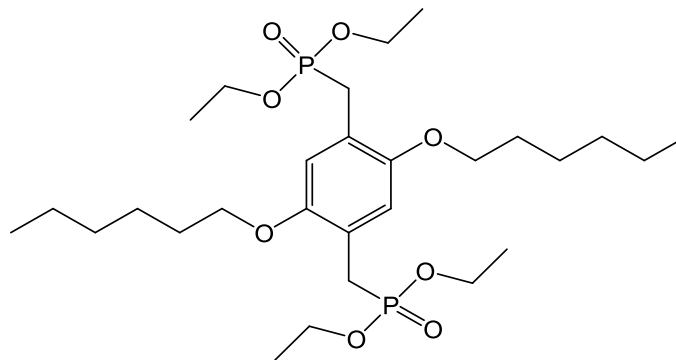
5.2.17 1,4-Bis(diethylphosphonatomethyl)-2,5-dihexyloxybenzene.

Adapted from a literature procedure.[12,13] 1,4-Bis(bromomethyl)-2,5-dihexyloxybenzene (4.60 g, 0.01 mols) was suspended in triethylphosphite (10 mL) in a microwave reaction tube. The reaction was irradiated to 150 °C at 300 W for 45 min, yielding a colorless solution. The triethyl phosphite was removed by vacuum distillation, and the remaining residue was allowed dry under vacuum for 24 h to give colorless, cubic crystals (5.80 g, 100%). ^{1}HNMR (400 MHz, CHCl3): δ (ppm) = 0.89 (t, 6H, J = 10 Hz), 1.22 (m, 12H), 1.32 (m, 8H), 1.43 (m, 4H), 1.74 (m, 4H), 3.20 (d, 4H, J = 20 Hz), 3.91 (t, 4H, J = 6 Hz), 4.00 (m, 8H), 6.90 (s, 2H). Mp = 49-51 °C.
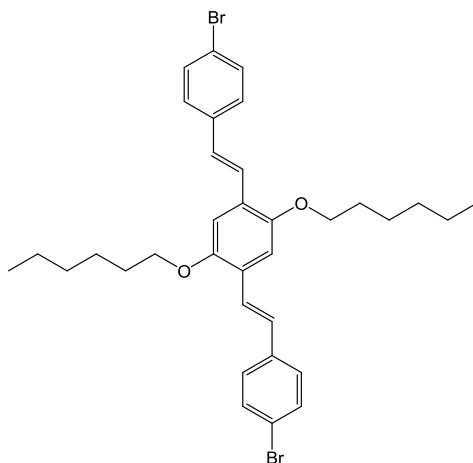
5.2.18 1,4-Bis(4-bromostyryl)-2,5-dihexyloxybenzene.

Adapted from literature procedures.[12,14] 1,4-Bis(diethylphosphonatomethyl)-2,5-dihexyloxybenzene (0.60 g, 0.001 mol) and 4-bromobenzaldeyde (0.44 g, 0.0024 mol) were combined with sodium hydride (0.12 g, 0.005 mols, oil stabilized) in a microwave reaction tube under a nitrogen atmosphere. Then, 25 mL of dry tetrahydrofuran was added, and the reaction was irradiated to 55 °C at 300 W for 5 min. The reaction was then poured into ice water, and the resultant yellow precipitate was collected and recrystallized from absolute ethanol to give yellow needles (0.60 g, 94%). ^{1}HNMR (400 MHz, CHCl$_3$): δ (ppm) = 0.93 (t, 6H, J = 6.8 Hz), 1.40 (m, 8H), 1.55 (m, 4H), 1.88 (m, 4H), 4.06 (t, 4H, J = 6.4 Hz), 7.09 (m, 4H), 7.44 (m, 10H). MS (EI) molecular ion peak m/z = 638.1:640.1:642.1 (Norm. Intensity = 0.575:1:0.688), calculated for C$_{34}$H$_{40}$Br$_2$O$_2$ m/z = 638:640.05:641 (Norm. Intensity = 0.492:1:0.545). Mp = 166-167 °C.
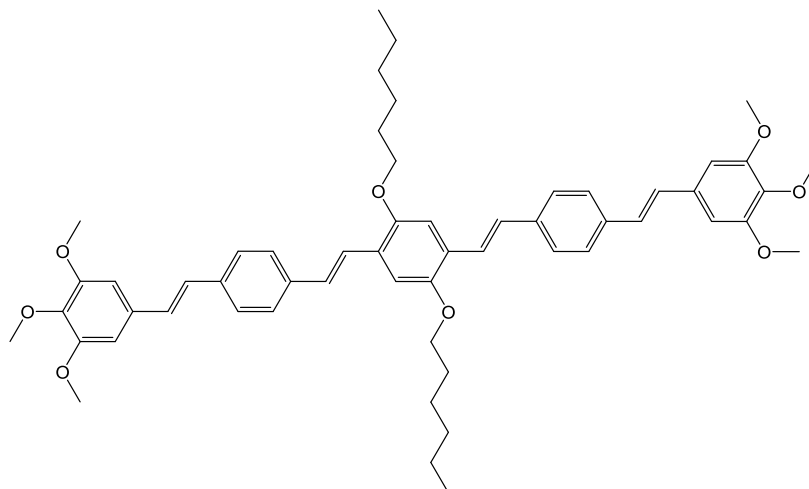
5.2.19 M0.

Adapted from a literature procedure[10]. 1,4-Bis(4-bromostyryl)-2,5-dihexyloxybenzene (0.5 g, 0.00078 mol) and 3,4,5-trimethoxystyrene (0.33 g, 0.0017 mol) were combined with palladium acetate (0.012 g, 0.07 eq) and tris(2-methylphenyl)phosphine (0.028 g, 0.12 eq) in a microwave reaction tube under a nitrogen atmosphere. Next, 15 mL of dry dimethylformamide and 2 mL of triethylamine were injected by syringe, and the reaction was irradiated to 125 °C at 300 W for 45 min. The reaction was poured into iced brine, and the crude orange precipitate was isolated by vacuum filtration, dissolved in chloroform and filtered through Celite. The product was further purified by flash column chromatography using 15% ethyl acetate in hexanes as the eluent to give an orange solid (0.20 g, 30%). ^{1}H-NMR (400 MHz, CDCl$_3$) δ (ppm) = 0.97 (t, 6H, J = 6 Hz), 1.41 (m, 8H), 1.56 (m, 4H), 1.89 (m, 4H), 3.90 (s, 6H), 3.96 (s, 12H), 4.10 (t, 4H, J = 6 Hz), 7.09 (m, 4H), 7.16 (m, 8H), 7.54 (m, 10H). UV-vis (CHCl$_3$; nm[ε=M^{-1}cm^{-1}]), 422[53,600]. Fluorescence (CHCl$_3$), excit = 420 nm; nm[φ = quantum yield]: 482 [φ = 0.58]. FT-IR (neat, cm^{-1}) 2957 (aliph C-H), 2853 (OCH$_2$-H), 1579

(C=C), 1126 (C-O), 958 (trans =CH out-of-plane bend). MS (EI) molecular ion peak m/z = 866.53, calculated for $C_{56}H_{66}O_8$ m/z = 866.48. Mp = 174-175 °C.
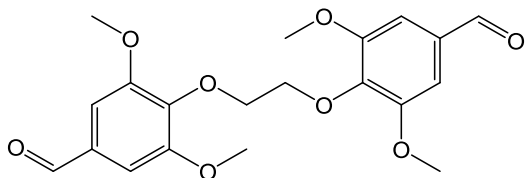
5.2.20 1,2-Bis(2,6-dimethoxy-4-formylphenoxy)ethane.

Adapted from literature procedure[6]. Syringaldehyde (5.46 g, 0.03 mols) and 4.5 g of anhydrous potassium carbonate were combined in a 3-neck round bottom flask under a nitrogen atmosphere. Then, 250-mL of dry dimethylformamide was injected and the solution was heated to 100 °C. 1,2-Dibromoethane (2.82 g, 0.015 mol) was then injected dropwise, and the reaction was allowed to stir for 24 h. The reaction was allowed to cool to room temperature and poured into 400 mL of water. After precipitation for 4 h, the resulting white solid was collected by vacuum filtration and was allowed to dry overnight. The solid was then recrystallized from absolute ethanol to give an off-white powder (5.01 g, 86% yield). ^{1}H NMR (400 MHz, CDCl$_3$): δ (ppm) = 3.91 (s, 12H), 4.16 (br s, 4H), 7.14 (s, 4H), 9.87 (s, 2H). Mp = 164-166°C.
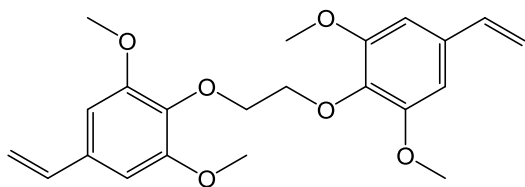
5.2.21 1,2-Bis(2,6-dimethoxy-4-vinylphenoxy)ethane.

Adapted from a literature procedure[6]. Methyltriphenylphosphonium bromide (11.00 g, 0.031 mol) was suspended in 70 mL of dry tetrahydrofuran in a 3-neck round

bottom flask under a nitrogen atmosphere. The suspension was cooled to 0 °C and 2.5 M of n-butyllithium (12.3 mL in hexanes, 0.031 mol) was added dropwise by syringe. The solution stirred and allowed to warm to 20 °C. Next, a solution of 1,2-bis(2,6-dimethoxy-4-formyloxy)ethane (2.80 g, 0.0072 mol) in 35 ml of dry tetrahydrofuran was added via cannula to the stirring ylide solution. The reaction was then heated to reflux for 24 h, allowed to cool to room temperature, and poured into 100 mL of water. The aqueous layer was extracted with diethyl ether (3×75 mL). The combined organic layers were dried over anhydrous magnesium sulfate, filtered and concentrated onto silica gel for column chromatography using diethyl ether as the eluent. The resultant yellow oil was then stirred with cold hexanes, giving a solid that was collected by filtration and air-dried to give a white powder (1.94 g, 93% yield). ^{1}H NMR (400 MHz, CDCl$_3$): δ (ppm) = 3.84 (s, 12H), 4.04 (br m, 4H), 5.21 (d, 2H, J = 11.2 Hz), 5.66 (d, 2H, J = 17.6 Hz), 6.63 (s, 4H). Mp = 51-52 °C.
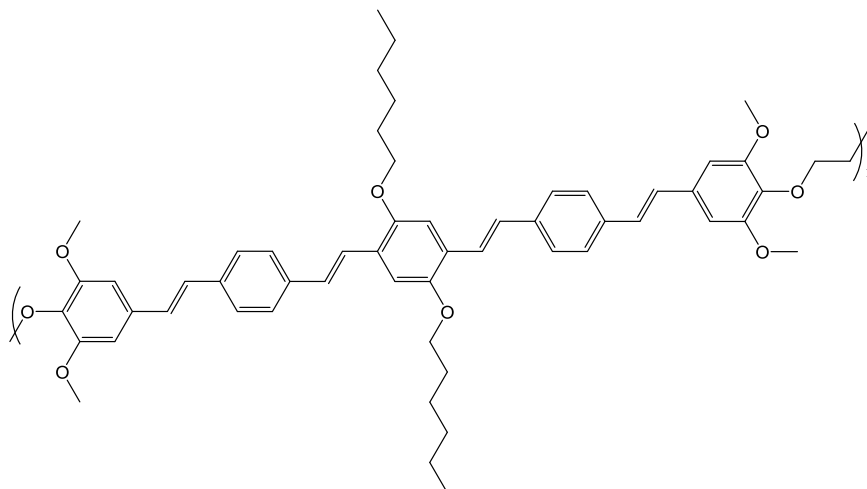
5.2.22 P2.

Adapted from a literature procedure[10]. 1,4-Dihexyloxy-2,5-bis(4-bromostyryl)benzene (0.33 g, 0.5 mmol) and 1,2-bis(2,6-dimethoxy-4-vinylphenoxy)ethane (0.20 g, 0.5 mmol) were combined with tris-2-methylphenyl phosphine (0.021 g, 0.15 eq) and palladium (II) acetate (0.008 g, 0.08 eq) in a 30 mL microwave reaction vessel under nitrogen atmosphere. Dimethylformamide (5 mL) and triethylamine (0.5 mL) were added by syringe, and the reaction vessel was irradiated at 300 W to reach 130 ºC for 45 min. The reaction was poured into water, and the resulting orange precipitate was isolated by vacuum filtration. The crude solid was purified by Soxhlet extraction with hexanes, then methanol. The remaining residue was dissolved in chloroform, filtered through Celite, and concentrated under reduced pressure to give an orange glassy solid (0.15 g, 34%). ^{1}H-NMR (400 MHz, CDCl$_3$) δ (ppm) = 0.95 (t, 6 H, J = 6 Hz), 1.41 (br m, 8 H), 1.58 (br m, 4 H), 1.89 (m, 4 H), 3.91 (m, 12 H), 4.08 (br t, 4 H, J = 6 Hz), 6.75 (s, 4 H), 7.10 (m, 8 H), 7.52 (m, 10H). UV-vis (CHCl$_3$; nm[ε=M^{-1}cm^{-1}]), 425[78,800]. Fluorescence (CHCl$_3$), excit = 420 nm; nm[φ = quantum yield]: 484 [φ = 0.53]. FT-IR (neat, cm^{-1}) 2924 (aliph C-H), 2853 (OCH$_2$-H), 1579 (C=C), 1123 (C-O),

956 (trans =CH out-of-plane bend). GPC (CHCl$_3$ eluent, vs. polystyrene standards): $\overline{M}_n$ = 3889; Đ = 2.65.
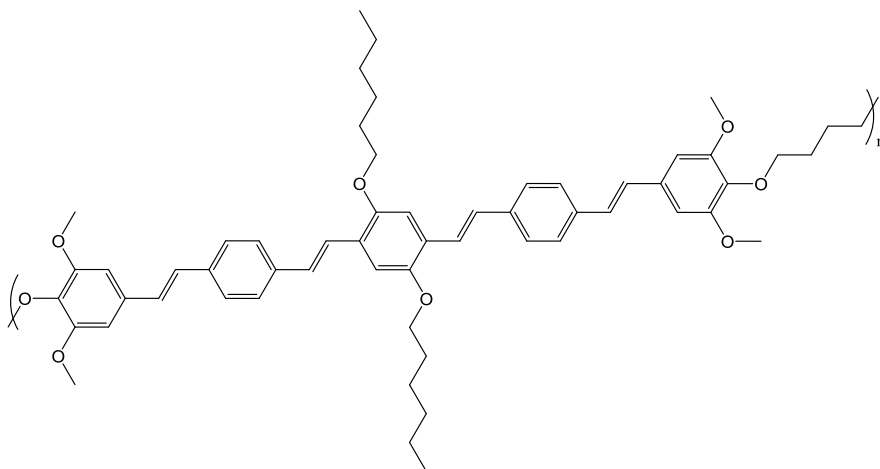
5.2.23 P4.

Adapted from a literature procedure[10]. 1,4-Dihexyloxy-2,5-bis(4-bromostyryl)benzene (0.32 g, 0.5 mmol) and 1,4-bis(2,6-dimethoxy-4-vinylphenoxy)butane (0.21 g, 0.5 mmol) were combined with tris-2-methylphenyl phosphine (0.02 g, 0.15 eq) and palladium (II) acetate (0.008 g, 0.08 eq) in a 30 mL microwave reaction vessel under nitrogen atmosphere. Dimethylformamide (5 mL) and triethylamine (0.5 mL) were added by syringe, and the vessel was irradiated at 300 W to reach 130 ºC for 45 min. The reaction was poured into water, and the resulting brown precipitate was isolated via vacuum filtration. The crude polymer was purified via Soxhlet extraction using hexanes, then methanol. The remaining residue was dissolved in chloroform, filtered through Celite, and concentrated under reduced pressure to give a brown solid (0.16 g, 36%). ^{1}H-NMR (400 MHz, CDCl$_3$) δ (ppm) = 0.94 (t, 6 H, J = 6 Hz), 1.40 (br. m, 8 H), 1.56 (br m, 4 H), 1.88 (br m, 4 H), 1.97 (br m, 4 H), 3.89 (m, 12 H),

4.07 (t, 4 H, J = 6 Hz), 6.76 (s, 4 H), 7.10 (m, 8 H), 7.52 (m, 10H). UV-vis (CHCl$_3$); nm[ε=M^{-1}cm^{-1}]), 415[58,400]. Fluorescence (CHCl$_3$), excit = 420 nm; nm[φ = quantum yield]: 482 [φ = 0.44]. FT-IR (neat, cm^{-1}) 2928 (aliph C-H), 2857 (OCH$_2$-H), 1578 (C=C), 1123(C-O), 955 (trans =CH out-of-plane bend). GPC (CHCl$_3$ eluent, vs. polystyrene standards): M̄$_n$ = 2858; Đ = 1.33.
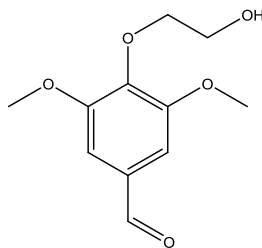
5.2.24 4-(2-Hydroxyethoxy)-3,5-dimethoxy-benzaldehyde

Syringaldehyde (3.64 g, 0.02 mols) and 3.0 g of anhydrous potassium carbonate were combined in a 3-neck round bottom flask under a nitrogen atmosphere. Then, 100-mL of dry dimethylformamide was injected and the solution was heated to 100 °C. 2-Bromoethanol (1.40 mL, 0.02 mol) was then injected dropwise, and the reaction was allowed to stir for 24 h. The reaction was allowed to cool to room temperature and poured into 350 mL of brine. The crude product was extracted with ethyl acetate (3×100 mL). The combined organic layers were then dried over anhydrous magnesium sulfate, filtered, and concentrated onto silica for column chromatography using 60% ethyl acetate in hexanes as the eluent. The pure product was isolated as a colorless oil (3.68 g, 81% yield). ^{1}H NMR (400 MHz, CDCl$_3$): δ (ppm) = 3.27 (t, 1H, J = 6 Hz), 3.74 (t, 2H, J = 6 Hz), 3.92 (s, 6H), 4.19 (t, 2H, J = 4 Hz), 7.13 (s, 2H), 9.86 (s, 1H).
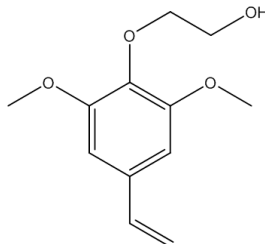
5.2.25 2-(2,6-Dimethoxy-4-vinylphenoxy)-ethanol

Methyltriphenylphosphonium bromide (4.73 g, 13.3 mmols) was suspended in 75 mL of dry tetrahydrofuran in a 3-neck round bottom flask under a nitrogen atmosphere. The suspension was cooled to 0 °C and 1.6 M n-butyllithium (8.5 mL in hexanes, 13.3 mmol) was injected dropwise by syringe. The color of the suspension slowly changed from white to orange. After stirring for 30 min, the solution was allowed to warm to 20 °C. A solution of 4-(2-Hydroxy-ethoxy)-3,5-dimethoxy-benzaldehyde (2.00 g, 8.8 mmol) in 15 mL of dry tetrahydrofuran was then added via cannula to the stirring ylide solution. After stirring at room temperature for 24 h, the reaction was carefully poured into 100 mL of water. The aqueous layer was extracted with diethyl ether (3×30-mL). The combined organic layers were dried over anhydrous magnesium sulfate, filtered and concentrated onto silica gel for column chromatography. The product was then purified by elution with diethyl ether, yielding a yellow oil (1.40 g, 71% yield). ^{1}H NMR (CDCl$_3$, 400 MHz): δ (ppm) = 3.48 (s, 1H), 3.71 (t, 2H, J = 4 Hz), 3.88 (s, 6H), 4.13 (t, 2H, J = 4 Hz), 5.23 (d, 1H, J = 10 Hz), 5.67 (d, 1H, J = 17 Hz), 6.63 (dd, 1H, J = 11 Hz), 6.64 (s, 2H).
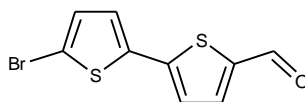
5.2.24 2-Bromo-5'-formyl-5,2'-bithiophene

Adapted from a literature procedure[15]. 2-Formylbithiophene (1.70 g, 0.0088 mols) was dissolved in a 110 mL of a 10:1 tetrahydrofuran:acetic acid mixture. N-Bromosuccinimide (1.53 g, 0.0096 mol) was added to the solution in portions, then the reaction was heated at 60 °C with stirring overnight. After cooling to room temperature, the reaction was poured into water, yielding a yellow precipitate that was collected by vacuum filtration. Recrystallization of the solid from absolute ethanol yielded the product as a yellow solid (2.10 g, 88%). ^{1}H-NMR (400 MHz, CDCl$_3$) δ (ppm) = 7.03 (d, 1 H, J = 4 Hz), 7.10 (d, 1 H, J = 4 Hz), 7.18 (d, 1 H, J = 4 Hz), 7.66 (d, 1H, J = 4 Hz), 9.87 (s, 1 H). Mp = 136-137 °C.
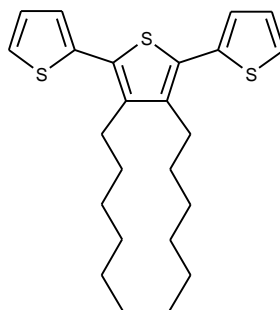
5.2.25 3'4'-Dihexyl-2,2',5',2''-terthiophene

Adapted from a literature procedure[16]. In a round-bottom flask, magnesium turnings (0.19 g, 0.0078 mol) were flame dried. A vacuum was applied to the still-hot flask, and then was filled with nitrogen gas. Diethyl ether was then added by syringe, and the resulting suspension was cooled to 0 °C. Next, 2-bromothiophene (0.6 mL, 0.006 mols) was added slowly by syringe over the course of 30 min. The brown suspension was

then allowed to warm to room temperature, and was cannulated into a separate, flame

dried round bottom flask charged with 1,1′-

bis(diphenylphosphino)ferrocene]dichloropalladium(II) (0.015 g, 0.018 mmols) and 2,5-

dibromo-3,4-dihexylthiophene (0.47 mL, 0.0015 mols) that had been cooled to 0 °C

under nitrogen. The reaction was stirred at room temperature overnight, poured carefully

into water and extracted with diethyl ether (3×100 mL). The combined organic layers

were washed with brine (3×100 mL), dried over anhydrous sodium sulfate, filtered, and

concentrated under vacuum to give the product as a brown, highly viscous oil (0.61 g,

98%). ^{1}H-NMR (400 MHz, CDCl$_3$) δ (ppm) = 0.91 (t, 6 H), 1.33 (m, 8 H), 1.42 (m, 4

H), 1.57 (m, 4H), 2.70 (m, 4 H), 7.07 (dd, 2H, J = 4 Hz), 7.14 (d, 2H, J = 4 Hz), 7.31 (d,

2H, J = 4 Hz).
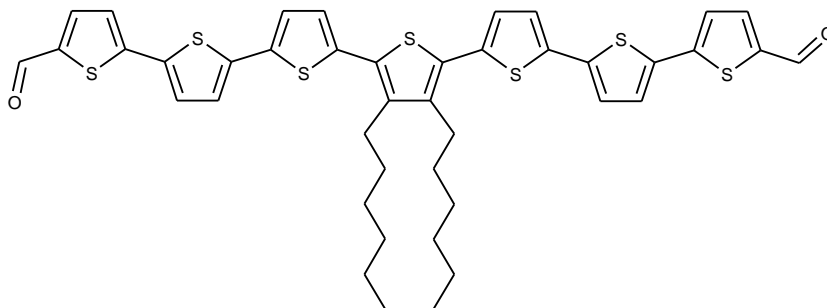
5.2.27 7TDA

Adapted from a literature procedure[17]. 3'4'-Dihexyl-2,2',5',2''-

terthiophene (0.20 g, 0.5 mmol) and 2-bromo-5'-formyl-5,2'-bithiophene (0.41 g, 1.5

mmol) were combined in a 3-neck, 50 mL round-bottom flask with

tris(dibenzylideneacetone)dipalladium(0) (0.007 g, 0.075 mmol), pivalic acid (0.15 g, 1.5

mmol), tris(o-methoxyphenyl)phosphine (0.011 g, 0.3 mmol), and cesium carbonate

(1.47 g, 4.5 mmol). The flask was evacuated and filled with nitrogen, charged with

tetrahydrofuran (20 mL), and then the reaction was heated to reflux and stirred for 72 h. After cooling to room temperature, the reaction was poured into water and extracted with chloroform (3×100 mL). The combined organic layers were washed with brine, dried over anhydrous sodium sulfate, filtered, and concentrated onto silica gel. The crude reaction mixture was subjected to column chromatography using 4:1 hexanes:ethyl acetate as the eluent. The product was obtained as a deep red powder (0.04 g, 10%). ^{1}H-NMR (400 MHz, CDCl$_3$) δ (ppm) = 0.93 (t, 6 H), 1.37 (m, 8 H), 1.47 (m, 4 H), 1.61 (m, 4H), 2.75 (m, 4 H), 7.10 (dd, 2H, J = 4 Hz), 7.16 (d, 2H, J = 4 Hz), 7.20 (d, 2H, J = 4 Hz), 7.26 (d, 2H, J = 4 Hz), 7.30 (d, 2H, J = 4 Hz), 7.69 (d, 2H, J = 4 Hz), 9.88 (s, 2H). MS (EI) molecular ion peak m/z = 800.2, calculated for C$_{56}$H$_{66}$O$_8$ m/z = 800.11. Mp = 164-165 °C.

5.3 References

(1)   Devadoss, C.; Bharathi, P.; Moore, J. S. Energy Transfer in Dendritic Macromolecules: Molecular Size Effects and the Role of an Energy Gradient. *Journal of the American Chemical Society* **1996**, *118*, 9635-9644.

(2)   Baghgar, M.; Labastide, J.; Bokel, F.; Dujovne, I.; McKenna, A.; Barnes, A. M.; Pentzer, E.; Emrick, T.; Hayward, R.; Barnes, M. D. Probing Inter- and Intrachain Exciton Coupling in Isolated Poly(3-hexylthiophene) Nanofibers: Effect of Solvation and Regioregularity. *The Journal of Physical Chemistry Letters* **2012**, *3*, 1674-1679.

(3)   Faler, C. A.; Joullié, M. M. The Kulinkovich Reaction in the Synthesis of Constrained N,N-Dialkyl Neurotransmitter Analogues. *Organic Letters* **2007**, *9*, 1987-1990.

(4)   Rathnayake, H. P.; Cirpan, A.; Karasz, F. E.; Odoi, M. Y.; Hammer, N. I.; Barnes, M. D.; Lahti, P. M. Luminescence of Molecular and Block Copolymeric 2,7-Bis(phenylethenyl)-fluorenones; Identifying Green-Band Emitter Sites in a Fluorene-Based Luminophore. *Chemistry of Materials* **2007**, *19*, 3265-3270.

(5)   Homnick, P. J.; Lahti, P. M. Modular electron donor group tuning of frontier energy levels in diarylaminofluorenone push-pull molecules. *Physical Chemistry Chemical Physics* **2012**, *14*, 11961-11968.

(6)   Yang, Z.; Karasz, F. E.; Geise, H. J. Intrinsically soluble copolymers with well-defined alternating substituted p-phenylenevinylene and ethylene oxide blocks. *Macromolecules* **1993**, *26*, 6570-6575.

(7)   Yang, Z.; Sokolik, I.; Karasz, F. E. A soluble blue-light-emitting polymer. *Macromolecules* **1993**, *26*, 1188-1190.

(8)   Banwell, M. G.; Chand, S.; Savage, G. P. An enantioselective total synthesis of the stilbenolignan (−)-aiphanol and the determination of its absolute stereochemistry. *Tetrahedron: Asymmetry* **2005**, *16*, 1645-1654.

(9)   Singh, M.; Argade, N. P. Palladium-Catalyzed Routes to Geranylated or Farnesylated Phenolic Stilbenes: Synthesis of Pawhuskin C and Schweinfurthin J. *Synthesis* **2012**, *44*, 2895-2902.

(10)   Rathnayake, H. P.; Cirpan, A.; Delen, Z.; Lahti, P. M.; Karasz, F. E. Optimizing OLED Efficacy of 2,7-Diconjugated 9,9-Dialkylfluorenes by Variation of Periphery Substitution and Conjugation Length. *Advanced Functional Materials* **2007**, *17*, 115-122.

(11)   Zhang, Y.; Zhu, W.; Wang, W.; Tian, H.; Su, J.; Wang, W. Synthesis and nonlinear optical properties of rod-like luminescent materials containing Schiff-base and naphthalimide units. *Journal of Materials Chemistry* **2002**, *12*, 1294-1300.

(12)   Zhu, X.; Traub, M. C.; Vanden Bout, D. A.; Plunkett, K. N. Well-Defined Alternating Copolymers of Oligo(phenylenevinylene)s and Flexible Chains. *Macromolecules* **2012**, *45*, 5051-5057.

(13)   Plater, M. J.; Jackson, T. Polyaromatic amines. Part 3: Synthesis of poly(diarylamino)styrenes and related compounds. *Tetrahedron* **2003**, *59*, 4673-4685.

(14)   Smith, T.; Modarelli, D. A. The efficient synthesis of unsymmetrical oligo(phenylenevinylenes). *Tetrahedron Letters* **2008**, *49*, 526-528.

(15)   Lu, Z.; Li, C.; Fang, T.; Li, G.; Bo, Z. Triindole-cored star-shaped molecules for organic solar cells. *Journal of Materials Chemistry A* **2013**, *1*, 7657-7665.

(16)   Vidal, P.-L.; Divisia-Blohorn, B.; Bidan, G.; Hazemann, J.-L.; Kern, J.-M.; Sauvage, J.-P. π-Conjugated Ligand Polymers Entwined around Copper Centres. *Chemistry – A European Journal* **2000**, *6*, 1663-1673.

(17)   Wakioka, M.; Kitano, Y.; Ozawa, F. A Highly Efficient Catalytic System for Polycondensation of 2,7-Dibromo-9,9-dioctylfluorene and 1,2,4,5-Tetrafluorobenzene via Direct Arylation. *Macromolecules* **2013**, *46*, 370-374.

APPENDIX

FERMI'S GOLDEN RULE APPLIED TO FOS
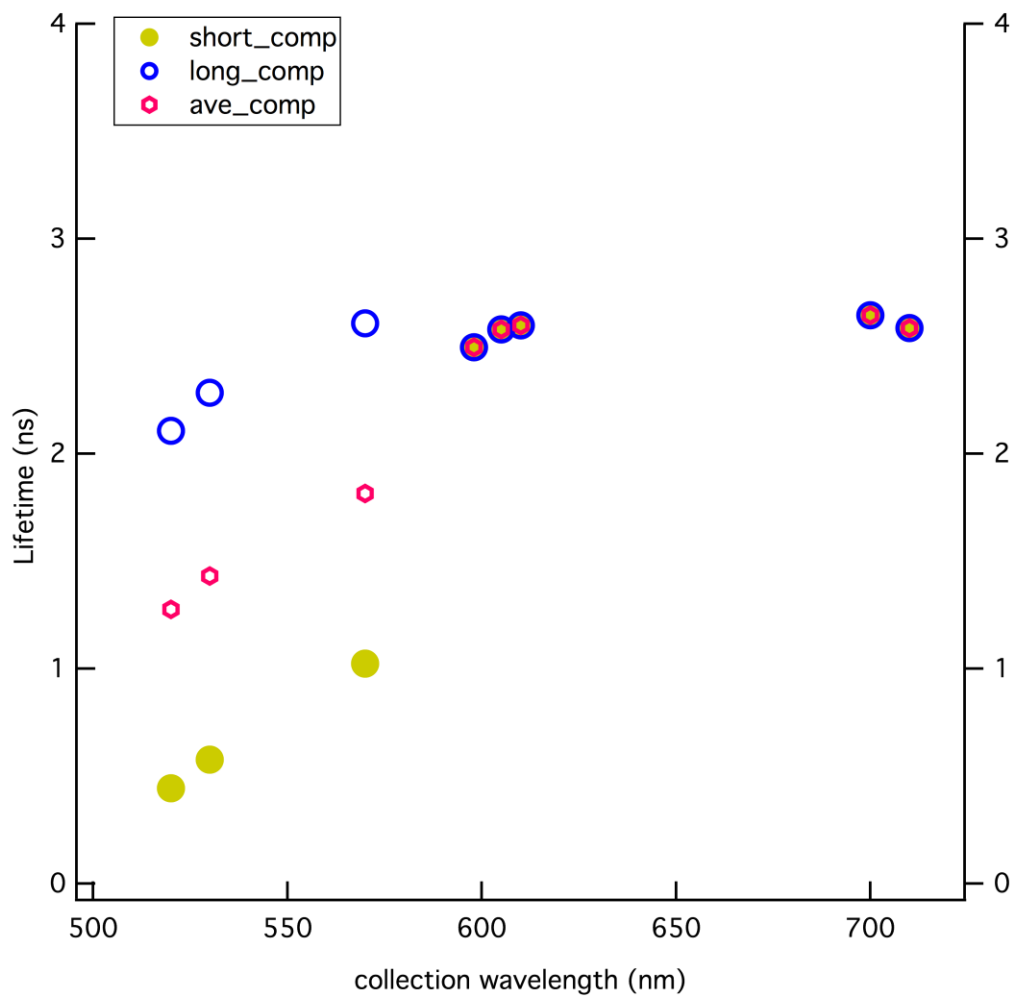
Figure A.1: Plot of fluorescent lifetimes versus collection wavelength for FOS (0.001 mM, excited at 440 nm).

BIBLIOGRAPHY

Aihara, J. Anomalous Solvatochromism of Charge-Transfer Absorption Bands. *Bulletin of the Chemical Society of Japan* **1981**, *54*, 1561-1562.

Ananthakrishnan, S. J.; Varathan, E.; Ravindran, E.; Somanathan, N.; Subramanian, V.; Mandal, A. B.; Sudha, J. D.; Ramakrishnan, R. A solution processable fluorene-fluorenone oligomer with aggregation induced emission enhancement. *Chemical Communications* **2013**, *49*, 10742-10744.

Anslyn, E. V.; Dougherty, D. A.: *Modern Physical Organic Chemistry*; University Science Books: Sausalito, California, 2006.

Baghgar, M.; Labastide, J.; Bokel, F.; Dujovne, I.; McKenna, A.; Barnes, A. M.; Pentzer, E.; Emrick, T.; Hayward, R.; Barnes, M. D. Probing Inter- and Intrachain Exciton Coupling in Isolated Poly(3-hexylthiophene) Nanofibers: Effect of Solvation and Regioregularity. *The Journal of Physical Chemistry Letters* **2012**, *3*, 1674-1679.

Banwell, M. G.; Chand, S.; Savage, G. P. An enantioselective total synthesis of the stilbenolignan (−)-aiphanol and the determination of its absolute stereochemistry

Tetrahedron: Asymmetry **2005**, *16*, 1645-1654.

Barnes, M. D.; Baghar, M. Optical probes of chain packing structure and exciton dynamics in polythiophene films, composites, and nanostructures. *Journal of Polymer Science Part B: Polymer Physics* **2012**, *50*, 1121-1129.

Basabe-Desmonts, L.; Reinhoudt, D. N.; Crego-Calama, M. Design of fluorescent materials for chemical sensing. *Chemical Society Reviews* **2007**, *36*, 993-1017.

Baughman, R. H.; Chance, R. R. Point defects in fully conjugated polymers. *Journal of Applied Physics* **1976**, *47*, 4295-4300.

Benvenho, A. R. V.; Hummelgen, I. A. Positive Charge Transport in an Alternative Oligo-p-phenylenevinylene-derivative/aliphatic-segment Block Copolymer. *Materials Research* **2001**, *4*, 133-136.

Bianchi, R. F.; Balogh, D. T.; Gonçalves, D.; Faria, R. M.; Irene, E. A. Photo-oxidation Phenomenon of MH-PPV Films Studied by Ellipsometry and Infrared Spectroscopy. *Molecular Crystals and Liquid Crystals* **2002**, *374*, 457-462.

Birckner, E.; Grummt, U. W.; Rost, H.; Hartmann, A.; Pfeiffer, S.; Tillmann, H.; Hörhold, H. H. Fluorescence spectroscopy of potential electroluminescent materials: Substituent effects on DSB and segmented PPV derivatives. *Journal of Fluorescence* **1998**, *8*, 73-80.

Birks, J. B. Excimers. *Reports on Progress in Physics* **1975**, *38*, 903-974.

Birks, J. B. Higher Excited States of Benzene and Toluene Excimers. *Chemical Physics Letters* **1968**, *1*, 625-626.

Birks, J. B.; Christophorou, L. G. `Excimer' Fluorescence. I. Solution Spectra of 1:2-Benzanthracene Derivatives. *Proceedings of the Royal Society of London. Series A. Mathematical and Physical Sciences* **1963**, *274*, 552-564.

Bounos, G.; Ghosh, S.; Lee, A. K.; Plunkett, K. N.; DuBay, K. H.; Bolinger, J. C.; Zhang, R.; Friesner, R. A.; Nuckolls, C.; Reichman, D. R.; Barbara, P. F. Controlling Chain Conformation in Conjugated Polymers Using Defect Inclusion Strategies. *Journal of the American Chemical Society* **2011**, *133*, 10155-10160.

Brouwer, H. J.; Krasnikov, V. V.; Pham, T. A.; Gill, R. E.; van Hutten, P. F.; Hadziioannou, G. Optical properties of single crystals and vacuum-deposited thin films of a substituted oligo(p-phenylene vinylene). *Chemical Physics* **1998**, *227*, 65-74.

Brunetti, F. G.; Kumar, R.; Wudl, F. Organic electronics from perylene to organic photovoltaics: painting a brief history with a broad brush. *Journal of Materials Chemistry* **2010**, *20*, 2934-2948.

Brunsveld, L.; Folmer, B. J. B.; Meijer, E. W.; Sijbesma, R. P. Supramolecular Polymers. *Chemical Reviews* **2001**, *101*, 4071-4098.

Bruzewicz, D. A.; Boncheva, M.; Winkleman, A.; St. Clair, J. M.; Engel, G. S.; Whitesides, G. M. Biomimetic Fabrication of 3D Structures by Spontaneous Folding of Tapes. *Journal of the American Chemical Society* **2006**, *128*, 9314-9315.

Campoy-Quiles, M.; Ferenczi, T.; Agostinelli, T.; Etchegoin, P. G.; Kim, Y.; Anthopoulos, T. D.; Stavrinou, P. N.; Bradley, D.; Nelson, J. Morphology Evolution Via Self-organization and Lateral and Vertical Diffusion in Polymer:fullerene Solar Cell Blends. *Nature Materials* **2008**, *7*, 158-164.

Chandross, E. A.; Dempster, C. J. Intramolecular excimer formation and fluorescence quenching in dinaphthylalkanes. *Journal of the American Chemical Society* **1970**, *92*, 3586-3593.

Chen, D.; Nakahara, A.; Wei, D.; Nordlund, D.; Russell, T. P. P3HT/PCBM Bulk Heterojunction Organic Photovoltaics: Correlating Efficiency and Morphology. *Nano Letters* **2010**, *11*, 561-567.

Chen, Z.; Cai, P.; Chen, J.; Liu, X.; Zhang, L.; Lan, L.; Peng, J.; Ma, Y.; Cao, Y. Low Band-Gap Conjugated Polymers with Strong Interchain Aggregation and Very High Hole Mobility Towards Highly Efficient Thick-Film Polymer Solar Cells. *Advanced Materials* **2014**, *26*, 2586-2591.

Christophorou, L. G.; Abu-Zeid, M. E. M.; Carter, J. G. Emission and Decay of Liquid-Benzene and Naphthalene Derivatives Excited by Electron Impact. *The Journal of Chemical Physics* **1968**, *49*, 3775-3782.

Chu, N. Y. C.; Kearns, D. R. Monomer Emission from Excimer Forming Crystals: Pyrene and Perylene. *Molecular Crystals and Liquid Crystals* **1972**, *16*, 61-74.

Clafton, S. N.; Beattie, D. A.; Mierczynska-Vasilev, A.; Acres, R. G.; Morgan, A. C.; Kee, T. W. Chemical Defects in the Highly Fluorescent Conjugated Polymer Dots. *Langmuir* **2010**, *26*, 17785-17789.

Cook, S.; Furube, A.; Katoh, R. Analysis of the excited states of regioregular polythiophene P3HT. *Energy & Environmental Science* **2008**, *1*, 294-299.

Cravino, A.; Zerza, G.; Maggini, M.; Bucella, S.; Svensson, M.; Andersson, M. R.; Neugebauer, H.; Sariciftci, N. S. A novel polythiophene with pendant fullerenes: toward donor/acceptor double-cable polymers. *Chemical Communications* **2000**, 2487-2488.

Detert, H.; Schollmeyer, D.; Sugiono, E. Synthesis, Structure and Solvatochromism of the Emission of Cyano-Substituted Oligo(phenylenevinylene)s. *European Journal of Organic Chemistry* **2001**, *2001*, 2927-2938.

Devadoss, C.; Bharathi, P.; Moore, J. S. Energy Transfer in Dendritic Macromolecules: Molecular Size Effects and the Role of an Energy Gradient. *Journal of the American Chemical Society* **1996**, *118*, 9635-9644.

Drori, T.; Utah, T. U. o.: *Optical Study of Pi-conjugated Polymers and Pi-conjugated Polymers/fullerene Blends*; The University of Utah, 2009.

Drury, A.; Maier, S.; Ruther, M.; Blau, W. J. Investigation of different synthetic routes to and structure-property relationships of poly(m-phenylenevinylene-co-2,5-dioctyloxy-p-phenylenevinylene). *Journal of Materials Chemistry* **2003**, *13*, 485-490.

Faler, C. A.; Joullié, M. M. The Kulinkovich Reaction in the Synthesis of Constrained N,N-Dialkyl Neurotransmitter Analogues. *Organic Letters* **2007**, *9*, 1987-1990.

Ferenczi, T.; Sims, M.; Bradley, D. D. C. On the nature of the fluorenone-based emission in oxidized poly(dialkyl-fluorene)s. *Journal of Physics: Condensed Matter* **2008**, *20*.

Fichou, D.; Horowitz, G.; Xu, B.; Garnier, F. Low temperature optical absorption of polycrystalline thin films of α-quaterthiophene, α-sexithiophene and α-octithiophene, three model oligomers of polythiophene. *Synthetic Metals* **1992**, *48*, 167-179.

Forster, T. Formation and Dissociation of Excited Dimers. *Pure and Applied Chemistry* **1963**, *7*, 73-78.

Gadermaier, C.; Lanzani, G. Photophysics of conjugated polymers: the contribution of ultrafast spectroscopy. *Journal of Physics: Condensed Matter* **202**, *14*.

Gamerith, S.; Gadermaier, C.; Scherf, U.; List, E. J. W.: The Origin of the Green Emission Band in Polyfluorene Type Polymers. In *Physics of Organic Semiconductors*; Wiley-VCH Verlag GmbH & Co. KGaA, 2006; pp 153-181.

Gebler, D. D.; Wang, Y. Z.; Fu, D.-K.; Swager, T. M.; Epstein, A. J. Exciplex emission from bilayers of poly(vinyl carbazole) and pyridine based conjugated copolymers. *The Journal of Chemical Physics* **1998**, *108*, 7842-7848.

Geddes, C. D.; Lakowicz, J. R.: *Advanced Concepts in Fluorescence Sensing: Part B: Macromolecular Sensing*; Springer, 2010.

Gierschner, J.; Park, S. Y. Luminescent distyrylbenzenes: tailoring molecular structure and crystalline morphology. *Journal of Materials Chemistry C* **2013**, *1*, 5818-5832.

Giridharagopal, R.; Ginger, D. S. Characterizing Morphology in Bulk Heterojunction Organic Photovoltaic Systems. *The Journal of Physical Chemistry Letters* **2010**, *1*, 1160-1169.

Gordon, M.; Ware, W. R.: *The Exciplex*; Academic Press: New York, 1975.

Grigoras, M.; Catargiu, A.-M.; Musteata, V.-E. Multi-Block Copolymers Containing Oligoaniline Pentamer as Electroactive Segment. *Soft Materials* **2011**, *11*, 90-97.

Grimme, S. Do Special Noncovalent π–π Stacking Interactions Really Exist? *Angewandte Chemie International Edition* **2008**, *47*, 3430-3434.

Grimme, S.; Ehrlich, S.; Goerigk, L. Effect of the damping function in dispersion corrected density functional theory. *Journal of Computational Chemistry* **2011**, *32*, 1456-1465.

Günes, S.; Neugebauer, H.; Sariciftci, N. S. Conjugated Polymer-Based Organic Solar Cells. *Chemical Reviews* **2007**, *107*, 1324-1338.

Hadjichristidis, N.; Hirao, A.; Tezuka, Y.; Du Prez, F.: *Complex Macromolecular Architectures: Synthesis, Characterization, and Self-Assembly*; Wiley, 2011.

Hammer, B. A. G.; Bokel, F. A.; Hayward, R. C.; Emrick, T. Cross-Linked Conjugated Polymer Fibrils: Robust Nanowires from Functional Polythiophene Diblock Copolymers. *Chemistry of Materials* **2011**, *23*, 4250-4256.

He, B.; Li, J.; Bo, Z.; Huang, Y. Studies of Green Emission in Polyfluorenes Using a Model Polymer. *Polymer* **2007**, *39*, 1345-1350.

Hedley, G. J.; Ward, A. J.; Alekseev, A.; Howells, C. T.; Martins, E. R.; Serrano, L. A.; Cooke, G.; Ruseckas, A.; Samuel, I. D. W.: Determining the optimum morphology in high-performance polymer-fullerene organic photovoltaic cells. In *Nature Communications*, 2013; Vol. 4.

Heidarsson, Pétur O.; Otazo, Mariela R.; Bellucci, L.; Mossa, A.; Imparato, A.; Paci, E.; Corni, S.; Di Felice, R.; Kragelund, Birthe B.; Cecconi, C. Single-Molecule Folding Mechanism of an EF-Hand Neuronal Calcium Sensor. *Structure*, *21*, 1812-1821.

Heldt, J. R.; Heldt, J.; Józefowicz, M.; Kamiński, J. Spectroscopic Studies of Fluorenone Derivatives. *Journal of Fluorescence* **2001**, *11*, 65-73.

Heun, S.; Mahrt, R. F.; Greiner, A.; Lemmer, U.; Bassler, H.; Halliday, D. A.; Bradley, D. D. C.; Burn, P. L.; Holmes, A. B. Conformational effects in poly(p-phenylene vinylene)s revealed by low-temperature site-selective fluorescence. *Journal of Physics: Condensed Matter* **1993**, *5*, 247-260.

Höfle, S.; Pfaff, M.; Do, H.; Bernhard, C.; Gerthsen, D.; Lemmer, U.; Colsmann, A. Suppressing molecular aggregation in solution processed small molecule organic light emitting diodes. *Organic Electronics* **2014**, *15*, 337-341.

Homnick, P. J.; Lahti, P. M. Modular electron donor group tuning of frontier energy levels in diarylaminofluorenone push-pull molecules. *Physical Chemistry Chemical Physics* **2012**, *14*, 11961-11968.

Homnick, P. J.; Tinkham, J. S.; Devaughn, R.; Lahti, P. M. Engineering Frontier Energy Levels in Donor–Acceptor Fluoren-9-ylidene Malononitriles versus Fluorenones. *The Journal of Physical Chemistry A* **2013**, *118*, 475-486.

Hu, D.; Yu, J.; Padmanaban, G.; Ramakrishnan, S.; Barbara, P. F. Spatial Confinement of Exciton Transfer and the Role of Conformational Order in Organic Nanoparticles. *Nano Letters* **2002**, *2*, 1121-1124.

Hu, D.; Yu, J.; Wong, K.; Bagchi, B.; Rossky, P. J.; Barbara, P. F. Collapse of Stiff Conjugated Polymers with Chemical Defects into Ordered Cylindrical Conformations. *Nature* **2000**, *405*, 1030-1033.

Huser, T.; Yan, M.; Rotherberg, L. J. Single chain spectroscopy of conformational dependence of conjugated polymer photophysics. *Proceedings of the National Academy of Sciences* **2000**, *97*, 11187-11191.

Husken, D.; Feijen, J.; Gaymans, R. J. Segmented Block Copolymers with Terephthalic-Extended Poly(ethylene oxide) Segments. *Macromolecular Chemistry and Physics* **2008**, *209*, 525-534.

Ichimura, K. Preparation of water-soluble photoresist derived from poly(vinyl alcohol). *Journal of Polymer Science: Polymer Chemistry Edition* **1982**, *20*, 1411-1417.

Ignatious, F.; Lu, C.; Kantor, S. W.; Lenz, R. W. Alternating, Block, and Random Copolymers of a Triad Mesogen with Alkylene Terephthalate Flexible Segments. *Macromolecules* **1994**, *27*, 7785-7793.

Jonkheijm, P.; van Duren, J. K. J.; Kemerink, M.; Janssen, R. A. J.; Schenning, A. P. H. J.; Meijer, E. W. Control of Film Morphology by Folding Hydrogen-Bonded Oligo(p-phenylenevinylene) Polymers in Solution. *Macromolecules* **2005**, *39*, 784-788.

Jozefowicz, M.; Heldt, J. R.; Heldt, J. The Red-edge Effect in the Spectra of Fluorenone and 4-Hydroxyfluorenone Alcohol Solutions. *Verlag der Zeitschrift für Naturforschung Tübingen* **2002**, *57 a*, 787-796.

Junkers, T.; Vandenbergh, J.; Adriaensens, P.; Lutsen, L.; Vanderzande, D. Synthesis of poly(p-phenylene vinylene) materials via the precursor routes. *Polymer Chemistry* **2012**, *3*, 275-285.

Khoshkhoo, M. S.; Taromi, F. A.; Kowsari, E.; Shalamzari, E. K. Contribution of chromophores with different numbers of repeat units to overall emission of MEH–PPV: An experimental and simulation study. *Polymer* **2013**, *54*, 4017-4029.

Kim, D. Y.; Grey, J. K.; Barbara, P. F. A detailed single molecule spectroscopy study of the vibronic states and energy transfer pathways of the conjugated polymer MEH-PPV. *Synthetic Metals* **2006**, *156*, 336-345.

Kolodiazhnyi, O. I.: *Phosphorus Ylides: Chemistry and Applications in Organic Synthesis*; Wiley, 2008.

Kulkarni, A. P.; Kong, X.; Jenekhe, S. A. Fluorenone-Containing Polyfluorenes and Oligofluorenes: Photophysics, Origin of the Green Emission and Efficient Green Electroluminescence†. *The Journal of Physical Chemistry B* **2004**, *108*, 8689-8701.

Labastide, J. A.; Baghgar, M.; Dujovne, I.; Venkatraman, B. H.; Ramsdell, D. C.; Venkataraman, D.; Barnes, M. D. Time- and Polarization-Resolved Photoluminescence of Individual Semicrystalline Polythiophene (P3HT) Nanoparticles. *The Journal of Physical Chemistry Letters* **2011**, *2*, 2089-2093.

Labastide, J. A.; Baghgar, M.; Dujovne, I.; Yang, Y.; Dinsmore, A. D.; G. Sumpter, B.; Venkataraman, D.; Barnes, M. D. Polymer Nanoparticle Superlattices for Organic Photovoltaic Applications. *The Journal of Physical Chemistry Letters* **2011**, *2*, 3085-3091.

Labastide, J. A.; Baghgar, M.; McKenna, A.; Barnes, M. D. Time- and Polarization-Resolved Photoluminescence Decay from Isolated Polythiophene (P3HT) Nanofibers. *The Journal of Physical Chemistry C* **2012**, *116*, 23803-23811.

Lakowicz, J. R.: *Principles of Fluorescence Spectroscopy*; Springer, 2007.

Lanzani, G.: *Photophysics of Molecular Materials: From Single Molecules to Single Crystals*; Wiley, 2006.

Lee, Y. J.; Kim, D. Y.; Barbara, P. F. Effect of Sample Preparation and Excitation Conditions on the Single Molecule Spectroscopy of Conjugated Polymers. *The Journal of Physical Chemistry B* **2006**, *110*, 9739-9742.

Li, Q.: *Self-Organized Organic Semiconductors: From Materials to Device Applications*; Wiley, 2011.

Liu, D.; Yin, S.; Xu, H.; Liu, X.; Sun, G.; Xie, Z.; Yang, B.; Ma, Y. Cis- and trans-isomerization-induced transition of charge transport property in PPV oligomers. *Chemical Physics* **2011**, *388*, 69-77.

Liu, F.; Gu, Y.; Shen, X.; Ferdous, S.; Wang, H.-W.; Russell, T. P. Characterization of the morphology of solution-processed bulk heterojunction organic photovoltaics. *Progress in Polymer Science* **2013**, *38*, 1990-2052.

Liu, F.; Zhao, W.; Tumbleston, J. R.; Wang, C.; Gu, Y.; Wang, D.; Briseno, A. L.; Ade, H.; Russell, T. P. Understanding the Morphology of PTB7:PCBM Blends in Organic Photovoltaics. *Advanced Energy Materials* **2014**, *4*, n/a-n/a.

Liu, L.; Lu, P.; Wang, H.; Tang, S.; Wang, Z.; Zhang, W.; Ma, Y. Role of nonemissive quenchers for the green emission in polyfluorene. *Journal of Physical Chemistry B* **2007**, *111*, 10639-10644.

Lowry, T. H.; Richardson, K. S.: *Mechanism and Theory in Organic Chemistry*; Harper and Row Publishers: New York, 1987.

Lu, Z.; Li, C.; Fang, T.; Li, G.; Bo, Z. Triindole-cored star-shaped molecules for organic solar cells. *Journal of Materials Chemistry A* **2013**, *1*, 7657-7665.

Maayan, G.; Albrecht, M.: Metallofoldamers: Supramolecular Architectures from Helicates to Biomimetics. Wiley: Weinheim, Germany, 2013.

Masse, M.; Martin, D.; Thomas, E.; Karasz, F.; Petermann, J. Crystal morphology in pristine and doped films of poly (p-phenylene vinylene). *J Mater Sci* **1990**, *25*, 311-320.

Mathauer, K.; Frank, C. W. Naphthalene chromophore tethered in the constrained environment of a self-assembled monolayer. *Langmuir* **1993**, *9*, 3002-3008.

Meier, H.; Stalmach, U.; Kolshorn, H. Effective conjugation length and UV/vis spectra of oligomers. *Acta Polymerica* **1997**, *48*, 379-384.

Moerner, W. E.; Fromm, D. P. Methods of single-molecule fluorescence spectroscopy and microscopy. *Review of Scientific Instruments* **2003**, *74*, 3597-3619.

Mohamad, D. K.; Chauhan, S. S.; Yi, H.; Cadby, A. J.; Lidzey, D. G.; Iraqi, A. A regioregular head to tail thiophene based "double-cable" polymer with pendant anthraquinone functional groups: Preparation, spectroscopy and photovoltaic properties. *Solar Energy Materials and Solar Cells* **2011**, *95*, 1723-1730.

Mohamad, D. K.; Fischereder, A.; Yi, H.; Cadby, A. J.; Lidzey, D. G.; Iraqi, A. A novel 2,7-linked carbazole based "double cable" polymer with pendant perylene diimide functional groups: preparation, spectroscopy and photovoltaic properties. *Journal of Materials Chemistry* **2011**, *21*, 851-862.

Morfa, A. J.; Barnes, T. M.; Ferguson, A. J.; Levi, D. H.; Rumbles, G.; Rowlen, K. L.; van de Lagemaat, J. Optical characterization of pristine poly(3-hexyl thiophene) films. *Journal of Polymer Science Part B: Polymer Physics* **2011**, *49*, 186-194.

Murphy, R. S.; Moorlag, C. P.; Green, W. H.; Bohne, C. Photophysical Characterization of Fluorenone Derivatives. *Journal of Photochemistry and Photobiology A Chemistry* **1997**, *110*, 123-129.

Nagarjuna, G.; Baghgar, M.; Labastide, J. A.; Algaier, D. D.; Barnes, M. D.; Venkataraman, D. Tuning Aggregation of Poly(3-hexylthiophene) within Nanoparticles. *ACS Nano* **2012**, *6*, 10750-10758.

Nalwa, H. S.: *Handbook of Advanced Electronic and Photonic Materials and Devices*; Academic Press, 2000.

Nayak, M. K.; Dogra, S. K. Photophysics of 1-hydroxy- and 1-methoxy-9-fluorenone: II. Non-radiative deactivation. *Journal of Photochemistry and Photobiology A Chemistry* **2005**, *169*, 299-307.

Nayyar, I. H.; Batista, E. R.; Tretiak, S.; Saxena, A.; Smith, D. L.; Martin, R. L. Effect of trans- and cis-isomeric defects on the localization of the charged excitations in π-conjugated organic polymers. *Journal of Polymer Science Part B: Polymer Physics* **2013**, *51*, 935-942.

Noriega, R.; Rivnay, J.; Vandewal, K.; Koch, F. P. V.; Stingelin, N.; Smith, P.; Toney, M. F.; Salleo, A. A general relationship between disorder, aggregation and charge transport in conjugated polymers. *Nature Materials* **2013**, *12*, 1038-1044.

Notestein, J. M.; Canlas, C.; Siegfried, J.; Moore, J. S. Covalent Grafting of m-Phenylene-Ethynylene Oligomers to Oxide Surfaces. *Chemistry of Materials* **2010**, *22*, 5319-5327.

Odoi, M. Y.; Hammer, N. I.; Rathnayake, H. P.; Lahti, P. M.; Barnes, M. D. Single-Molecule Studies of a Model Fluorenone. *ChemPhysChem* **2007**, *8*, 1481-1486.

Oh, K. J.; Cash, K. J.; Plaxco, K. W. Beyond molecular beacons: optical sensors based on the binding-induced folding of proteins and polypeptides. *Chemistry* **2009**, *15*, 2244-2251.

Olsen, B. D.; Alcazar, D.; Krikorian, V.; Toney, M. F.; Thomas, E. L.; Segalman, R. A. Crystalline Structure in Thin Films of DEH−PPV Homopolymer and PPV-b-PI Rod−Coil Block Copolymers. *Macromolecules* **2007**, *41*, 58-66.

Padmanaban, G.; Ramakrishnan, S. Fluorescence Spectroscopic Studies of Solvent- and Temperature-Induced Conformational Transition in Segmented Poly[2-methoxy-5-(2'-ethylhexyl)oxy-1,4-phenylenevinylene] (MEHPPV). *The Journal of Physical Chemistry B* **2004**, *108*, 14933-14941.

Pandit, B.; Gautam, B. R.; Basel, T. P.; Vardeny, Z. V. Correlation between ultrafast transient photomodulation spectroscopy and organic photovoltaic solar cell efficiency based on RR-P3HT/PCBM blends. *Organic Electronics* **2014**, *15*, 1149-1154.

Perkampus, H.; Pohl, L. Uber die Fluoreszenzspektren dunner Filme aromatischer Kohlenwasserstoffe. *Zeitschrift für Physikalische Chemie* **1964**, *40*, 162-188.

Plater, M. J.; Jackson, T. Polyaromatic amines. Part 3: Synthesis of poly(diarylamino)styrenes and related compounds. *Tetrahedron* **2003**, *59*, 4673-4685.

Rani, S. A.; Sobhanadri, J.; Prasada, R. Solvent and Concentration Effects on the Steady State Fluorescence of Fluorenone. *Journal of Photochemistry and Photobiology A: Chemistry* **1996**, *94*, 1-5.

Rathnayake, H. P.; Cirpan, A.; Delen, Z.; Lahti, P. M.; Karasz, F. E. Optimizing OLED Efficacy of 2,7-Diconjugated 9,9-Dialkylfluorenes by Variation of Periphery Substitution and Conjugation Length. *Advanced Functional Materials* **2007**, *17*, 115-122.

Rathnayake, H. P.; Cirpan, A.; Karasz, F. E.; Odoi, M. Y.; Hammer, N. I.; Barnes, M. D.; Lahti, P. M. Luminescence of Molecular and Block Copolymeric 2,7-Bis(phenylethenyl)-fluorenones; Identifying Green-Band Emitter Sites in a Fluorene-Based Luminophore. *Chemistry of Materials* **2007**, *19*, 3265-3270.

Ray, B.; Lundstrom, M. S.; Alam, M. A. Can morphology tailoring improve the open circuit voltage of organic solar cells? *Applied Physics Letters* **2012**, *100*, -.

Reid, O. G.; Malik, J. A. N.; Latini, G.; Dayal, S.; Kopidakis, N.; Silva, C.; Stingelin, N.; Rumbles, G. The influence of solid-state microstructure on the origin and yield of long-lived photogenerated charge in neat semiconducting polymers. *Journal of Polymer Science Part B: Polymer Physics* **2012**, *50*, 27-37.

Rissler, J. Effective conjugation length of π-conjugated systems. *Chemical Physics Letters* **2004**, *395*, 92-96.

Romaner, L.; Pogantsch, A.; Scandiucci de Freitas, P.; Scherf, U.; Gaal, M.; Zojer, E.; List, E. J. W. The Origin of Green Emission in Polyfluorene-Based Conjugated Polymers: On-Chain Defect Fluorescence. *Advanced Functional Materials* **2003**, *13*, 597-601.

Saini, S.; Bagchi, B. Photophysics of conjugated polymers: interplay between Förster energy migration and defect concentration in shaping a photochemical funnel in PPV. *Physical Chemistry Chemical Physics* **2010**, *12*, 7427-7433.

Salamone, J. C.: *Polymeric materials encyclopedia*; CRC Press, 1996.

Schweikart, K. H.; Hohloch, M.; Steinhuber, E.; Hanack, M.; Lüer, L.; Gierschner, J.; Egelhaaf, H. J.; Oelkrug, D. Highly luminescent oligo(phenylenevinylene) films: the stereochemical approach. *Synthetic Metals* **2001**, *121*, 1641-1642.

Scott, J. L.; Yamada, T.; Tanaka, K. Guest specific solid-state fluorescence rationalised by reference to solid-state structures and specific intermolecular interactions. *New Journal of Chemistry* **2004**, *28*, 447-450.

Selinger, B. The photoassociation of some substituted naphthalenes. I. Rate constants and thermodynamic data for excited dimer formation. *Australian Journal of Chemistry* **1966**, *19*, 825-834.

Shigeta, M.; Morita, M.; Konishi, G.-i. Selective Formation of Twisted Intramolecular Charge Transfer and Excimer Emissions on 2,7-bis(4-Diethylaminophenyl)-fluorenone by Choice of Solvent. *Molecules* **2012**, *17*, 4452-4459.

Siddiqui, S.; Spano, F. C. H- and J-aggregates of conjugated polymers and oligomers: A theoretical investigation. *Chemical Physics Letters* **1999**, *308*, 99-105.

Singh, K. A.; Sauvé, G.; Zhang, R.; Kowalewski, T.; McCullough, R. D.; Porter, L. M. Dependence of field-effect mobility and contact resistance on nanostructure in regioregular poly(3-hexylthiophene) thin film transistors. *Applied Physics Letters* **2008**, *92*, 263303.

Singh, M.; Argade, N. P. Palladium-Catalyzed Routes to Geranylated or Farnesylated Phenolic Stilbenes: Synthesis of Pawhuskin C and Schweinfurthin J. *Synthesis* **2012**, *44*, 2895-2902.

Sirringhaus, H.; Brown, P. J.; Friend, R. H.; Nielsen, M. M.; Bechgaard, K.; Langeveld-Voss, B. M. W.; Spiering, A. J. H.; Janssen, R. A. J.; Meijer, E. W.; Herwig, P.; de Leeuw, D. M. Two-dimensional charge transport in self-organized, high-mobility conjugated polymers. *Nature* **1999**, *401*, 685.

Smith, T.; Modarelli, D. A. The efficient synthesis of unsymmetrical oligo(phenylenevinylenes). *Tetrahedron Letters* **2008**, *49*, 526-528.

Spano, F. C. Emission from aggregates of oligo-phenylene vinylenes: a recipe for superradiant H-aggregates. *Chemical Physics Letters* **2000**, *331*, 7-13.

Spano, F. C. Temperature dependent exciton emission from herringbone aggregates of conjugated oligomers. *The Journal of Chemical Physics* **2004**, *120*, 7643-7658.

Spano, F. C.; Silva, C. H- and J-Aggregate Behavior in Polymeric Semiconductors. *Annual Review of Physical Chemistry* **2014**, *65*, 477-500.

Spencer, S. D.; Bougher, C.; Heaphy, P. J.; Murcia, V. M.; Gallivan, C. P.; Monfette, A.; Andersen, J. D.; Cody, J. A.; Conrad, B. R.; Collison, C. J. The effect of controllable thin film crystal growth on the aggregation of a novel high panchromaticity squaraine viable for organic solar cells. *Solar Energy Materials and Solar Cells* **2013**, *112*, 202-208.

Stefani, M. Protein misfolding and aggregation: new examples in medicine and biology of the dark side of the protein world. *Biochimica et Biophysica Acta (BBA) - Molecular Basis of Disease* **2004**, *1739*, 5-25.

Stevens, B.; Hutton, E. Radiative Life-time of the Pyrene Dimer and the Possible Role of Excited Dimers in Energy Transfer Processes. *Nature* **1960**, *186*, 1045-1046.

Strobl, G. R.: *The Physics of Polymers: Concepts for Understanding Their Structures and Behavior*; Springer, 2007.

Summers, M. A.; Bazan, G. C.; Buratto, S. K. Matrix-Induced Intensity Fluctuations in the Fluorescence from Single Oligo(phenylenevinylene) Molecules. *Journal of the American Chemical Society* **2005**, *127*, 16202-16206.

Summers, M. A.; Robinson, M. R.; Bazan, G. C.; Buratto, S. K. Optical Microscopy of Polycrystalline Oligo(phenylenevinylene) Films. *Synthetic Metals* **2003**, *137*, 957-958.

Titov, A. V.; Wang, B.; Sint, K.; Král, P. Controllable Synthetic Molecular Channels: Biomimetic Ammonia Switch. *The Journal of Physical Chemistry B* **2009**, *114*, 1174-1179.

Tretiak, S.; Mukamel, S. Density Matrix Analysis and Simulation of Electronic Excitations in Conjugated and Aggregated Molecules. *Chemical Reviews* **2002**, *102*, 3171-3212.

Turner, A. P. F. Biosensors: Sense and sensibility. *Chemical Society Reviews* **2013**, *42*, 3175-3648.

van Hutten, P. F.; Krasnikov, V. V.; Brouwer, H. J.; Hadziioannou, G. Excimer luminescence from single crystals and films of a cyano-substituted phenylene–vinylene model compound. *Chemical Physics* **1999**, *241*, 139-154.

van Hutten, P. F.; Wildeman, J.; Meetsma, A.; Hadziioannou, G. Molecular Packing in Unsubstituted Semiconducting Phenylenevinylene Oligomer and Polymer. *Journal of the American Chemical Society* **1999**, *121*, 5910-5918.

Venkataraman, D.; Yurt, S.; Venkatraman, B. H.; Gavvalapalli, N. Role of Molecular Architecture in Organic Photovoltaic Cells. *The Journal of Physical Chemistry Letters* **2010**, *1*, 947-958.

Vidal, P.-L.; Divisia-Blohorn, B.; Bidan, G.; Hazemann, J.-L.; Kern, J.-M.; Sauvage, J.-P. π-Conjugated Ligand Polymers Entwined around Copper Centres. *Chemistry – A European Journal* **2000**, *6*, 1663-1673.

Wakioka, M.; Kitano, Y.; Ozawa, F. A Highly Efficient Catalytic System for Polycondensation of 2,7-Dibromo-9,9-dioctylfluorene and 1,2,4,5-Tetrafluorobenzene via Direct Arylation. *Macromolecules* **2013**, *46*, 370-374.

Wang, H.; Ng, M.-K.; Wang, L.; Yu, L.; Lin, B.; Meron, M.; Xiao, Y. Synthesis and Characterization of Conjugated Diblock Copolymers. *Chemistry – A European Journal* **2002**, *8*, 3246-3253.

Wang, H.; Sun, Q.; Li, Y.; Duan, L.; Qiu, Y.; Li, X. Synthesis and electroluminescent properties of a novel copolymer with short alternating conjugated and non-conjugated blocks. *Polymer International* **2003**, *52*, 343-346.

Wohlgenannt, M. Confind and delocalized polarons in pi-conjugated oligomers and polymers: A study of the effective conjugation length. *Physical Review B* **2004**, *69*.

Wolfbeis, O.; Berberan-Santos, M.: Fluorescence of Supermolecules, Polymers and Nanosystems. Springer: Verlag Berlin Heidelberg, 2008.

Yan, D.; Zhao, Y.; Wei, M.; Liang, R.; Lu, J.; Evans, D. G.; Duan, X. Regular assembly of 9-fluorenone-2,7-dicarboxylate within layered double hydroxide and its solid-state photoluminescence: a combined experiment and computational study. *RSC Advances* **2013**, *3*, 4303-4310.

Yang, Z.; Karasz, F. E.; Geise, H. J. Intrinsically soluble copolymers with well-defined alternating substituted p-phenylenevinylene and ethylene oxide blocks. *Macromolecules* **1993**, *26*, 6570-6575.

Yang, Z.; Sokolik, I.; Karasz, F. E. A soluble blue-light-emitting polymer. *Macromolecules* **1993**, *26*, 1188-1190.

Yoo, H.; Yang, J.; Yousef, A.; Wasielewski, M. R.; Kim, D. Excimer Formation Dynamics of Intramolecular π-Stacked Perylenediimides Probed by Single-Molecule Fluorescence Spectroscopy. *Journal of the American Chemical Society* **2010**, *132*, 3939-3944.

Yu, C.; Yam, V. W.-W. Glucose sensing via polyanion formation and induced pyrene excimer emission. *Chemical Communications* **2009**, 1347-1349.

Yu, Z.; Barbara, P. F. Low-Temperature Single-Molecule Spectroscopy of MEH-PPV Conjugated Polymer Molecules. *The Journal of Physical Chemistry B* **2004**, *108*, 11321-11326.

Yuan, M.-S.; Wang, D.-E.; Xue, P.; Wang, W.; Wang, J.-C.; Tu, Q.; Liu, Z.; Liu, Y.; Zhang, Y.; Wang, J. Fluorenone Organic Crystals: Two-Color Luminescence Switching and Reversible Phase Transformations between π–π Stacking-Directed Packing and Hydrogen Bond-Directed Packing. *Chemistry of Materials* **2014**, *26*, 2467-2477.

Zereg, M.; Durand, P.; Paidarová, I. About the Fermi golden rule and the computation of lifetimes of quantum resonances. *Physics Letters A* **1992**, *169*, 71-76.

Zhang, Y.; Zhu, W.; Wang, W.; Tian, H.; Su, J.; Wang, W. Synthesis and nonlinear optical properties of rod-like luminescent materials containing Schiff-base and naphthalimide units. *Journal of Materials Chemistry* **2002**, *12*, 1294-1300.

Zhu, X.; Traub, M. C.; Vanden Bout, D. A.; Plunkett, K. N. Well-Defined Alternating Copolymers of Oligo(phenylenevinylene)s and Flexible Chains. *Macromolecules* **2012**, *45*, 5051-5057.